UNIVERSIDAD DE CONCEPCION
ESCUELA DE GRADUADOS
CONCEPCION–CHILE

METODOS DE ELEMENTOS FINITOS PARA ESTRUCTURAS DELGADAS

Tesis para optar al grado de
Doctor en Ciencias Aplicadas con mención en Ingeniería Matemática

Frank Emilio Sanhueza E.

FACULTAD DE CIENCIAS FISICAS Y MATEMATICAS
DEPARTAMENTO DE INGENIERIA MATEMATICA

2010

METODOS DE ELEMENTOS FINITOS PARA ESTRUCTURAS DELGADAS

Frank Emilio Sanhueza

Directores de Tesis: Dr. Rodolfo Rodríguez A. y Dr. Ricardo G. Durán

Director de Programa: Dr. Raimund Burger.

COMISION EVALUADORA

Dr. Lourenço Beirão da Veiga, Universita degli Studi di Milano, Italia.
Dr. Richard Falk, Rutgers University,Estados Unidos.
Dr. Gabriel Gatica, Universidad de Concepción, Chile.
Dr. Rolf Stenberg, Helsinki University of Technology, Finlandia.

COMISION EXAMINADORA

Firma: _____
Dr. Lourenço Beirão da Veiga
Universita degli Studi di Milano, Italia

Firma: _____
Dr. Ricardo Durán
Universidad de Buenos Aires, Argentina

Firma: _____
Dr. Gabriel Gatica
Universidad de Concepción, Chile

Firma: _____
Dr. Rodolfo Rodríguez
Universidad de Concepción, Chile

Firma: _____
Dr. Rolf Stenberg
Helsinki University of Technology, Finlandia.

Fecha Examen de Grado: _____

Calificación: _____

Concepción–Enero 2010

Resumen

El objetivo de la tesis es analizar diferentes problemas relacionados con estructuras delgadas y su discretización por elementos finitos. Estudiamos tres problemas, que son:

- Computación de los modos de vibrar de una barra curva de Timoshenko de geometría arbitraria;
- Aproximación de los modos de vibrar de una placa laminada modelada por ecuaciones de Reissner-Mindlin;
- Un método de elementos finitos para placas rigidizadas conformada por una placa de Reissner- Mindlin y una Barra de Timoshenko.

En el primer problema, probamos estimaciones del error de orden óptimo para los desplazamientos, rotaciones y esfuerzos de corte y un doble orden de convergencia para las frecuencias de vibración, todas esas estimaciones independientes del espesor de la barra. Presentamos experimentos numéricos que confirman los resultados teóricos y el carácter libre de bloqueo del método.

En el segundo problema, estudiamos la convergencia del método propuesto. Probamos una adecuada estimación *a-priori* del problema fuente asociado y obtenemos óptimos órdenes de convergencia de las estimaciones del error para los desplazamientos en el plano y transversales en norma L^2 y H^1 y doble orden de convergencia para las frecuencias de vibración. Todas esas estimaciones son otra vez independientes del espesor de la placa. testeos numéricos confirman que el método presentado es libre de bloqueo.

En el último trabajo, probamos que el problema que resulta está bien puesto y estudiamos el caso en que el rigidizador es concéntrico con respecto a la placa. El problema se descompone en dos problemas como ocurre para las placas estándar. El problema rigidizado en el plano resulta en un análisis típico y no depende del espesor de la placa. El problema de flexión rigidizado es mucho más desafiante. Mostramos que la solución está acotada por arriba y por abajo independientemente del espesor. Óptimas estimaciones del error se prueban para los desplazamientos, rotaciones y esfuerzos de corte tanto para la placa como para el rigidizador. Finalmente experimentos numéricos muestran el carácter libre de bloqueo del método.

Abstract

The aim of this thesis is to analyze different problems involving thin structures and their discretization by finite element methods. We study three problems, namely:

- The computation of the vibration modes of a Timoshenko curved rod with arbitrary geometry;
- The approximation of the vibration modes of a laminated plate modeled by Reissner-Mindlin equations;
- A finite element method for stiffened plates composed by a Reissner-Mindlin plate and a Timoshenko rod.

In the first problem, we prove optimal order error estimates for displacements, rotations and shear stresses and a double order of convergence for the vibration frequencies, all of these estimates independent of the thickness of the rod. We present numerical experiments that confirm the theoretical results and the free-locking character of the method.

In the second problem, we study the convergence of the proposed method. We prove an adequate *a-priori* estimate for the associated load problem and obtain optimal order error estimates for the in-plane and transverse displacements and the rotations in L^2 and H^1 norms and double order of convergence for the vibration frequencies. All of these estimates are again independent of the thickness of the plate. Numerical tests which confirm that the method is locking-free are presented.

In the last work, we prove that the resulting problem is well posed and study the case in that the stiffener is located *concentrically* with respect to the plate. The problem is decoupled into two problems as for standard Reissner-Mindlin plates. The stiffened in-plane problem results in a standard analysis and not depending on the plate thickness. The stiffened bending problem is more challenging. We show that the solution is bounded above and below independently on the plate thickness. Optimal error estimates are proved for displacements, rotations and shear stresses for the plate and the stiffener. Finally numerical experiments demonstrate the locking-free character of the method.

Contents

Introducción

0.1 Introducción

0.1.1 Motivación

El estudio de las estructuras delgadas ha tomado una gran importancia en los últimos decenios tanto en la ingeniería civil como en el análisis numérico de ecuaciones diferenciales parciales. La búsqueda de elementos estructurales más eficientes desde el punto de vista económico, del peso y de las propiedades mecánicas ha introducido la necesidad de realizar modelaciones especiales consistentes en sistemas estructurales acoplados, el uso de geometrías complejas o el uso de materiales cuyas propiedades mecánicas varían tanto en su composición como en su distribución espacial. Ejemplos de estas situaciones se presentan en cascos de barcos, submarinos, aviones y naves espaciales; también están presentes en losas de puentes, pisos y estructuras de techumbres por nombrar a algunas.

Para la resolución de este tipo de situaciones el enfoque inicial ha sido el uso de herramientas analíticas para obtener soluciones cerradas o vía series infinitas, que sólo pueden obtenerse en casos sencillos y limitados (ver por ejemplo ([47]) para el caso de placas). Posteriormente los métodos numéricos, en particular el método de los elementos finitos, se han convertido en una herramienta poderosa debido a su versatilidad, eficiencia y robustez en los resultados.

Para abordar un problema de estructuras delgadas existen por lo menos dos grandes teorías. La primera es solamente para estructuras muy delgadas y que en placas y cáscaras se denomina teoría de Kirchhoff-Love y en vigas, arcos y barras se denomina teoría de vigas de Navier-Bernoulli. El segundo enfoque es una teoría para estructuras moderadamente gruesas que en placas se denomina teoría de Reissner-Mindlin y en vigas, teoría de Timoshenko. En este trabajo seguimos este segundo enfoque. La ventaja de esta perspectiva es que permite estudiar tanto estructuras delgadas como estructuras gruesas.

La utilización de modelos más enriquecidos como la teoría de Reissner-Mindlin (Timoshenko) trae aparejado serios desafíos que han concentrado por mucho tiempo el interés tanto de ingenieros civiles como de matemáticos especialistas en el análisis numérico

de ecuaciones diferenciales parciales.

El fenómeno más interesante es justamente el "locking" o bloqueo. Éste consiste en que si se utilizan elementos finitos estándar entonces se produce una sobrerigidización del término de corte (generalmente) y a medida que se considera la estructura cada vez más y más delgada este efecto se acentúa, disminuyendo artificialmente los desplazamientos hasta hacerse nulos (la estructura se bloquea). Luego para obtener resultados aceptables es necesario hacer una discretización prohibitivamente fina para evitarla. En el análisis numérico se observa que las estimaciones del error *a priori* para estos métodos dependen del espesor de la estructura que degenera cuando este parámetro se hace cada vez más pequeño.

La solución a este problema pasa por utilizar elementos finitos especiales que aseguren un buen comportamiento matemático independientemente del espesor de la estructura.

El primer artículo que propuso una solución matemática a esta implementación fue Arnold [1] para el problema de una viga de Timoshenko usando una formulación variacional mixta y demostrando que ésta es equivalente a una integración reducida del término de corte en la formulación primal. Posteriormente algunos modelos de arco fueron desarrollados por Kikuchi [33], Loula *et al.* [36] y Reddy & Volphi [42] resultados que fueron generalizados y extendidos por Arunakirinathar & Reddy [3] para barras de Timoshenko de geometría arbitraria. Una formulación alternativa a este modelo fue presentada posteriormente por Chapelle [14] a través de un esquema no conforme.

Otro problema de interés es el problema de vibraciones libres de una viga, arco o barra. Solamente hay referencias en revistas de ingeniería, sobre la implementación numérica y modelación [37, 31].

El análisis matemático de problemas de vibraciones hace uso de la teoría de operadores compactos que son presentados con suficiente detalle en [6]. Este problema ha sido abordado en placas homogéneas de Reissner-Mindlin como se puede observar en [20, 21] para diferentes elementos finitos.

0.1.2 Vibraciones en barras de Timoshenko

En el Capítulo 2 se aborda el problema de vibraciones libres de una barra de geometría arbitraria de Timoshenko. Para esto seguimos el planteamiento establecido por Arunakirinathar & Reddy [3] para el problema de cargas, pero usamos hipótesis un poco más generales al no considerar que la base de Frenet elegida que sigue la línea de los centroides de la sección transversal sea un conjunto de ejes principales; además se permite que los coeficientes geométricos y mecánicos varíen suavemente a lo largo de la barra. Se tiene una barra de geometría arbitraria cuyas secciones transversales están descritas por medio de una parametrización suficientemente suave en su longitud de arco $s \in \mathrm{I} := [0, L]$

donde L es la longitud de la curva. A través de su parametrización se define una base de Frenet consistentes en t, n y b que son el vector tangencial, normal y binormal de la curva. Estos vectores cambian punto a punto y forman una base ortogonal de $\mathbb{R}^3$ en cada punto. Llamamos S a la sección transversal de la barra y por (η,ξ) las coordenadas en el sistema $n-b$ que contiene a S. Las hipótesis de Reissner-Mindlin aplicadas en este caso particular se traducen en que:

- El vector normal a la sección transversal en un punto puede ser no necesariamente paralelo al vector tangencial definido por la línea de controides después de la deformación.
- Los puntos contenidos en el plano $n-b$ de una sección transversal de la barra tienen el mismo desplazamiento en ese plano despues de la deformación.

Definimos como $u := (u,v,w)$ el vector de desplazamientos de la línea media (curva paramétrica) en términos de la base de Frenet y $\theta := (\theta,\varphi,\psi)$ el respectivo vector de rotaciones de la línea media. los vectores u y θ son funciones de s. De aquí en adelante por sencillez de notación se omitirá esta dependencia, al igual que para los vectores de la base de Frenet. Para la formulación del problema variacional que describe una barra de Timoshenko en vibración libre es necesario considerar los desplazamientos admisibles, relacionar estos desplazamientos con la deformación y usar ecuaciones constitutivas que se apliquen al modelo considerado. En ese sentido, los desplazamientos admisibles de la barra quedan representados por:

$$U = u + \theta \times (0,\eta,\xi)\,.$$

En particular, el vector de desplazamientos queda

$$U = \begin{pmatrix} u - \eta\psi + \xi\varphi \\ v - \xi\theta \\ w + \eta\theta \end{pmatrix},$$

la diferencial del vector de desplazamientos queda

$$DU = \begin{pmatrix} u' + \xi\varphi' - \eta\psi' & -\psi & \varphi \\ v' - \xi\varphi & 0 & -\theta \\ w' + \eta\theta & \theta & 0 \end{pmatrix}$$

y el tensor de deformaciones

$$\begin{aligned} \varepsilon(U) &= \frac{1}{2}\left(DU + DU^T\right) \\ &= \begin{pmatrix} u' + \xi\varphi' - \eta\psi' & \frac{1}{2}(v' - \xi\varphi - \psi) & \frac{1}{2}(w' + \eta\theta' + \varphi) \\ \frac{1}{2}(v' - \xi\varphi' - \psi) & 0 & 0 \\ \frac{1}{2}(w' + \eta\theta' + \varphi) & 0 & 0 \end{pmatrix}. \end{aligned} \tag{1}$$

Usamos las ecuaciones constitutivas de la elasticidad 3D para un material elástico lineal caracterizado por las propiedades

$$\lambda = \frac{E\nu}{(1+\nu)(1-2\nu)} \quad \text{y} \quad \mu = \frac{E}{2(1+\nu)} = \frac{G}{2}.$$

Donde E es el módulo de Young, ν es el coeficiente de Poisson y G es el módulo de corte. Usando los supuestos de una barra en flexión, es decir tomando $\sigma_{nn} = \sigma_{nb} = \sigma_{bb} = 0$ se introducen las relaciones:

$$\begin{aligned} \sigma_{nn} = 0 = (\lambda + 2\mu)\,\varepsilon_{nn} + \lambda\,(\varepsilon_{tt} + \varepsilon_{bb}), \\ \sigma_{bb} = 0 = (\lambda + 2\mu)\,\varepsilon_{bb} + \lambda\,(\varepsilon_{tt} + \varepsilon_{nn}), \\ \sigma_{nb} = 0 = G\varepsilon_{nb}, \end{aligned}$$

obteniéndose una ley constitutiva simplificada:

$$\sigma_{tt} = E\varepsilon_{tt}, \quad \sigma_{tn} = G\varepsilon_{tn} \qquad \text{y} \qquad \sigma_{tb} = G\varepsilon_{tb}. \tag{2}$$

Usando la simetría del tensor de esfuerzos se obtiene que $\sigma_{tn} = \sigma_{nt}$, $\sigma_{tb} = \sigma_{bt}$ y $\sigma_{nb} = \sigma_{bn} = 0$. Consideramos sólo la respuesta estacionaria asociada al problema de vibraciones que tiene la forma:

$$U = \tilde{U}e^{i\omega t}.$$

Recordamos que la ecuación que rige el comportamiento de un sólido deformable está dada por

$$-\operatorname{div}\sigma(U) = \rho\ddot{U},$$

donde

$$\sigma = \begin{bmatrix} \sigma_{tt} & \sigma_{tn} & \sigma_{tb} \\ \sigma_{tn} & 0 & 0 \\ \sigma_{tb} & 0 & 0 \end{bmatrix},$$

lo que conduce al problema

$$-\operatorname{div}\sigma\left(\tilde{U}\right) = \rho\omega^2\tilde{U}.$$

El problema que se aborda es el problema de Dirichlet homogéneo, es decir u y θ se anulan en los extremos de la barra. Por simplicidad en la notación omitiremos el tilde que explicita la amplitud de la solución. Multiplicando con funciones test V que satisfagan las condiciones de contorno, integrando en el volumen e integrando por partes en el lado izquierdo se tiene

$$\int_0^L \int_A \sigma(U) : \varepsilon(V) = \omega^2 \int_0^L \int_A \rho U \cdot V.$$

De este modo, se puede escribir la energía de deformación de una barra de geometría arbitraria en forma simplificada:

$$\begin{aligned}\frac{1}{2}\int_0^L \int_A \sigma : \varepsilon &= \frac{1}{2}\int_0^L \int_A \Big(E\left(u'(s) + \xi\,\varphi(s) - \eta\,\psi'(s)\right)^2 \\ &\quad + \mu\left(v' - \xi\,\varphi - \psi\right)^2 + \mu\left(w' + \eta\,\theta' + \varphi\right)^2 \Big).\end{aligned}$$

Integrando en la sección se tiene la energía, expresada en la forma

$$\begin{aligned}\frac{1}{2}\int_0^L \int_S \sigma : \varepsilon &= \frac{1}{2}\int_0^L \left\{ \begin{pmatrix} u' \\ v' - \psi \\ w' + \varphi \end{pmatrix}^T \begin{pmatrix} EA & 0 & 0 \\ 0 & GA & 0 \\ 0 & 0 & GA \end{pmatrix} \begin{pmatrix} u' \\ v' - \psi \\ w' + \varphi \end{pmatrix} \right. \\ &\quad \left. + \begin{pmatrix} \theta' \\ \varphi' \\ \psi' \end{pmatrix}^T \begin{pmatrix} GJ & 0 & 0 \\ 0 & EI_{\xi\xi} & -EI_{\eta\xi} \\ 0 & -EI_{\eta\xi} & EI_{\eta\eta} \end{pmatrix} \begin{pmatrix} \theta' \\ \varphi' \\ \psi' \end{pmatrix} \right\}.\end{aligned}$$

Definiendo

$$\mathbb{D} := \begin{pmatrix} EA & 0 & 0 \\ 0 & k_1 GA & 0 \\ 0 & 0 & k_2 GA \end{pmatrix}, \qquad \mathbb{E} := \begin{pmatrix} GJ & 0 & 0 \\ 0 & EI_{\eta\eta} & -EI_{\eta\xi} \\ 0 & -EI_{\eta\xi} & EI_{\xi\xi} \end{pmatrix},$$

$$\mathbb{J} := \begin{pmatrix} J & 0 & 0 \\ 0 & I_{\eta\eta} & -I_{\eta\xi} \\ 0 & -I_{\eta\xi} & I_{\xi\xi} \end{pmatrix},$$

la energía de deformación de la barra queda:

$$\frac{1}{2}\int_0^L \int_S \sigma : \varepsilon = \frac{1}{2}\int_0^L \left(u' - \theta \times t\right)^T \mathbb{D}\,\left(u' - \theta \times t\right) + {\theta'}^T \mathbb{E}\,\theta',$$

donde las constantes k_1 y k_2 en $\mathbb{D}$ se llaman factores de corrección de corte. El uso de estos factores no es completamente satisfactorio desde el punto de vista matemático, pero es considerado apropiado desde el punto de vista de la ingeniería. De las ecuaciones (1) y (2) observamos que σ_{tn} es constante en η, σ_{tb} es constante en ξ y $\sigma_{nb} = 0$. Sin embargo dichas tensiones en realidad son parabólicas con la condición que en las caras exteriores vale cero y tiene un valor máximo en el centroide de la sección ([45]). De allí que sea necesario introducir estos factores de corrección que dependen también de las condiciones de borde del problema.

Finalmente, el problema de vibraciones libres de la barra empotrada queda: Hallar $(u, \theta) \in H_0^1(\mathrm{I})^3 \times H_0^1(\mathrm{I})^3$ no nulos y $\omega > 0$ tales que

$$\begin{aligned}\int_0^L \left(u' - \theta \times t\right)^T \mathbb{D}\,\left(v' - \phi \times t\right) + {\theta'}^T \mathbb{E}\,\phi' &= \omega^2 \int_0^L \rho\left(Au \cdot v + \theta^T \mathbb{J}\phi\right) \\ &\forall (v, \phi) \in H_0^1(\mathrm{I})^3 \times H_0^1(\mathrm{I})^3.\end{aligned}$$

Después de escalar el problema, definir el operador resolvente y el operador resolvente del problema límite, se demuestra convergencia del operador resolvente al problema límite y por lo tanto convergencia espectral al espectro del problema límite. En el estudio del problema discreto se utilizan para las variables principales polinomiales de grado r a trozos y continuas y en el corte (multiplicadores de Lagrange) polinomiales discontinuas de grado $r-1$. Se propone una demostración alternativa a la inf-sup propuesta en [1]. Se demuestra convergencia de orden r al espectro en norma H^1 y de orden $(r+1)$ en norma L^2 asociado a autovalores simples. Por último se demuestra doble orden de convergencia para las frecuencias de vibración.

El estudio del problema de vibraciones de una barra de geometría arbitraria de Timoshenko dio origen a la publicación:

- Erwin Hernandez, Enrique Otárola, Rodolfo Rodríguez, Frank Sanhueza: Approximation of the vibration modes of a Timoshenko curved rod of arbitrary geometry. IMA Journal of Numerical Analysis, vol 29 pp. 86-108, (2009).

0.1.3 Vibraciones en placas laminadas

El estudio de placas de Reissner-Mindlin por Métodos de Elementos Finitos concentró la atención de gran parte de la comunidad matemática, produciendo en la década de los 90 una gran cantidad de artículos en los que se tratan diversas formas de resolver el problema de *locking*. En el libro de Brezzi & Fortin [10], se presenta en forma general la temática de las placas de Reissner-Mindlin, el estudio de la existencia y unicidad de la solución, algunos resultados de regularidad de la solución y algunos métodos de elementos finitos satisfactorios con estimaciones del error, resultados que son complementados en los artículos de Brezzi & Fortin [10] y Arnold & Falk [2].

Se han desarrollado múltiples familias de elementos finitos que resuelvan apropiadamente el problema de bloqueo en placas homogéneas de Reissner-Mindlin ([10, 2, 9] entre otros). Entre los estudios desarrollados se destaca el artículo de Durán & Liberman [22] que presenta una manera de estudiar en forma sistemática diferentes métodos de elementos finitos encontrando estimaciones del error satisfactorias. Además se desarrolla un elemento finito de bajo orden denominado posteriormente como DL3.

El problema de la placa laminada fue estudiado fundamentalmente por la comunidad de Ingeniería [39, 43]. Sin embargo Aurichio *et al.* [4], estudiaron el problema de flexión de una placa sometida a cargas transversales siguiendo el análisis realizado por Durán *et al* ([22]) para placas homogéneas. Utilizando este último artículo y ([4]) se estudia el problema de vibraciones de una placa laminada utilizando una teoría de primer orden denominada First Shear Deformation Theory (FSDT,[5]).

La formulación del problema variacional sigue un camino similar al de las barras de geometría arbitraria. Se considera una placa elástica de espesor t con la configuración de referencia $\Omega \times \left(-\frac{t}{2}, \frac{t}{2}\right)$, donde $\Omega \subset \mathbb{R}^2$ es un dominio poligonal convexo. Por sencillez asumiremos que la placa está hecha de dos materiales diferentes ocupando cada uno de ellos los subdominios $\Omega \times \left(-\frac{t}{2}, 0\right)$ y $\Omega \times \left(0, \frac{t}{2}\right)$. Se definen ciertos desplazamientos fundamentales que describirán el movimiento de la placa. Llamaremos (u^*, w^*) los desplazamientos de la superficie media con $u^* = (u_1^*, u_2^*)$ los desplazamientos en el plano de la placa y w^* el desplazamiento transversal, ambos en cada punto (x_1, x_2) del plano medio de la placa. Se definen también $\beta^* = (\beta_1^*, \beta_2^*)$ las rotaciones de las fibras inicialmente ortogonales a la superficie media de la placa. Se utilizan las hipótesis de Reissner-Mindlin que vinculan los desplazamientos con las rotaciones proponiendo los siguientes desplazamientos admisibles:

$$U^* = \begin{pmatrix} u^* - \beta^* x_3 \\ w^* \end{pmatrix}$$

La diferencial queda

$$DU^* = \begin{pmatrix} Du^* - x_3 \nabla \beta^* & -\beta^* \\ \nabla w^* & 0 \end{pmatrix}$$

y el tensor de deformación

$$\varepsilon(U) = \begin{pmatrix} \varepsilon(u^*) - x_3 \varepsilon(\beta^*) & \frac{1}{2}(\nabla w^* - \beta^*) \\ \frac{1}{2}(\nabla w^* - \beta^*)^T & 0 \end{pmatrix}.$$

Dado que la placa laminada está formada por dos materiales diferentes, tendrá distintas propiedades elásticas en cada lámina, lo que se traduce en ecuaciones constitutivas para cada zona. para las deformaciones en el plano, la ley constitutiva es

$$\sigma(\zeta) = \lambda_i (\operatorname{tr} \varepsilon(\zeta)) I + 2\mu_i \varepsilon(\zeta)$$
$$\text{con} \quad \lambda_i = \frac{E_i \nu_i}{(1+\nu_i)(1-2\nu_i)}, \quad \mu_i = \frac{E_i}{2(1+\nu_i)}, \quad i = 1, 2.$$

donde E_i y ν_i son los módulos de Young y de Poisson en cada lámina de la placa.

Para las deformaciones por flexión utilizando las hipótesis de tensión plana en cada lámina de la placa, es decir $\sigma_{zz} = \sigma_{zx} = \sigma_{zy} = 0$, se tiene una modificación sólo de λ_i para adaptarla al modelo de tensión plana:

$$\tilde{\lambda}_i = \frac{E \nu_i}{1 - \nu_i^2}.$$

Consideramos nuevamente sólo la respuesta estacionaria asociada al problema de vibraciones que tiene la forma,

$$U = \tilde{U} e^{i\omega t}.$$

Recordamos que la ecuación que rige el comportamiento de un sólido deformable está dada por:

$$-\operatorname{div}\sigma(U)=\rho\ddot{U},$$

que conduce al problema

$$-\operatorname{div}\sigma\left(\tilde{U}\right)=\rho\omega^2\tilde{U}.$$

Por simplicidad en la notación omitiremos el tilde que explicita la amplitud de los desplazamientos. La energía de deformación de la placa laminada queda

$$\begin{aligned}\frac{1}{2}\int_{-\frac{t}{2}}^{\frac{t}{2}}\int_\Omega \sigma(U):\varepsilon(U)=\frac{1}{2}\Big(&t\left(\mathscr{A}\varepsilon(u^*),\varepsilon(u^*)\right)+2t^2\left(\mathscr{B}\varepsilon(u^*),\varepsilon(\beta^*)\right)\\&+t^3\left(\mathscr{D}\varepsilon(\beta^*),\varepsilon(\beta^*)\right)+t\kappa(\beta^*-\nabla w^*,\beta^*-\nabla w^*)\Big),\end{aligned}$$

donde hemos integrado en el espesor t, utilizado las leyes constitutivas asociadas a cada lámina de la placa y la siguiente definición de los tensores de cuarto orden $\mathscr{A}$, $\mathscr{B}$ y $\mathscr{D}$:

$$\mathscr{A}(\tau):=\frac{1}{2}(\mathscr{C}_1+\mathscr{C}_2)\tau,\quad \mathscr{B}(\tau):=\frac{1}{8}(\mathscr{C}_1-\mathscr{C}_2)\tau,\quad \mathscr{D}(\tau):=\frac{1}{24}(\mathscr{C}_1+\mathscr{C}_2)\tau,$$

con $\mathscr{C}_1$ y $\mathscr{C}_2$ operadores de elasticidad lineal en cada medio:

$$\mathscr{C}_i:=\lambda_i\operatorname{tr}(\tau)I+2\mu_i\tau,\qquad i=1,2.$$

Finalmente $\kappa:=k(\mu_1+\mu_2)/2$ es el módulo de corte de la placa laminada, siendo k el factor de corrección de corte que se toma como $5/6$ para una placa empotrada.

La energía de vibración de la parte estacionaria queda

$$\begin{aligned}\frac{\omega^2}{2}\int_{-\frac{t}{2}}^{\frac{t}{2}}\int_\Omega \rho U\cdot U=\frac{\omega^2}{2}\Big\{&\frac{t}{2}(\rho_1+\rho_2)(u^*,u^*)+\frac{t}{2}(\rho_1+\rho_2)(w^*,w^*)\\&+\frac{t^3}{24}(\rho_1+\rho_2)(\beta^*,\beta^*)+\frac{t^2}{4}(\rho_1-\rho_2)(\beta^*,u^*)\Big\}\end{aligned}$$

Finalmente el problema variacional queda:

Hallar $\omega>0$ y $(u^*,\beta^*,w^*)\in V$ no trivial, tales que

$$\begin{aligned}&t\left(\mathscr{A}\varepsilon(u^*),\varepsilon(v)\right)+t^2\left[\left(\mathscr{B}\varepsilon(u^*),\varepsilon(\eta)\right)+\left(\mathscr{B}\varepsilon(\beta^*),\varepsilon(v)\right)\right]\\&+t^3\left(\mathscr{D}\varepsilon(\beta^*),\varepsilon(\eta)\right)+t\kappa(\beta^*-\nabla w^*,\eta-\nabla z)\\&\quad=\omega^2\Big\{\frac{t}{2}(\rho_1+\rho_2)(u^*,v)+\frac{t^3}{24}(\rho_1+\rho_2)(\beta^*,\eta)\\&\qquad+\frac{t}{2}(\rho_1+\rho_2)(w^*,z)+\frac{t^2}{8}(\rho_1-\rho_2)\left[(\beta^*,v)+(u^*,\eta)\right]\Big\}\quad\forall(v,\eta,z)\in V,\end{aligned}$$

donde

$$V := H_0^1(\Omega)^2 \times H_0^1(\Omega)^2 \times H_0^1(\Omega).$$

En el Capítulo 2 se estudia el problema de vibraciones libres de una placa laminada usando la teoría de operadores compactos descrita en ([6]). Después de escalar adecuadamente el problema de vibraciones libres, se definen los operadores resolventes del problema de placas laminadas así como su respectivo problema límite. Se demuestra convergencia hacia el operador resolvente del problema límite cuando el espesor de la placa tiende a cero. En la definición del problema discreto se utiliza el elemento finito DL3 [22] para las variables de la placa y para los desplazamientos en el plano se utilizan elementos lineales a trozos y continuos. Se prueba orden de convergencia lineal para las autofunciones en norma H^1 y cuadrático en norma L^2, así como doble orden de convergencia para las frecuencias de vibración. Todos estos resultados dan origen al artículo:

- Approximation of the vibration modes of a Reissner-Mindlin laminated Plate (Enviado)

0.1.4 Problema de placas rigidizadas de Reissner-Mindlin

Otro problema de mucho interés en la ingeniería se refiere a las placas rigidizadas. Una placa rigidizada es una placa acoplada con una barra que generalmente tiene propiedades mecánicas mucho más resistentes aumentando su capacidad resistente a flexión, o bien, evitando el pandeo de una placa cuando está sometida a carga en su propio plano. Se han aplicado diferentes ideas para modelar placas rigidizadas desde el punto de vista de la ingeniera civil. A pesar de que se pueden distinguir varios tipos, los agrupamos en dos categorías.

El primero consiste en utilizar un modelos aproximados de una estructura típicamente con una topología diferente pero que dentro de criterios ingenieriles puede considerarse una aproximación simplificada del problema. Por ejemplo, modelar la placa rigidizada como una placa ortotrópica o alternativamente, como un envigado en donde las propiedades equivalentes de las vigas son consideradas a partir de un ancho efectivo de la placa. Otra posibilidad es agrupar la masa de los rigidizadores desplazándola a los bordes de los elementos de la placa. Claramente la debilidad de estos enfoques es que hay un error en la modelación que es difícil de evaluar (ver [28] para un breve recuento de estos modelos y las referencias de ese artículo).

Un segundo enfoque consiste en modelar la placa rigidizada por medio de elementos de placas y los rigidizadores por elementos de vigas. En este caso hay dos posibilidades, usar una malla arbitraria de manera que en general habrá elementos atravesados por trozos de rigidizador o usar una malla en la que los rigidizadores coinciden con los lados de los elementos. En nuestro análisis consideramos sólo la segunda posibilidad.

Muchos artículos han abordado el problema de las placas rigidizadas desde el punto de vista de la ingeniería. En [40] se estudia el problema de la placa rigidizada para placas y vigas esbeltas. Se escribe la energía de la placa, la energía de la viga y se introducen multiplicadores de Lagrange que vincula los desplazamientos de la placa y el rigidizador. En [17] se estudia el problema de cargas de la placa rigidizada usando la teoría de Reissner Mindlin utilizando varias formulaciones, entre ellas se muestra una formulación ortotrópica. En [38] se ha estudiado también el problema de vibraciones de una placa rigidizada de acuerdo a la teoría de Reissner-Mindlin para rigidizadores excéntricos, es decir tales que no necesariamente la línea media del rigidizador coincida con la superficie media de la placa. En [28] se presenta también el problema de vibraciones libres de una placa rigidizada excéntrica, pero utiliza el elemento MITC9 lo que permite evitar el "locking" en la placa rigidizada.

Desde el punto de vista matemático el único artículo sobre placas rigidizadas es [19] donde se estudia una placa esbelta usando la técnica de descomposición de dominios. En ese artículo se estudia una placa con el rigidizador puesto simétricamente con respecto a la línea media de la placa. En el Capítulo 3 de esta tesis se presenta la formulación del problema y las condiciones de compatibilidad geométrica entre la placa y el rigidizador. Se estudia la existencia y unicidad, la estabilidad de la solución y su discretización.

Para el análisis numérico nos restringimos a analizar el caso en que el rigidizador es simétrico con respecto al plano medio de la placa. En este caso los problemas de las deformaciones de la placa rigidizada en el plano y de flexión se desacoplan completamente.

Como resultado de esta investigación se tiene el siguiente artículo:

- A finite element method for Reissner-Mindlin stiffened plates (en preparación).

Chapter 1

Approximation of the vibration modes of a Timoshenko curved rod of arbitrary geometry

The aim of this chapter is to analyze a mixed finite element method for computing the vibration modes of a Timoshenko curved rod with arbitrary geometry. Optimal order error estimates are proved for displacements, rotations and shear stresses of the vibration modes, as well as a double order of convergence for the vibration frequencies. These estimates are essentially independent of the thickness of the rod, which leads to the conclusion that the method is locking free. Numerical tests are reported in order to assess the performance of the method.

1.1 Introduction

It is very well known that standard finite elements applied to models of thin structures, like beams, rods, plates and shells, are subject to the so-called *locking* phenomenon. This means that they produce very unsatisfactory results when the thickness is small with respect to the other dimensions of the structure (see for instance [7]). From the point of view of the numerical analysis, this phenomenon usually reveals itself in that the a priori error estimates for these methods depend on the thickness of the structure in such a way that they degenerate when this parameter becomes small. To avoid locking, special methods based on reduced integration or mixed formulations have been devised and are typically used (see, for instance, [10]).

Very likely, the first mathematical piece of work dealing with numerical locking and how to avoid it is the paper by [1], where a thorough analysis for the Timoshenko beam bending model is developed. In that paper, it is proved that locking arises because of the

shear terms and a locking-free method based on a mixed formulation is introduced and analyzed. It is also shown that this mixed method is equivalent to use a reduced-order scheme for the integration of the shear terms in the primal formulation.

Subsequently, several methods to avoid locking on different models of circular arches were developed by [33], [36] and [42]. The analysis of the latter was extended by [3] to Timoshenko rods of rather arbitrary geometry. An alternative approach to deal with this same kind of rods was developed and analyzed by [14], where a numerical method based on standard beam finite elements was used.

All the above references deal only with load problems. The literature devoted to the dynamic analysis of rods is less rich. There exist a few papers introducing finite element methods and assessing their performance by means of numerical experiments (see [31, 35] and references therein). Papers dealing with the numerical analysis of the eigenvalue problems arising from the computation of the vibration modes for thin structures are much less frequent; among them we mention [20, 21], where MITC methods for computing bending vibration modes of plates were analyzed. One reason for this is that the extension of mathematical results from load to vibration problems is not quite straightforward for mixed methods. [12, 13] showed that eigenvalue problems for mixed formulations show peculiar features that make them substantially different from the same methods applied to the corresponding source problems. In particular, they showed that the standard inf-sup and ellipticity in the kernel conditions, which ensure convergence for the mixed formulation of source problems, are not enough to attain the same goal in the corresponding eigenvalue problem.

In this paper we analyze a mixed finite element method to compute the vibration modes of an elastic curved rod. For the stiffness terms, we follow the approach proposed by [3] for the load problem. We settle the corresponding spectral problem by including the mass terms arising from displacement and rotational inertia in the model, as proposed in [31]. Our assumptions on the rods are slightly weaker than those in these references. On the one hand we do not assume that the Frenet basis associated with the line of cross-section centroids is a set of principal axes. On the other hand, we allow for non-constant geometric and physical coefficients varying smoothly along the rod. We prove that the resulting method yields optimal order approximation of displacements, rotations and shear stresses of the vibration modes, as well as a double order of convergence for the vibration frequencies. Under mild assumptions, we also prove that the error estimates do not degenerate as the thickness becomes small, which allows us to conclude that the method is locking free.

The outline of the paper is as follows. In Sect. 1.2, we recall the basic geometric and physical assumptions to settle the vibration problem for a Timoshenko rod of arbitrary geometry. The resulting spectral problem is shown to be well posed. Its eigenvalues and

eigenfunctions are proved to converge to the corresponding ones of the limit problem as the thickness of the rod goes to zero, which corresponds to a Bernoulli-like rod model. A finite element discretization with piecewise polynomials of arbitrary degree is introduced and analyzed in Sect. 1.3. Optimal orders of convergence are proved for the eigenfunctions and the corresponding shear stresses. Finally a double order of convergence is proved for the eigenvalues and, whence, for the vibration frequencies. All these error estimates are proved to be independent of the thickness of the rod, which allows us to conclude that the method is locking-free. In Sect. 1.4, we report several numerical tests, which allow assessing the performance of the lowest-degree method. The experiments include different geometries and even boundary conditions not covered by the theoretical analysis. All the tests show optimal orders of convergence for all the variables. They also show that the method is thoroughly locking-free.

1.2 The vibration problem for an elastic rod of arbitrary geometry

A curved rod in undeformed reference state is described by means of a smooth three-dimensional curve, the *line of centroids*, which passes through the centroids of cross-sections of the rod. These cross-sections are initially plane and normal to the line of centroids. The curve is parametrized by its arc length $s \in \mathrm{I} := [0, L]$, L being the total length of the curve.

We recall some basic concepts and definitions; for further details see [3], for instance. We use standard notation for Sobolev spaces and norms.

The basis in which the equations are formulated is the *Frenet basis* consisting of t, n and b, which are the tangential, normal and binormal vectors of the curve, respectively. These vectors change smoothly from point to point and form an orthogonal basis of $\mathbb{R}^3$ at each point.

Let S denote a cross-section of the rod. We denote by (η, ζ) the coordinates in the coordinate system $\{n, b\}$ of the plane containing S (see Fig. 1.1).

The geometric properties of the cross-section are determined by the following parameters (recall that the first moments of area, $\int_S \eta \, d\eta \, d\zeta$ and $\int_S \zeta \, d\eta \, d\zeta$, vanish, because the center of coordinates is the centroid of S):

- area of S: $A := \int_S d\eta \, d\zeta$;
- second moments of area with respect to the axis n, $I_n := \int_S \zeta^2 \, d\eta \, d\zeta$, and b, $I_b := \int_S \eta^2 \, d\eta \, d\zeta$;
- polar moment of area: $J := \int_S \left(\eta^2 + \zeta^2\right) d\eta \, d\zeta = I_n + I_b$;
- $I_{nb} := \int_S \eta \, \zeta \, d\eta \, d\zeta$.

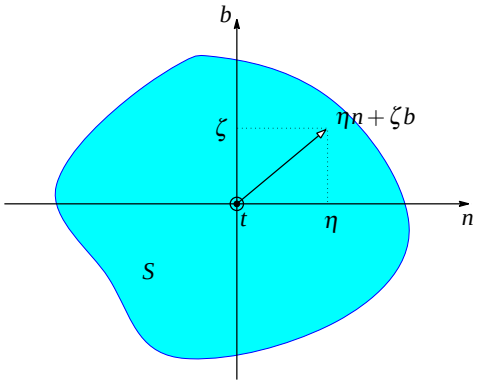

Figure 1.1: Cross-section. Coordinate system.

These parameters are not necessarily constant, but they are assumed to vary smoothly along the rod. For a non-degenerate rod, A is bounded above and below far from zero. Consequently, the same happens for the area moments, I_n, I_b and J.

Remark 1.2.1 *For any planar set S, there exists an orthogonal coordinate system, named the set of principal axes, such that I_{nb} vanishes when computed in these coordinates. For particularly symmetric geometries of S, for instance when the cross-section of the rod is a circle or a square, I_{nb} vanishes in any orthogonal coordinate system. However, in general, there is no reason for n and b to be principal axes, so that I_{nb} does not necessarily vanish. In any case, it is straightforward to prove that the matrix*

$$\begin{pmatrix} I_n & -I_{nb} \\ -I_{nb} & I_b \end{pmatrix}$$

is always positive definite.

Vector fields defined on the line of centroids will be always written in the Frenet basis:

$$v = v_1 t + v_2 n + v_3 b, \qquad \text{with} \quad v_1, v_2, v_3 : \mathrm{I} \longrightarrow \mathbb{R}.$$

We emphasize that v_1, v_2 and v_3 are not the components of v in a fixed basis of $\mathbb{R}^3$, but in the Frenet basis $\{t, n, b\}$, which changes from point to point of the curve.

Since t, n and b are smooth functions of the arc-length parameter s, we have that

$$v' = v_1' t + v_2' n + v_3' b + v_1 t' + v_2 n' + v_3 b'.$$

If we denote

$$\dot{v} := v_1' t + v_2' n + v_3' b, \tag{1.1}$$

then, by using the *Frenet-Serret formulas* (see, for instance, [3]), there holds

$$v' = \dot{v} + \Gamma^{\mathrm{t}} v, \qquad \text{with} \quad \Gamma(s) := \begin{pmatrix} 0 & \kappa(s) & 0 \\ -\kappa(s) & 0 & \tau(s) \\ 0 & -\tau(s) & 0 \end{pmatrix},$$

where κ and τ are the curvature and the torsion of the rod, which are smooth functions of s, too. Therefore, $v = v_1 t + v_2 n + v_3 b \in \mathrm{H}^1(\mathrm{I})^3$ if and only if $v_i \in \mathrm{L}^2(\mathrm{I})$ and $\dot{v}_i \in \mathrm{L}^2(\mathrm{I})$, $i = 1,2,3$.

Since we will confine our attention to elastic rods clamped at both ends, we proceed as in [3] and consider

$$\mathscr{V} := \left\{ v \in \mathrm{L}^2(\mathrm{I})^3 : \ \dot{v} \in \mathrm{L}^2(\mathrm{I})^3 \text{ and } v(0) = v(L) = 0 \right\},$$

endowed with its natural norm

$$\|v\|_1 := \left[\int_0^L \left(|v|^2 + |\dot{v}|^2 \right) ds \right]^{1/2};$$

namely, $\mathscr{V}$ is the space of vector fields defined on the line of centroids such that their components in the Frenet basis are in $\mathrm{H}^1_0(\mathrm{I})$.

We will systematically use in what follows the total derivative $v' = \dot{v} + \Gamma^{\mathrm{t}} v$. Since t, n and b are assumed to be smooth functions, $\|v'\|_0$ is a norm on $\mathscr{V}$ equivalent to $\|\cdot\|_1$ (see [3, Theorem 3.1]). This is the reason why we denote $\|\cdot\|_1$ the norm of $\mathscr{V}$. However, the total derivative v' should be distinguished from the vector $\dot{v}$ of derivatives of the components of v in the Frenet basis, as defined by (1.1).

The kinematic hypotheses of Timoshenko are used for the problem formulation. The deformation of the rod is described by the displacement of the line of centroids, $u \in \mathbb{R}^3$, and the rotation of the cross-sections, $\theta \in \mathbb{R}^3$. The physical properties of the rod are determined by the elastic and the shear moduli E and G, respectively, the shear correcting factors k_1 and k_2, and the volumetric density ρ, all of them strictly positive coefficients. These coefficients are not necessarily constant; they are allowed to vary along the rod, but they are also assumed to be smooth functions of the arc-length s.

We consider the problem of computing the free vibration modes of an elastic rod clamped at both ends. The variational formulation of this problem consists in finding non-trivial $(u,\theta) \in \mathscr{W} := \mathscr{V} \times \mathscr{V}$ and $\omega > 0$ such that

$$\begin{aligned} \int_0^L \mathbb{E}\theta' \cdot \psi' \, ds + \int_0^L \mathbb{D}\left(u' - \theta \times t\right) \cdot \left(v' - \psi \times t\right) ds \\ = \omega^2 \left(\int_0^L \rho A u \cdot v \, ds + \int_0^L \rho \mathbb{J}\theta \cdot \psi \, ds \right) \qquad \forall (v,\psi) \in \mathscr{W} \end{aligned} \tag{1.2}$$

where ω is the vibration frequency and u and θ are the amplitudes of the displacements and the rotations, respectively (see [31]). The coefficients $\mathbb{D}$, $\mathbb{E}$ and $\mathbb{J}$ are 3×3 matrices, which in the Frenet basis are written as follows:

$$\mathbb{D} := \begin{pmatrix} EA & 0 & 0 \\ 0 & k_1GA & 0 \\ 0 & 0 & k_2GA \end{pmatrix}, \quad \mathbb{E} := \begin{pmatrix} GJ & 0 & 0 \\ 0 & EI_n & -EI_{nb} \\ 0 & -EI_{nb} & EI_b \end{pmatrix},$$

$$\mathbb{J} := \begin{pmatrix} J & 0 & 0 \\ 0 & I_n & -I_{nb} \\ 0 & -I_{nb} & I_b \end{pmatrix}.$$

In [31], as in most references ([3, 14], for instance), the Frenet basis is assumed to be a set of principal axes, so that $I_{nb} = 0$ and the three matrices above are diagonal. We do not make this assumption in this paper.

Remark 1.2.2 *The vibration problem above can be formally obtained from the three-dimensional linear elasticity equations as follows: According to the Timoshenko hypotheses, the admissible displacements at each point $\eta n + \zeta b \in S$ (see Fig. 1.1) are of the form $u + \theta \times (\eta n + \zeta b)$, with u, θ, n and b being functions of the arc-length coordinate s. Test and trial displacements of this form are taken in the variational formulation of the linear elasticity equations for the vibration problem of the three-dimensional rod. By integrating over the cross-sections and multiplying the shear terms by correcting factors k_1 and k_2, one arrives at problem (1.2).*

It is well known that standard finite element methods applied to equations like (1.2) are subject to *numerical locking*: they lead to unacceptably poor results for very thin structures, unless the mesh-size is excessively small. This phenomenon is due to the different scales with respect to the thickness of the rod of the two terms on the left-hand side of this equation. An adequate framework for the mathematical analysis of locking is obtained by rescaling the equations in order to obtain a family of problems with a well-posed limit as the thickness becomes infinitely small.

With this purpose, we introduce the following non-dimensional parameter, characteristic of the thickness of the rod:

$$d^2 := \frac{1}{L}\int_0^L \frac{J}{AL^2}\, ds.$$

By defining

$$\lambda := \frac{\omega^2\rho}{d^2}, \qquad \widehat{\mathbb{D}} := \frac{1}{d^2}\mathbb{D}, \qquad \widehat{\mathbb{E}} := \frac{1}{d^4}\mathbb{E}, \qquad \widehat{\mathbb{J}} := \frac{1}{d^4}\mathbb{J} \qquad \text{and} \qquad \widehat{A} := \frac{A}{d^2},$$

problem (1.2) can be equivalently written as follows: Find non-trivial $(u,\theta)\in\mathscr{W}$ and $\lambda\in\mathbb{R}$ such that

$$\int_0^L \widehat{\mathbb{E}}\theta'\cdot\psi'\,ds+\frac{1}{d^2}\int_0^L \widehat{\mathbb{D}}\left(u'-\theta\times t\right)\cdot\left(v'-\psi\times t\right)ds = \lambda\left(\int_0^L \widehat{A}u\cdot v\,ds+d^2\int_0^L \widehat{\mathbb{J}}\theta\cdot\psi\,ds\right)\qquad \forall\,(v,\psi)\in\mathscr{W}. \tag{1.3}$$

The values of interest of d are obviously bounded above, so we restrict our attention to $d\in(0,d_{\max}]$. The coefficients of the matrices $\widehat{\mathbb{D}}$, $\widehat{\mathbb{E}}$ and $\widehat{\mathbb{J}}$, as well as $\widehat{A}$, are assumed to be functions of s which do not vary with d. This corresponds to considering a family of problems where the size of the cross-sections are uniformly scaled by d at all point of the line of centroids, while their shapes as well as the geometry of the curve and the material properties remain fixed.

Remark 1.2.3 *Matrices $\widehat{\mathbb{D}}$, $\widehat{\mathbb{E}}$ and $\widehat{\mathbb{J}}$ are positive definite for all $s\in\mathrm{I}$, the last two because of Remark 1.2.1. Moreover, since all the coefficients are continuous functions of s, the eigenvalues of each of these matrices are uniformly bounded below away from zero for all $s\in\mathrm{I}$.*

Remark 1.2.4 *The eigenvalues λ of problem (1.3) are strictly positive, because of the symmetry and the positiveness of the bilinear forms on its left and right-hand sides. The positiveness of the latter is a straightforward consequence of Remark 1.2.3, whereas that of the former follows from the ellipticity of this bilinear form in $\mathscr{W}$. This can be proved by using Remark 1.2.3 again and proceeding as in the proof of Lemma 3.4 (a) from [3], where the same result appears for particular constant coefficients (see also [14, Proposition 1]).*

We introduce the scaled shear stress $\gamma:=\frac{1}{d^2}\widehat{\mathbb{D}}\left(u'-\theta\times t\right)$ to rewrite problem (1.3) as follows:

$$\left(\widehat{\mathbb{E}}\theta',\psi'\right)+\left(\gamma,v'-\psi\times t\right)=\lambda\left[\left(\widehat{A}u,v\right)+d^2\left(\widehat{\mathbb{J}}\theta,\psi\right)\right]\qquad\forall\,(v,\psi)\in\mathscr{W}, \tag{1.4}$$

$$\gamma=\frac{1}{d^2}\widehat{\mathbb{D}}\left(u'-\theta\times t\right). \tag{1.5}$$

where $(\cdot,\cdot)$ denotes the $\mathrm{L}^2(\mathrm{I})^3$ inner product.

To analyze this problem, we introduce the operator

$$T:\ \mathrm{L}^2(\mathrm{I})^3\times\mathrm{L}^2(\mathrm{I})^3\longrightarrow\mathrm{L}^2(\mathrm{I})^3\times\mathrm{L}^2(\mathrm{I})^3,$$

defined by $T(f,\phi):=(u,\theta)$, where $(u,\theta)\in\mathscr{W}$ is the solution of the associated load problem:

$$\left(\widehat{\mathbb{E}}\theta',\psi'\right)+\left(\gamma,v'-\psi\times t\right)=\left(\widehat{A}f,v\right)+d^2\left(\widehat{\mathbb{J}}\phi,\psi\right)\qquad\forall\,(v,\psi)\in\mathscr{W}, \tag{1.6}$$

$$\gamma=\frac{1}{d^2}\widehat{\mathbb{D}}\left(u'-\theta\times t\right). \tag{1.7}$$

Taking into account that (1.7) can be equivalently written as follows:

$$\left(u' - \theta \times t, q\right) - d^2 \left(\widehat{\mathbb{D}}^{-1}\gamma, q\right) = 0 \qquad \forall q \in \mathscr{Q} := \mathrm{L}^2(\mathrm{I})^3,$$

we note that the load problem falls in the framework of the mixed formulations considered in [10]. In this reference, the results from [1] are extended to cover this kind of problems. In particular, according to [10, Theorem II.1.2], to prove the well posedness it is enough to verify the classical properties of mixed problems:

i) *ellipticity in the kernel*: $\exists \alpha > 0$ such that

$$\left(\widehat{\mathbb{E}}\psi', \psi'\right) \geq \alpha \left(\|v\|_1^2 + \|\psi\|_1^2\right) \qquad \forall (v, \psi) \in \mathscr{W}_0,$$

where $\mathscr{W}_0 := \{(v, \psi) \in \mathscr{W} : \ v' - \psi \times t = 0 \ \text{ in I}\}$;

ii) *inf-sup condition*: $\exists \beta > 0$ such that

$$\sup_{(0,0)\neq(v,\psi)\in\mathscr{W}} \frac{(q, v' - \psi \times t)}{\|v\|_1 + \|\psi\|_1} \geq \beta \|q\|_0 \qquad \forall q \in \mathscr{Q}.$$

Property (i) has been proved in [3, Lemma 3.6] for $\widehat{\mathbb{E}}$ being the identity matrix. The extension to $\widehat{\mathbb{E}}$ positive definite uniformly in s is quite straightforward. Property (ii) has been proved in [3, Lemma 3.7]. An alternative simpler proof of an equivalent inf-sup condition appears in [14, Proposition 2].

Therefore, according to [10, Theorem II.1.2], problem (1.6)–(1.7) has a unique solution $(u, \theta, \gamma) \in \mathscr{W} \times \mathscr{Q}$ and this solution satisfies

$$\|u\|_1 + \|\theta\|_1 + \|\gamma\|_0 \leq C \left(\|f\|_0 + d^2 \|\phi\|_0\right). \tag{1.8}$$

Here and thereafter, C denotes a strictly positive constant, not necessarily the same at each occurrence, but always independent of d and of the mesh-size h, which will be introduced in the next section.

Because of the estimate above and the compact embedding $\mathrm{H}^1(\mathrm{I}) \hookrightarrow \mathrm{L}^2(\mathrm{I})$, the operator T is compact. Moreover, by substituting (1.7) into (1.6), from the symmetry of the resulting bilinear forms, it is immediate to show that T is self-adjoint with respect to the 'weighted' $\mathrm{L}^2(\mathrm{I})^3 \times \mathrm{L}^2(\mathrm{I})^3$ inner product in the right-hand side of (1.6). Therefore, apart of $\mu = 0$, the spectrum of T consists of a sequence of finite-multiplicity real eigenvalues converging to zero, all with ascent 1.

Note that λ is a non-zero eigenvalue of problem (1.3) if and only if $\mu := 1/\lambda$ is a non-zero eigenvalue of T, with the same multiplicity and corresponding eigenfunctions. Recall that these eigenvalues are strictly positive (cf. Remark 1.2.4).

Next, we define T_0 by means of the limit problem of (1.6)–(1.7) as $d \to 0$:

$$T_0 : \mathrm{L}^2(\mathrm{I})^3 \times \mathrm{L}^2(\mathrm{I})^3 \longrightarrow \mathrm{L}^2(\mathrm{I})^3 \times \mathrm{L}^2(\mathrm{I})^3,$$

where $T_0(f,\phi) := (u_0,\theta_0) \in \mathscr{W}$ is such that there exists $\gamma_0 \in \mathscr{Q}$ satisfying:

$$\left(\widehat{\mathbb{E}}\theta_0', \psi'\right) + \left(\gamma_0, v' - \psi \times t\right) = \left(\widehat{A}f, v\right) \qquad \forall (v,\psi) \in \mathscr{W}, \tag{1.9}$$

$$u_0' - \theta_0 \times t = 0. \tag{1.10}$$

The above mentioned existence and uniqueness results covers this problem as well.

Our next goal is to prove that T converges to T_0 as d goes to zero. With this purpose, we will use the following a priori estimates for the solutions of problems (1.6)–(1.7) and (1.9)–(1.10), whose proof is based on the same arguments as those used to prove Proposition 3 in [14]: if $f,\phi \in \mathrm{H}^{k-2}(\mathrm{I})^3$, $k \geq 2$, then

$$\|u\|_k + \|\theta\|_k + \|\gamma\|_{k-1} \leq C\left(\|f\|_{k-2} + d^2\|\phi\|_{k-2}\right), \tag{1.11}$$

$$\|u_0\|_k + \|\theta_0\|_k + \|\gamma_0\|_{k-1} \leq C\|f\|_{k-2}. \tag{1.12}$$

In the following lemma and thereafter, $\|\cdot\|_1$ denotes the natural product norm in $\mathscr{W} = \mathscr{V} \times \mathscr{V}$.

Lemma 1.2.1 *There exists a constant $C > 0$, independent of d, such that*

$$\|(T - T_0)(f,\phi)\|_1 \leq Cd\left(\|f\|_0 + d\|\phi\|_0\right) \qquad \forall f,\phi \in \mathrm{L}^2(\mathrm{I})^3.$$

Proof. Given $f,\phi \in \mathrm{L}^2(\mathrm{I})^3$, let $(u,\theta) := T(f,\phi)$ and $(u_0,\theta_0) := T_0(f,\phi)$. Subtracting (1.9) from (1.6) and (1.10) from (1.7), we have

$$\left(\widehat{\mathbb{E}}\left(\theta' - \theta_0'\right), \psi'\right) + \left(\gamma - \gamma_0, v' - \psi \times t\right) = d^2\left(\widehat{\mathbb{J}}\phi, \psi\right) \qquad \forall (v,\psi) \in \mathscr{W}, \tag{1.13}$$

$$\gamma = \frac{1}{d^2}\widehat{\mathbb{D}}\left(u' - u_0' - (\theta - \theta_0) \times t\right). \tag{1.14}$$

Taking $\psi = \theta - \theta_0$ and $v = u - u_0$, we obtain

$$\left(\widehat{\mathbb{E}}\left(\theta' - \theta_0'\right), \theta' - \theta_0'\right) = d^2\left(\widehat{\mathbb{J}}\phi, (\theta - \theta_0)\right) - d^2(\gamma - \gamma_0, \gamma).$$

Using the ellipticity of the bilinear form on the left-hand side, Cauchy-Schwartz inequality, (1.11) and (1.12), we have

$$\begin{aligned}\|\theta - \theta_0\|_1^2 &\leq Cd^2\|\phi\|_0\|\theta - \theta_0\|_0 + Cd^2\left(\|\gamma\|_0 + \|\gamma_0\|_0\right)\|\gamma\|_0 \\ &\leq Cd^2\|\phi\|_0\|\theta - \theta_0\|_0 + Cd^2\left(\|f\|_0 + d^2\|\phi\|_0\right)\|f\|_0,\end{aligned}$$

whence

$$\|\theta-\theta_0\|_1 \leq Cd\left(\|f\|_0+d\,\|\phi\|_0\right). \tag{1.15}$$

On the other hand, observe that from (1.14),

$$u'-u_0' = d^2\widehat{\mathbb{D}}^{-1}\gamma+(\theta-\theta_0)\times t.$$

Hence, using (1.8) and Poincaré inequality, we obtain

$$\|u-u_0\|_1 \leq Cd^2\left(\|f\|_0+d\,\|\phi\|_0\right)+\|\theta-\theta_0\|_0,$$

which together with (1.15) allow us to end the proof. □

As a consequence of this lemma, T converges in norm to T_0 as d goes to zero. Therefore, standard properties of separation of isolated parts of the spectrum (see for instance [32]) yield the following result:

Lemma 1.2.2 *Let $\mu_0>0$ be an eigenvalue of T_0 of multiplicity m. Let D be any disc in the complex plane centered at μ_0 and containing no other element of the spectrum of T_0. Then, for d small enough, D contains exactly m eigenvalues of T (repeated according to their respective multiplicities). Consequently, each eigenvalue $\mu_0>0$ of T_0 is a limit of eigenvalues μ of T, as d goes to zero.*

Moreover, for any compact subset K of the complex plane not intersecting the spectrum of T_0, there exists $d_K>0$ such that for all $d<d_K$, K does not intersect the spectrum of T, either.

1.3 Finite elements discretization

Two different finite element discretizations of the load problem for Timoshenko curved rods have been analyzed in [3] and [14]. The two methods differ in the variables being discretized: the components of vector fields v in the Frenet basis, v_1, v_2 and v_3, are discretized by piecewise polynomial continuous functions in the former, whereas the discretized variable is the vector field $v=v_1t+v_2n+v_3b$ in the latter. We follow the approach from [3].

Consider a family $\{\mathscr{T}_h\}$ of partitions of the interval I:

$$\mathscr{T}_h:\ 0=s_0<s_1<\cdots<s_n=L,$$

with mesh-size

$$h:=\max_{j=1,\ldots,n}\left(s_j-s_{j-1}\right).$$

We define the following finite element subspaces of $\mathscr{V}$ and $\mathscr{Q}$, respectively:

$$\mathscr{V}_h := \left\{ v \in \mathscr{V} : \ v_i|_{[s_{j-1},s_j]} \in \mathscr{P}_r, \ j = 1,\dots,n, \ i = 1,2,3 \right\},$$
$$\mathscr{Q}_h := \left\{ q \in \mathscr{Q} : \ q_i|_{[s_{j-1},s_j]} \in \mathscr{P}_{r-1}, \ j = 1,\dots,n, \ i = 1,2,3 \right\},$$

where v_i, $i = 1,2,3$, are the components of v in the Frenet basis, $\mathscr{P}_k$ are the spaces of polynomials of degree lower than or equal to k, and $r \geq 1$.

Let $\mathscr{W}_h := \mathscr{V}_h \times \mathscr{V}_h$. The following is the discrete vibration problem in mixed form: Find non-trivial $(u_h, \theta_h, \gamma_h) \in \mathscr{W}_h \times \mathscr{Q}_h$ and $\lambda_h \in \mathbb{R}$ such that:

$$\left(\widehat{\mathbb{E}}\theta_h', \psi_h'\right) + \left(\gamma_h, v_h' - \psi_h \times t\right) = \lambda_h \left[\left(\widehat{A}u_h, v_h\right) + d^2 \left(\widehat{\mathbb{J}}\theta_h, \psi_h\right) \right] \qquad \forall (v_h, \psi_h) \in \mathscr{W}_h, \tag{1.16}$$

$$\left(u_h' - \theta_h \times t, q_h\right) - d^2 \left(\widehat{\mathbb{D}}^{-1}\gamma_h, q_h\right) = 0 \qquad \forall q_h \in \mathscr{Q}_h. \tag{1.17}$$

In the same manner as in the continuous case, we introduce the operator

$$T_h : \ \mathrm{L}^2(\mathrm{I})^3 \times \mathrm{L}^2(\mathrm{I})^3 \longrightarrow \mathrm{L}^2(\mathrm{I})^3 \times \mathrm{L}^2(\mathrm{I})^3,$$

defined by $T_h(f,\phi) := (u_h, \theta_h)$, where $(u_h, \theta_h, \gamma_h) \in \mathscr{W}_h \times \mathscr{Q}_h$ is the solution of the associated discrete load problem:

$$\left(\widehat{\mathbb{E}}\theta_h', \psi_h'\right) + \left(\gamma_h, v_h' - \theta_h \times t\right) = \left(\widehat{A}f, v_h\right) + d^2 \left(\widehat{\mathbb{J}}\phi, \psi_h\right) \qquad \forall (v_h, \psi_h) \in \mathscr{W}_h, \tag{1.18}$$

$$\left(u_h' - \theta_h \times t, q_h\right) - d^2 \left(\widehat{\mathbb{D}}^{-1}\gamma_h, q_h\right) = 0 \qquad \forall q_h \in \mathscr{Q}_h. \tag{1.19}$$

This problem falls in the framework of the discrete mixed formulations considered in [10, Section II.2.4]. In order to apply the results from this reference, we have to verify the following classical properties, for h small enough:

i) *ellipticity in the discrete kernel*: $\exists \alpha_* > 0$, independent of h, such that

$$\left(\widehat{\mathbb{E}}\psi_h', \psi_h'\right) \geq \alpha_* \left(\|v_h\|_1^2 + \|\psi_h\|_1^2 \right) \qquad \forall (v_h, \psi_h) \in \mathscr{W}_{0h}, \tag{1.20}$$

where $\mathscr{W}_{0h} := \left\{ (v_h, \psi_h) \in \mathscr{W}_h : \ \left(q_h, v_h' - \psi_h \times t\right) = 0 \quad \forall q_h \in \mathscr{Q}_h \right\}$;

ii) *discrete inf-sup condition*: $\exists \beta_* > 0$, independent of h, such that

$$\sup_{(0,0) \neq (v_h, \psi_h) \in \mathscr{W}_h} \frac{\left(q_h, v_h' - \psi_h \times t\right)}{\|v_h\|_1 + \|\psi_h\|_1} \geq \beta_* \|q_h\|_0 \qquad \forall q_h \in \mathscr{Q}_h.$$

Property (i) has been proved in [3, Lemma 4.2] for $\widehat{\mathbb{E}}$ being the identity matrix and $h > 0$ sufficiently small. The extension to $\widehat{\mathbb{E}}$ positive definite uniformly in s is quite straightforward. Property (ii) has been also proved in [3, Lemma 4.3] by means of a laborious constructive procedure, which is not fully detailed in this reference. In what follows we provide an alternative simpler proof based on the arguments used by [14, Lemma 3, Step (ii)] for the discrete inf-sup condition arising from another discretization.

With this purpose we will use the following lemma, which holds true as far as the rod is not a simple straight beam and whose proof can be found in [14, Lemma 1]:

Lemma 1.3.1 *If $t(s)$ is not a constant vector for all $s \in \mathrm{I}$, then there exists a linear mapping*

$$\begin{aligned} \phi : \mathbb{R}^3 &\longrightarrow \mathscr{C}^1(\mathrm{I},\mathbb{R}^3) \\ x &\longmapsto \phi_x \end{aligned}$$

such that, for any $x \in \mathbb{R}^3$:

$$\phi_x(0) = \phi_x(L) = 0, \tag{1.21}$$

$$\int_0^L \phi_x(s) \times t(s)\, ds = x, \tag{1.22}$$

$$\|\phi_x\|_{\mathscr{C}^1(\mathrm{I},\mathbb{R}^3)} \leq C\,|x|\,. \tag{1.23}$$

Note that the tangent vector t is constant throughout the length of the rod if and only if the rod is actually a straight beam. The finite element scheme is perfectly well fitted in this case too (see the numerical results reported in Sect. 1.4.1 below). However, in such a case, the inf-sup condition in the following lemma must be proved by adapting the arguments used in [1, p. 414]), where a similar condition has been proved in a two-dimensional simpler framework. For a curved rod there holds the following result:

Lemma 1.3.2 *For h small enough, there exists $\beta_* > 0$, independent of h, such that*

$$\sup_{(0,0)\neq(v_h,\psi_h)\in\mathscr{W}_h} \frac{\left(q_h, v_h' - \psi_h \times t\right)}{\|v_h\|_1 + \|\psi_h\|_1} \geq \beta_* \|q_h\|_0 \qquad \forall q_h \in \mathscr{Q}_h.$$

Proof. Given $q_h \in \mathscr{Q}_h$, let $v \in \mathrm{H}^1(\mathrm{I})^3$ be the solution of the following initial value problem:

$$\begin{cases} v' \equiv \dot{v} + \Gamma^{\mathrm{t}} v = q_h & \text{in I}, \\ v(0) = 0. \end{cases}$$

Since $v(0) = 0$, Poincaré inequality leads to $\|v\|_0 \leq C\,\|v'\|_0$. Hence,

$$\|v\|_1 = \left(\|v\|_0^2 + \|\dot{v}\|_0^2\right)^{1/2} \leq C\,\|q_h\|_0\,. \tag{1.24}$$

Let $\widehat{v} := \widehat{v}_1 t + \widehat{v}_2 n + \widehat{v}_3 b$, with

$$\widehat{v}_i(s) := \int_0^s \Pi v_i'(\sigma)\, d\sigma, \qquad 0 \le s \le L, \qquad i = 1,2,3,$$

where v_i are the components of v in the Frenet basis and Π is the $\mathrm{L}^2(\mathrm{I})$-orthogonal projection onto

$$\mathscr{Q}_h := \left\{ q \in \mathrm{L}^2(\mathrm{I}) :\ q|_{[s_{j-1},s_j]} \in \mathscr{P}_{r-1},\ j = 1,\dots,n \right\}.$$

Clearly $\widehat{v}_i' = \Pi v_i'$ and $\widehat{v}_i(0) = 0$, so that, from Poincaré inequality, the boundedness of Π and (1.24),

$$\|\widehat{v}\|_1 \le C \left(\sum_{i=1}^3 \left\| \Pi v_i' \right\|_0^2 \right)^{1/2} \le C \left(\sum_{i=1}^3 \left\| v_i' \right\|_0^2 \right)^{1/2} \le C \|q_h\|_0 . \tag{1.25}$$

Now, for all points s_j of the partition $\mathscr{T}_h$, there holds

$$\widehat{v}_i(s_j) - v_i(s_j) = \int_0^{s_j} \left[\Pi v_i'(\sigma) - v_i'(\sigma) \right] d\sigma = 0,$$

because the characteristic function of the interval $[0, s_j]$ belongs to $\mathscr{Q}_h$. Therefore, from Cauchy-Schwartz inequality, we have for all $s \in [s_j, s_{j+1}]$,

$$|\widehat{v}_i(s) - v_i(s)|^2 = \left| \int_{s_j}^s \left[\Pi v_i'(\sigma) - v_i'(\sigma) \right] d\sigma \right|^2 \le |s - s_j| \int_{s_j}^{s_{j+1}} \left| \Pi v_i'(\sigma) - v_i'(\sigma) \right|^2 d\sigma.$$

By integrating on $[s_j, s_{j+1}]$ and summing up for $j = 0, \dots, n-1$, we obtain

$$\|\widehat{v}_i - v_i\|_0^2 \le \frac{h^2}{2} \left\| \Pi v_i' - v_i' \right\|_0^2 \le h^2 \left\| v_i' \right\|_0^2,$$

which together with (1.24) yield

$$\|\widehat{v} - v\|_0 \le h \|\dot{v}\|_0 \le Ch \|q_h\|_0 . \tag{1.26}$$

On the other hand, since $\widehat{v}_i' = \Pi v_i'$ and the components of q_h belong to $\mathscr{Q}_h$, according to the definition (1.1) of $\dot{v}$ and $\dot{\widehat{v}}$, there holds

$$\left(q_h, \dot{\widehat{v}}\right) = \left(q_h, \dot{v}\right) = \left(q_h, v'\right) - \left(q_h, \Gamma^{\mathrm{t}} v\right),$$

which together with the definition of v lead to

$$\left(q_h, \widehat{v}'\right) = \left(q_h, \dot{\widehat{v}}\right) + \left(q_h, \Gamma^{\mathrm{t}} \widehat{v}\right) = \left(q_h, v'\right) + \left(q_h, \Gamma^{\mathrm{t}} (\widehat{v} - v)\right) = \|q_h\|_0^2 + \left(q_h, \Gamma^{\mathrm{t}} (\widehat{v} - v)\right).$$

Thus, from (1.26), we obtain

$$\left(q_h, \widehat{\nu}'\right) \geq (1-Ch)\,\|q_h\|_0^2. \tag{1.27}$$

According to its definition, $\widehat{\nu}_i$ are piecewise $\mathscr{P}_r$ continuous functions vanishing at $s=0$. However, in general, $\widehat{\nu}(L) \neq 0$, so that $\widehat{\nu} \notin \mathscr{V}_h$. Because of this, we resort to Lemma 1.3.1.

Let $x := -\widehat{\nu}(L)$ and ϕ_x be as in Lemma 1.3.1. From (1.23) and (1.25), there holds

$$\|\phi_x\|_1 \leq C\,\|\phi_x\|_{\mathscr{C}^1(\mathrm{I},\mathbb{R}^3)} \leq C\,|x| \leq C\,\|\widehat{\nu}\|_1 \leq C\,\|q_h\|_0.$$

Let

$$w(s) := \int_0^s \phi_x(\sigma) \times t(\sigma)\,d\sigma, \qquad 0 \leq s \leq L.$$

Clearly, $w(0)=0$ and $w' = \phi_x \times t$. Hence, from Poincaré inequality,

$$\|w\|_1 \leq C\left\|w'\right\|_0 \leq C\,\|\phi_x\|_0 \leq C\,\|q_h\|_0.$$

Let ϕ_x^{I} and w^{I} be the vector fields whose components in the Frenet basis are the Lagrange interpolants of degree r of the respective components of ϕ_x and w in the same basis. Standard properties of the one-dimensional Lagrange interpolant yield

$$\left\|\phi_x^{\mathrm{I}}\right\|_1 \leq C\,\|\phi_x\|_1 \leq C\,\|q_h\|_0 \qquad \text{and} \qquad \left\|w^{\mathrm{I}}\right\|_1 \leq C\,\|w\|_1 \leq C\,\|q_h\|_0, \tag{1.28}$$

as well as

$$\begin{aligned}
&\left\|\phi_x - \phi_x^{\mathrm{I}}\right\|_0 \leq Ch\left\|\dot{\phi}_x\right\|_0 \leq Ch\,\|q_h\|_0,\\
&\left\|\left(w^{\mathrm{I}} - w\right)'\right\|_0 \leq \left\|\left(w^{\mathrm{I}} - w\right)^{\cdot}\right\|_0 + \left\|\Gamma^{\mathrm{t}}\left(w^{\mathrm{I}} - w\right)\right\|_0 \leq Ch\left(\|\ddot{w}\|_0 + \|\dot{w}\|_0\right) \leq Ch\,\|q_h\|_0,
\end{aligned}$$

the latter because $\ddot{w} = (w' - \Gamma^{\mathrm{t}} w)^{\cdot} = (\phi_x \times t)^{\cdot} - (\Gamma^{\mathrm{t}} w)^{\cdot}$ and, consequently, we have that $\|\ddot{w}\|_0 \leq C\left(\|\phi_x\|_1 + \|w\|_1\right)$. Therefore,

$$\left|\left(q_h, \left(w^{\mathrm{I}}\right)' - \phi_x^{\mathrm{I}} \times t\right)\right| = \left|\left(q_h, \left(w^{\mathrm{I}} - w\right)'\right) + \left(q_h, \left(\phi_x - \phi_x^{\mathrm{I}}\right) \times t\right)\right| \leq Ch\,\|q_h\|_0^2. \tag{1.29}$$

Finally, let $v_h := \widehat{\nu} + w^{\mathrm{I}}$ and $\psi_h := \phi_x^{\mathrm{I}}$. Because of (1.21) and (1.22), both belong to $\mathscr{W}_h$. From (1.25) and (1.28), there holds

$$\|v_h\|_1 + \|\psi_h\|_1 \leq C\,\|q_h\|_0,$$

whereas from (1.27) and (1.29),

$$\left(q_h, v_h' - \psi_h \times t\right) \geq (1-Ch)\,\|q_h\|_0^2.$$

The last two inequalities allow us to conclude the lemma. □

Now we are in a position to prove that T_h is well defined and converges to T as $h \to 0$:

Theorem 1.3.1 *For sufficiently small $h>0$, problem (1.18)–(1.19) has a unique solution $(u_h,\theta_h,\gamma_h)\in\mathscr{W}_h\times\mathscr{Q}_h$. This solution satisfies*

$$\|u_h\|_1+\|\theta_h\|_1+\|\gamma_h\|_0\leq C\left(\|f\|_0+d^2\,\|\phi\|_0\right), \tag{1.30}$$

where $C>0$ is independent of h and d.

Let $(u,\theta,\gamma)\in\mathscr{W}\times\mathscr{Q}$ be the solution of problem (1.6)–(1.7). If $f,\phi\in H^{k-1}(\mathrm{I})^3$, $1\leq k\leq r$, then

$$\|u-u_h\|_1+\|\theta-\theta_h\|_1+\|\gamma-\gamma_h\|_0\leq Ch^k\left(\|f\|_{k-1}+d^2\,\|\phi\|_{k-1}\right), \tag{1.31}$$

$$\|u-u_h\|_0+\|\theta-\theta_h\|_0\leq Ch^{k+1}\left(\|f\|_{k-1}+d^2\,\|\phi\|_{k-1}\right), \tag{1.32}$$

with $C>0$ independent of h and d.

Proof. By virtue of (1.20) and Lemma 1.3.2, the well posedness of problem (1.18)–(1.19) as well as the error estimate (1.31) are consequences of Proposition II.2.11 from [10]. On the other hand, (1.32) is obtained by adapting to our case the duality argument used to prove Theorem 2 from [14]. □

By adding (1.18) and (1.19), from the symmetry of the resulting bilinear forms, it is immediate to show that T_h is self-adjoint with respect to the 'weighted' $\mathrm{L}^2(\mathrm{I})^3\times\mathrm{L}^2(\mathrm{I})^3$ inner product in the right-hand side of (1.18). Therefore, apart of $\mu_h=0$, the spectrum of T_h consists of a finite number of finite-multiplicity real eigenvalues with ascent 1.

Once more the spectrum of the operator T_h is related with the eigenvalues of the spectral problem (1.16)–(1.17): λ_h is a non-zero eigenvalue of this problem if and only if $\mu_h:=1/\lambda_h$ is a non-zero eigenvalue of T_h, with the same multiplicity and corresponding eigenfunctions. These eigenvalues are strictly positive. Indeed, by taking $v_h=u_h$, $\psi_h=\theta_h$ and $q_h=\gamma_h$ in problem (1.16)–(1.17), by subtracting the second equation from the first one, we have

$$\lambda_h=\frac{\left(\widehat{\mathbb{E}}\theta_h',\theta_h'\right)+d^2\left(\widehat{\mathbb{D}}^{-1}\gamma_h,\gamma_h\right)}{\left(\widehat{A}u_h,u_h\right)+d^2\left(\widehat{\mathbb{J}}\theta_h,\theta_h\right)}\geq 0.$$

Moreover, the eigenvalues cannot vanish. In fact, according to the expression above, since $\widehat{\mathbb{E}}$ and $\widehat{\mathbb{D}}$ are positive definite (see Remark 1.2.3), $\lambda_h=0$ would imply $\gamma_h=0$. Then, (1.17) would imply that $(u_h,\theta_h)\in\mathscr{W}_{0h}$ and, hence, u_h and θ_h would vanish too because of (1.20).

Our aim is to use the spectral theory for compact operators (see [6], for instance) to prove convergence of the eigenvalues and eigenfunctions of T_h towards those of T. However, some further considerations will be needed to show that the error estimates do not deteriorate as d becomes small. With this purpose, we will use the following result:

$$\|(T-T_h)(f,\phi)\|_1\leq Ch\left(\|f\|_0+d^2\,\|\phi\|_0\right), \tag{1.33}$$

which follows from (1.31) with $k = 1$. As a consequence of this estimate, T_h converges in norm to T as h goes to zero. Hence, standard results of spectral approximation (see for instance [32]) show that if μ is an eigenvalue of T with multiplicity m, then exactly m eigenvalues $\mu_h^{(1)}, \ldots, \mu_h^{(m)}$ of T_h (repeated according to their respective multiplicities) converge to μ.

The estimate above can be improved when the source term is an eigenfunction (u, θ) of T. Indeed, in such a case, the same arguments used to prove (1.11) allow us to show that, for all $k \geq 2$ and d sufficiently small, there holds

$$\|u\|_k + \|\theta\|_k + \|\gamma\|_{k-1} \leq C \left(\|u\|_0 + d^2 \|\theta\|_0 \right), \tag{1.34}$$

with C depending on k and on the eigenvalue of T associated with (u, θ). Note that in principle the constant C should depend also on d, because the eigenvalue does it. However, according to Lemma 1.2.2, for d sufficiently small we can choose C independent of d. Hence, from (1.31)–(1.32) with $k = r$, we obtain:

$$\|(T - T_h)(u, \theta)\|_1 \leq C h^r \|(u, \theta)\|_1, \tag{1.35}$$

$$\|(T - T_h)(u, \theta)\|_0 \leq C h^{r+1} \|(u, \theta)\|_0. \tag{1.36}$$

Here and thereafter, $\|\cdot\|_0$ denotes the standard product norm in $\mathrm{L}^2(\mathrm{I})^3 \times \mathrm{L}^2(\mathrm{I})^3$.

We remind the definition of the *gap* or symmetric distance $\widehat{\delta}_k$ between closed subspaces $\mathscr{Y}$ and $\mathscr{Z}$ of $\mathscr{W}$ in norm $\|\cdot\|_k$, $k = 0, 1$:

$$\widehat{\delta}_k(\mathscr{Y}, \mathscr{Z}) := \max \{ \delta_k(\mathscr{Y}, \mathscr{Z}), \delta_k(\mathscr{Z}, \mathscr{Y}) \},$$

with

$$\delta_k(\mathscr{Y}, \mathscr{Z}) := \sup_{\substack{(\nu, \psi) \in \mathscr{Y} \\ \|(\nu, \psi)\|_k = 1}} \left[\inf_{(\widehat{\nu}, \widehat{\psi}) \in \mathscr{Z}} \|(\nu - \widehat{\nu}, \psi - \widehat{\psi})\|_k \right].$$

For the sake of simplicity we state our results for eigenvalues of T converging to a simple eigenvalue of T_0 as $d \to 0$ (at the end of this section we will discuss this assumption). The following theorem yields d-independent error estimates for the approximate eigenvalues and eigenfunctions.

Theorem 1.3.2 *Let μ be an eigenvalue of T converging to a simple eigenvalue μ_0 of T_0 as d tends to zero, Let μ_h be the eigenvalue of T_h that converges to μ as h tends to zero. Let $\mathscr{E}$ and $\mathscr{E}_h$ be the corresponding eigenspaces. Then, for d and h small enough,*

$$\widehat{\delta}_1(\mathscr{E}, \mathscr{E}_h) \leq C h^r, \tag{1.37}$$

$$\widehat{\delta}_0(\mathscr{E}, \mathscr{E}_h) \leq C h^{r+1}, \tag{1.38}$$

$$|\mu - \mu_h| \leq C h^r, \tag{1.39}$$

with $C > 0$ independent of d and h.

Proof. The estimates are direct consequences of (1.35)–(1.36) and Theorems 7.1 and 7.2 from [6], in all cases with C depending on the constants in (1.35)–(1.36) and on the inverse of the distance from μ to the rest of the spectrum of T. Now, using Lemma 1.2.2, we have that for d small enough this distance is bounded below in terms of the distance from μ_0 to the rest of the spectrum of T_0, which obviously depends neither on d nor on h. This allows us to conclude the proof. □

This theorem yields optimal order error estimates for the approximate eigenfunctions in norms $\|\cdot\|_1$ and $\|\cdot\|_0$. In fact, the theorem implies that the eigenfunctions (u,θ) of T and (u_h,θ_h) of T_h, corresponding to the eigenvalues μ and μ_h, respectively, can be chosen normalized in $\|\cdot\|_k$, $k=0,1$, and so that:

$$\|u-u_h\|_1+\|\theta-\theta_h\|_1\le Ch^r \qquad (k=1), \tag{1.40}$$

$$\|u-u_h\|_0+\|\theta-\theta_h\|_0\le Ch^{r+1} \qquad (k=0), \tag{1.41}$$

which are the optimal orders for the finite elements used. Instead, the order of the error estimate (1.39) is not optimal. To improve this result, we will have to study first the convergence of the shear stresses of the vibration modes:

Lemma 1.3.3 *Let μ and μ_h be as in Theorem 1.3.2. Let (u,θ,γ) be a solution of problem (1.4)–(1.5) with $\lambda=\frac{1}{\mu}$, and (u_h,θ_h,γ_h) a solution of problem (1.16)–(1.17) with $\lambda_h=\frac{1}{\mu_h}$, such that $\|(u,\theta)\|_1=\|(u_h,\theta_h)\|_1=1$ and (1.40) holds true. Then, for d and h small enough,*

$$\|\gamma-\gamma_h\|_0\le Ch^r,$$

with $C>0$ independent of d and h.

Proof. From (1.16) and (1.4) we have $\forall\,(v_h,\psi_h)\in\mathscr{W}_h$,

$$\begin{aligned}\left(\gamma-\gamma_h,v_h'-\psi_h\times t\right)&=\lambda\left[\left(\widehat{A}\left(u-u_h\right),v_h\right)+d^2\left(\widehat{\mathbb{J}}\left(\theta-\theta_h\right),\psi_h\right)\right]\\&\quad+(\lambda-\lambda_h)\left[\left(\widehat{A}u_h,v_h\right)+d^2\left(\widehat{\mathbb{J}}\theta_h,\psi_h\right)\right]-\left(\widehat{\mathbb{E}}\left(\theta'-\theta_h'\right),\psi_h'\right)\\&\le Ch^r\left(\|v_h\|_1+\|\psi_h\|_1\right),\end{aligned}$$

where we have used (1.39) and (1.40) for the last inequality. Note that the constant C depends on the eigenvalue λ, but not on d or h, for d small enough (Lemma 1.2.2). Using this estimate, we have $\forall\widehat{\gamma}\in\mathscr{Q}_h$ and $\forall\,(v_h,\psi_h)\in\mathscr{W}_h$,

$$\left(\widehat{\gamma}-\gamma_h,v_h'-\psi_h\times t\right)\le\left(\widehat{\gamma}-\gamma,v_h'-\psi_h\times t\right)+Ch^r\left(\|v_h\|_1+\|\psi_h\|_1\right).$$

Therefore, from Lemma 1.3.2, we have $\forall\widehat{\gamma}\in\mathscr{Q}_h$

$$\beta_*\|\widehat{\gamma}-\gamma_h\|_0\le\sup_{(0,0)\neq(v_h,\psi_h)\in\mathscr{W}_h}\frac{\left(\widehat{\gamma}-\gamma_h,v_h'-\psi_h\times t\right)}{\|v_h\|_1+\|\psi_h\|_1}\le C\left(\|\widehat{\gamma}-\gamma\|_0+h^r\right).$$

Hence, by choosing $\widehat{\gamma}$ as the $\mathrm{L}^2(\mathrm{I})^3$-projection of γ onto $\mathscr{Q}_h$, the theorem follows from the triangular inequality, standard error estimates of the projection, and (1.34). □

Now we are in a position to prove an optimal order of convergence for the approximate eigenvalues by adapting to our problem a standard argument for variationally posed eigenvalue problems (see [6, Lemma 9.1], for instance).

Theorem 1.3.3 *Let $\lambda = \frac{1}{\mu}$ and $\lambda_h = \frac{1}{\mu_h}$, with μ and μ_h as in Theorem 1.3.2. Then, for d and h small enough,*

$$|\lambda - \lambda_h| \leq Ch^{2r}, \tag{1.42}$$

with $C > 0$ independent of d and h.

Proof. Let $\mathscr{A}_d$ and $\mathscr{B}_d$ denote the symmetric and continuous bilinear forms defined in $\mathscr{W} \times \mathscr{Q}$ by:

$$\mathscr{A}_d\left((u,\theta,\gamma),(v,\psi,q)\right) := \left(\widehat{\mathbb{E}}\theta', \psi'\right) + \left(\gamma, v' - \psi \times t\right) + \left(u' - \theta \times t, q\right) - d^2\left(\widehat{\mathbb{D}}^{-1}\gamma, q\right),$$
$$\mathscr{B}_d\left((u,\theta,\gamma),(v,\psi,q)\right) := \left(\widehat{A}u, v\right) + d^2\left(\widehat{\mathbb{J}}\theta, \psi\right).$$

Using this notation, problems (1.4)–(1.5) and (1.16)–(1.17) are respectively written as follows:

$$\mathscr{A}_d\left((u,\theta,\gamma),(v,\psi,q)\right) = \lambda\mathscr{B}_d\left((u,\theta,\gamma),(v,\psi,q)\right) \qquad \forall (v,\psi) \in \mathscr{W} \quad \forall q \in \mathscr{Q};$$
$$\mathscr{A}_d\left((u_h,\theta_h,\gamma_h),(v_h,\psi_h,q_h)\right) = \lambda_h\mathscr{B}_d\left((u_h,\theta_h,\gamma_h),(v_h,\psi_h,q_h)\right)$$
$$\forall (v_h,\psi_h) \in \mathscr{W}_h \qquad \forall q_h \in \mathscr{Q}_h.$$

Consider eigenfunctions satisfying $\|(u,\theta)\|_1 = \|(u_h,\theta_h)\|_1 = 1$ and (1.40).

From the symmetry of the bilinear forms, straightforward computations lead to

$$\begin{aligned}(\lambda - \lambda_h)&\mathscr{B}_d\left((u_h,\theta_h,\gamma_h),(u_h,\theta_h,\gamma_h)\right)\\ &= \lambda\mathscr{B}_d\left((u-u_h,\theta-\theta_h,\gamma-\gamma_h),(u-u_h,\theta-\theta_h,\gamma-\gamma_h)\right)\\ &\quad - \mathscr{A}_d\left((u-u_h,\theta-\theta_h,\gamma-\gamma_h),(u-u_h,\theta-\theta_h,\gamma-\gamma_h)\right).\end{aligned}$$

By using (1.30) with $f = \lambda_h u_h$ and $\phi = \lambda_h\theta_h$, we have that

$$\mathscr{B}_d\left((u_h,\theta_h,\gamma_h),(u_h,\theta_h,\gamma_h)\right) \geq C\left(\|u_h\|_0^2 + d^2\|\theta_h\|_0^2\right) \geq \frac{C}{\lambda_h^2}\left(\|u_h\|_1^2 + \|\theta_h\|_1^2\right) = \frac{C}{\lambda_h^2}.$$

Hence, from the continuity of the bilinear forms, we obtain

$$|\lambda - \lambda_h| \leq C\left(\|u-u_h\|_1 + \|\theta-\theta_h\|_1 + \|\gamma-\gamma_h\|_0\right)^2,$$

with C depending on λ and λ_h, but neither on d nor on h, for d and h sufficiently small (Lemma 1.2.2 and (1.39)). Thus, (1.40) and Lemma 1.3.3 allow us to conclude the proof. □

The last three theorems have been settled for eigenvalues of T converging to simple eigenvalues of T_0 as $d \to 0$. A multiple eigenvalue of T_0 usually arises because of symmetries in the geometry of the rod; in such a case, the eigenvalue of T converging to it has the same multiplicity. The proofs of these theorems extend trivially to cover this case.

Instead, if T_0 had a multiple eigenvalue not due to symmetry reasons, it could split into different eigenvalues of T. In this case, the proofs of the theorems above do not provide estimates independent of the thickness. In fact, the constants therein might in principle blow up as the distance between the eigenvalues becomes smaller.

However, by combining Lemma 1.2.1 and (1.33) we have that

$$\|(T_h - T_0)(f,\phi)\|_1 \leq C(d+h)\left(\|f\|_0 + d^2\|\phi\|_0\right) \qquad \forall f,\phi \in \mathrm{L}^2(\mathrm{I})^3.$$

This estimate can be used to prove spectral convergence as d and h both converge to zero. In fact, if μ_0 is an eigenvalue of T_0 with multiplicity m, then there exist exactly m eigenvalues $\mu_h^{(1)}, \ldots, \mu_h^{(m)}$ of T_h (repeated according to their respective multiplicities) converging to μ_0 as d and h go to zero (see again [32]). Let $\mathscr{E}_0$ be the eigenspace of T_0 corresponding to μ_0 and $\mathscr{E}_h$ be the direct sum of the eigenspaces of T_h corresponding to $\mu_h^{(1)}, \ldots, \mu_h^{(m)}$. Then, by proceeding as in the proof of Theorem 1.3.2, we obtain

$$\widehat{\delta}_1(\mathscr{E}_0, \mathscr{E}_h) \leq C(d+h^r),$$
$$\widehat{\delta}_0(\mathscr{E}_0, \mathscr{E}_h) \leq C\left(d+h^{r+1}\right).$$

Moreover, the arguments in the proofs of Lemma 1.3.3 and Theorem 1.3.3 can be easily adapted to take into account some additional $\mathscr{O}(d^2)$ terms, leading to similar results. In particular, the following estimate holds true for $\lambda_0 = \frac{1}{\mu_0}$ and $\lambda_h^{(j)} = \frac{1}{\mu_h^{(j)}}$:

$$\left|\lambda_0 - \lambda_h^{(j)}\right| \leq C\left(d^2 + h^{2r}\right), \qquad j = 1, \ldots, m.$$

1.4 Numerical results

We report in this section the results of some numerical tests computed with a MATLAB code implementing the finite element method described above. We have used the lowest possible order: $r = 1$; namely, piecewise linear continuous elements for the displacements u_h and the rotations θ_h, and piecewise constant discontinuous elements for the shear stresses γ_h.

We have computed the vibration modes with lowest frequencies $\omega^h := \sqrt{\lambda_h}$ for straight, circular and helical rods, with different sections, thickness and boundary conditions. To help identifying the different modes, we report two-dimensional plots of the computed components of displacements and rotations in the Frenet basis, as well as the three-dimensional deformed rods. For the latter, we have used MODULEF to create an auxiliary hexahedral mesh of the actual three-dimensional rod and the displacements at each node of this auxiliary mesh have been computed from u_h and θ_h as described in Remark 1.2.2. The resulting deformed rods have been plotted with MODULEF, too.

In all cases we have computed the lowest vibration frequencies $\omega_1^h < \omega_2^h < \omega_3^h < \cdots$ by using uniform meshes of N elements, with different values of N. Also in all cases, we have used the following physical parameters, which correspond to steel:

- elastic moduli: $E = 2.1 \times 10^6\,\mathrm{kgf/cm^2}$ ($1\,\mathrm{kgf} = 980\,\mathrm{kg\,cm/s^2}$);
- Poisson coefficient: $\nu = 0.3 \quad (G = E/[2(1+\nu)])$;
- density: $\rho = 7.85 \times 10^{-3}\,\mathrm{kg/cm^3}$;
- correction factors: $k_1 = k_2 = 1$.

1.4.1 Test 1: a straight beam

The aim of this first test is to validate the computer code by solving a problem with known analytical solution. With this purpose, we have computed the vibration modes of a beam (i.e., a straight rod, which corresponds to $\kappa = \tau = 0$). We have taken the beam clamped at both ends, with a total length $L = 120\,\mathrm{cm}$, and a square cross section of side-length $b = 20\,\mathrm{cm}$. Therefore, the non-dimensional thickness parameter is in this case $d = 0.068$. Figure 1.2 shows the undeformed beam.

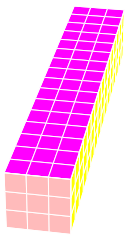

Figure 1.2: Undeformed straight beam.

To estimate the order of convergence of the method, we have compared the computed vibration frequencies with the closed form solution given in [29] for the flexural modes.

The analytical solution of the torsional and axial modes have been obtained by means of straightforward algebraic manipulations.

Table 1.1 shows the lowest vibration frequencies computed on successively refined meshes. It also includes the computed orders of convergence and the corresponding exact vibration frequencies ω_{ex}. Finally "d" and "s" point out if the vibration frequencies correspond to double or simple eigenvalues, respectively.

Table 1.1: Angular vibration frequencies of a straight beam

Mode	$N = 16$	$N = 32$	$N = 64$	$N = 128$	order	ω_{ex}	d/s
ω_1^h	4034.05	4005.16	3997.99	3996.20	2.00	3995.61	d
ω_2^h	8326.58	8316.57	8314.06	8313.44	2.00	8313.22	s
ω_3^h	9818.49	9656.86	9617.04	9607.11	2.01	9603.80	d
ω_4^h	13426.22	13410.07	13406.03	13405.03	2.00	13404.69	s
ω_5^h	17101.68	16639.02	16525.57	16497.37	2.01	16487.94	d
ω_6^h	16733.53	16653.17	16633.13	16628.13	2.00	16626.47	s

Figures 1.3–1.5 show the lowest-frequency vibration modes. Those corresponding to the frequencies ω_1 and ω_3 are flexural modes, whereas that corresponding to the frequency ω_2 is torsional. For each mode, the figures show the components in the Frenet basis of the displacements, u, and the rotations, θ, as well as the deformed beam.

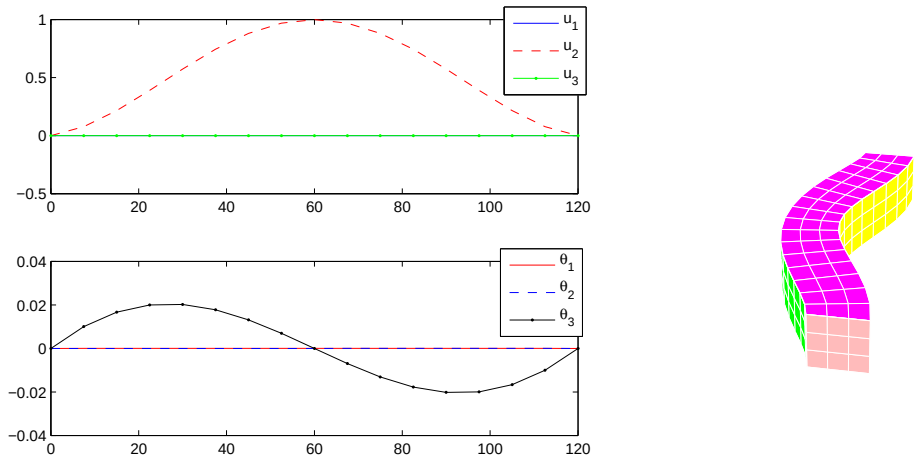

Figure 1.3: Straight beam. Vibration mode of frequency ω_1. Displacements and rotations (left). Deformed beam (right).

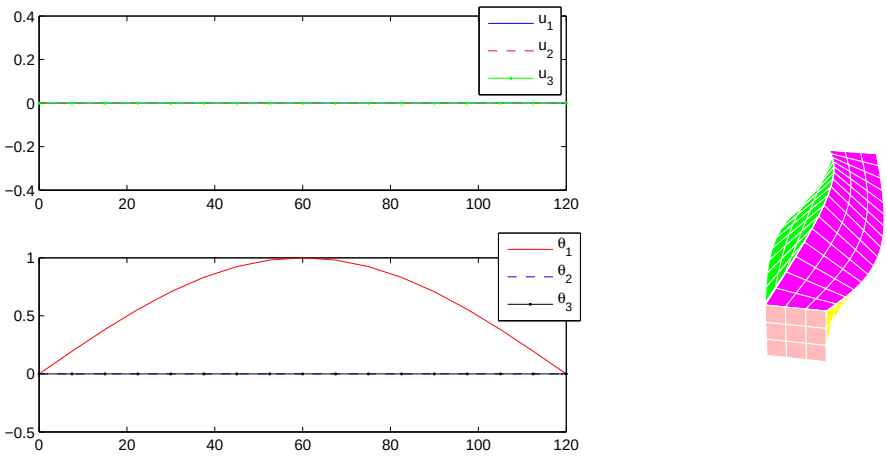

Figure 1.4: Straight beam. Vibration mode of frequency ω_2. Displacements and rotations (left). Deformed beam (right).

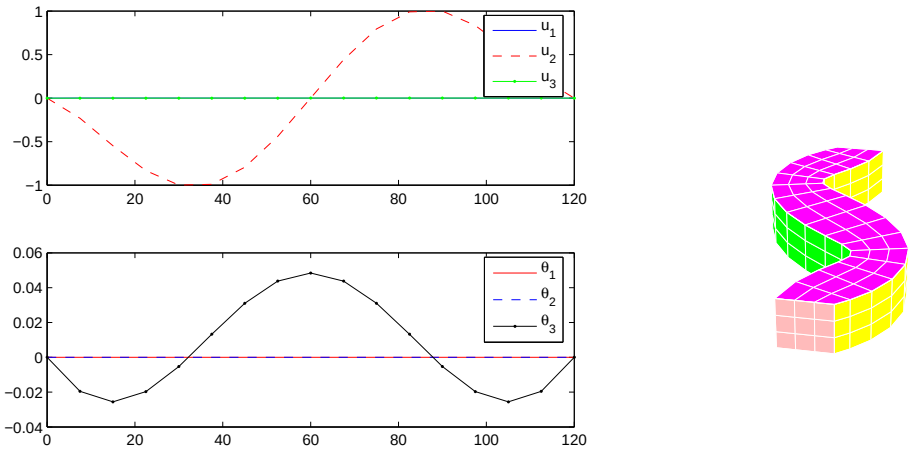

Figure 1.5: Straight beam. Vibration mode of frequency ω_3. Displacements and rotations (left). Deformed beam (right).

As indicated in Table 1.1, ω_1 and ω_3 correspond to double-multiplicity eigenvalues. The planar vibration modes shown in Figs. 1.3 and 1.5 only involve deformations in the plane spanned by t and n. The eigenspaces of each of these eigenvalues also contain other planar vibration modes involving deformations in the plane spanned by t and b. They are not shown because they are exactly the same as those in Figs. 1.3 and 1.5 rotated 90

degrees with respect to the axis t.

1.4.2 Test 2: a helical rod

The aim of this test is to apply the finite element method to a more general curved non-planar rod with non-vanishing curvature and torsion. We have considered a helix with eight turns, clamped at both ends. The equation of the helix centroids line parametrized by its arc-length is as follows:

$$r(s) = \left(A\cos\frac{s}{n}, A\sin\frac{s}{n}, C\frac{s}{n}\right), \qquad \text{with} \quad n = \sqrt{A^2 + C^2}; \tag{1.43}$$

the curvature is $\kappa = A/n^2$, the torsion $\tau = C/n^2$, and the length of the eight-turns helix is $L = 8 \times 2\pi n$. We have taken $A = 100\,\text{cm}$, $C = 25/\pi\,\text{cm}$ and a square of side-length $b = 20\,\text{cm}$ as the cross section of the rod. Thus, the thickness parameter is in this case $d = 0.0016$. Figure 1.6 shows the undeformed helix.

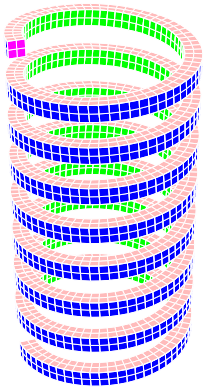

Figure 1.6: Undeformed helical rod.

Since no analytical solution is available for this rod, we have estimated the order of convergence by means of a least squares fitting of the model

$$\omega_j^h \approx \omega_{\text{ex}} + Ch^t.$$

Table 1.2 shows the lowest vibration frequencies computed on successively refined meshes. It also includes the computed orders of convergence t and the 'exact' vibration frequencies ω_{ex}, obtained with this fitting.

Table 1.2: Angular vibration frequencies of a helical rod

Mode	$N = 1024$	$N = 2048$	$N = 3072$	$N = 4096$	order	ω_{ex}
ω_1^h	15.9146	15.9104	15.9096	15.9094	1.97	15.9090
ω_2^h	18.2507	18.2497	18.2495	18.2494	1.94	18.2493
ω_3^h	19.0345	18.9807	18.9707	18.9672	1.99	18.9626
ω_4^h	19.2888	19.2359	19.2260	19.2226	1.99	19.2181
ω_5^h	31.4845	31.4813	31.4807	31.4805	1.97	31.4802
ω_6^h	35.5888	35.4752	35.4540	35.4466	1.99	35.4369

Figures 1.7–1.9 show the lowest-frequency vibration modes. The first one is a typical spring mode, the second one is an extensional mode, and the third one is a kind of 'phone rope' vibration mode.

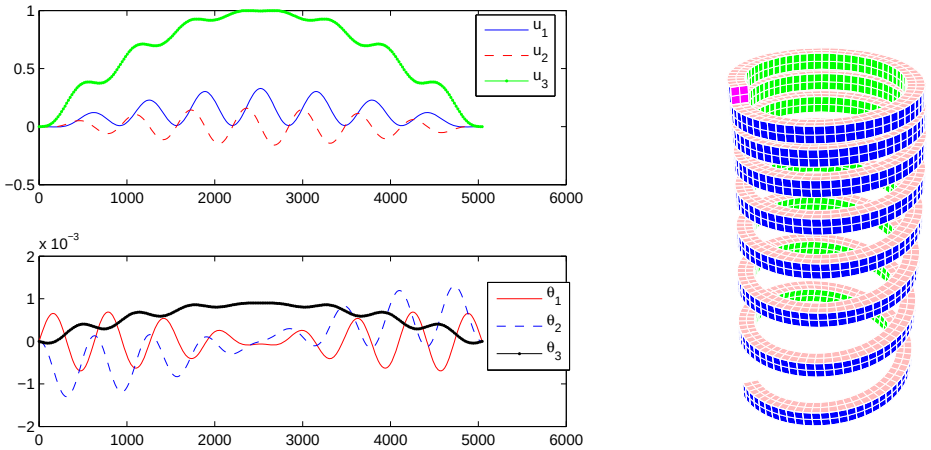

Figure 1.7: Helical rod. Vibration mode of frequency ω_1. Displacements and rotations (left). Deformed helix (right).

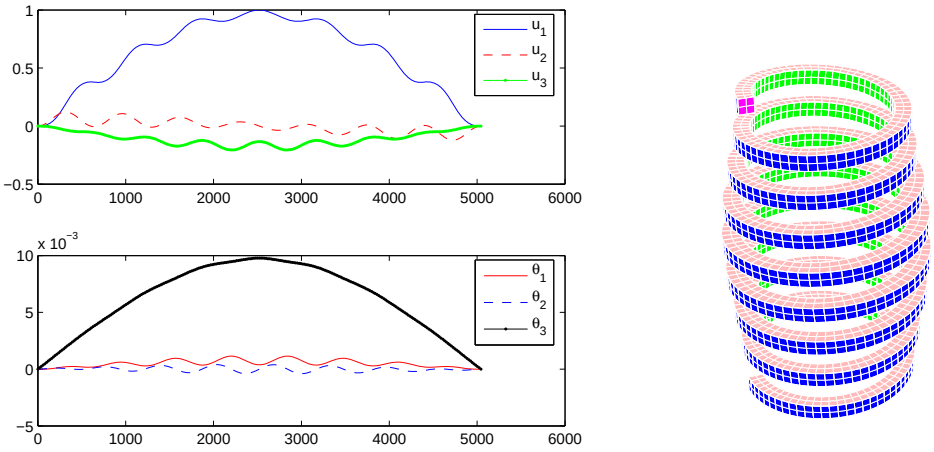

Figure 1.8: Helical rod. Vibration mode of frequency ω_2. Displacements and rotations (left). Deformed helix (right).

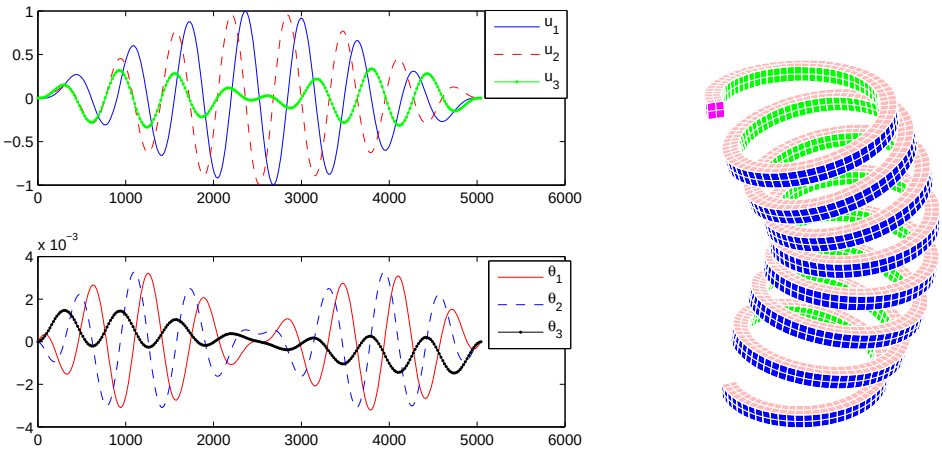

Figure 1.9: Helical rod. Vibration mode of frequency ω_3. Displacements and rotations (left). Deformed helix (right).

1.4.3 Test 3: a rod with principal axes not coinciding with the Frenet basis

The aim of this test is to apply the finite element method to a rod in which the Frenet basis is not a set of principal axes, so that the off-diagonal term of the inertia matrix I_{nb}

does not vanish (see Remark 1.2.1). With this purpose, we have considered a semicircular rod clamped at both ends, with radius of the centroids line $R = 50$ cm (curvature: $\kappa = 1/R$; torsion: $\tau = 0$; length: $L = \pi R$). The cross section of the rod is the parallelogram S shown in Fig. 1.10. In this case $d = 0.025$.

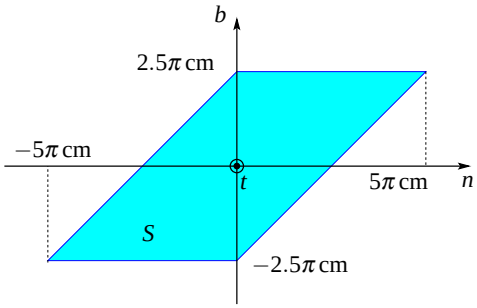

Figure 1.10: Cross-section of the semicircular rod.

Figure 1.11 shows the undeformed rod, seen from two different observation points.

Figure 1.11: Undeformed semicircular rod seen from two observation points.

Table 1.3 shows the lowest vibration frequencies computed on successively refined meshes. It also includes the computed orders of convergence and the 'exact' vibration frequencies ω_{ex}, obtained again by a least squares fitting.

Figures 1.12 and 1.13 show the lowest-frequency vibration modes.

Table 1.3: Angular vibration frequencies of a semicircular rod

Mode	$N = 32$	$N = 64$	$N = 128$	$N = 256$	order	ω_{ex}
ω_1^h	836.09	832.71	831.84	831.65	2.00	831.55
ω_2^h	1446.95	1435.02	1432.05	1431.29	2.01	1431.07
ω_3^h	3065.13	3024.53	3014.48	3011.97	2.01	3011.16
ω_4^h	3186.88	3164.30	3158.70	3157.29	2.01	3156.85
ω_5^h	5359.50	5252.03	5225.64	5219.10	2.02	5216.94
ω_6^h	6072.41	6011.77	5996.62	5992.80	2.00	5991.55

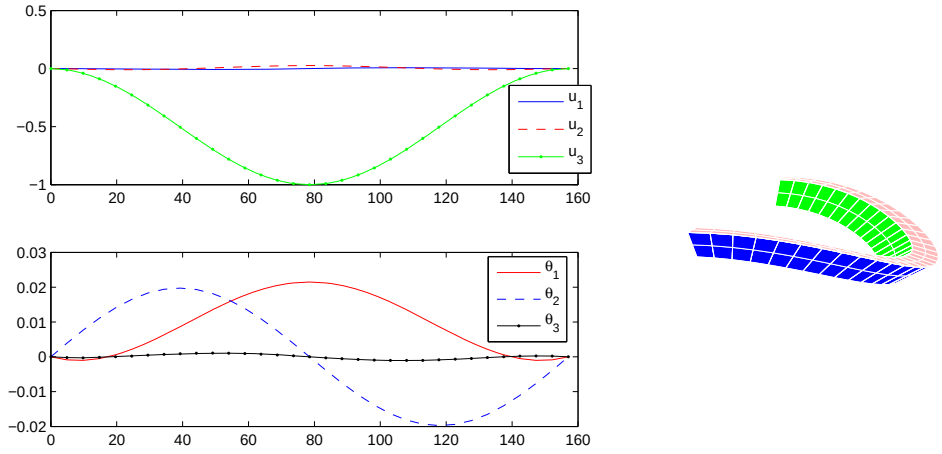

Figure 1.12: Semicircular rod. Vibration mode of frequency ω_1. Displacements and rotations (left). Deformed rod (right).

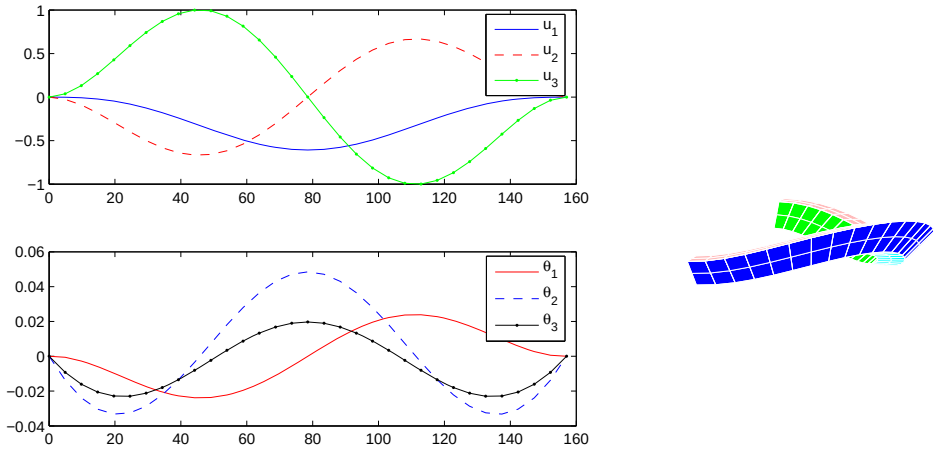

Figure 1.13: Semicircular rod. Vibration mode of frequency ω_2. Displacements and rotations (left). Deformed rod (right).

1.4.4 Test 4: a free ring

The aim of this test is to assess the performance of the finite element method applied to rods subject to boundary conditions different to those used to prove the theoretical results of the previous sections. In particular, we consider a free ring, namely, a circular rod whose centroids line is a whole circle subject to periodical boundary conditions.

The radius of the centroids line has been taken again $R = 50\,\text{cm}$ (curvature: $\kappa = 1/R$; torsion: $\tau = 0$; length: $L = 2\pi R$) and the cross section a square of side-length $b = 5\pi\,\text{cm}$. Hence, $d = 0.0204$. Figure 1.14 shows the undeformed ring.

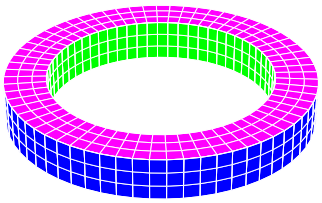

Figure 1.14: Undeformed ring.

In this case, 0 is an eigenvalue of the continuous and the discrete problems, both with multiplicity 6. The corresponding eigenspace is in both cases the set of admissible rigid

motions. Table 1.4 presents the lowest positive vibration frequencies computed on successively refined meshes. The table also includes computed orders of convergence and extrapolated 'exact' vibration frequencies ω_{ex} obtained by least squares fitting. Finally, "d" and "s" point out if the vibration frequencies correspond to double or simple eigenvalues, respectively.

Table 1.4: Angular vibration frequencies of a free ring

Mode	$N = 64$	$N = 128$	$N = 256$	$N = 512$	order	ω_{ex}	d/s
ω_1^h	2310.12	2294.90	2291.12	2290.15	2.00	2289.83	d
ω_2^h	2371.63	2358.77	2355.54	2354.73	2.00	2354.48	d
ω_3^h	6255.36	6195.63	6180.79	6177.06	2.01	6175.84	d
ω_4^h	6345.58	6288.95	6274.89	6271.38	2.01	6270.23	d
ω_5^h	7241.09	7241.09	7241.09	7241.09	—	7241.09	s
ω_6^h	9532.42	9531.20	9530.89	9530.79	2.00	9530.79	d
ω_7^h	10240.41	10240.41	10240.41	10240.41	—	10240.41	s
ω_8^h	11305.06	11147.82	11108.91	11099.20	2.01	11095.98	d

It can be seen from Table 1.4 that the computed fifth and seventh vibration frequencies coincide for all meshes. The fifth one corresponds to a purely torsional mode: a constant rotation with respect to the tangential vector. For this mode, θ_1 is constant and θ_2, θ_3 and all the components of u vanish (see Fig. 1.17 below). On the other hand, the seventh mode corresponds to a constant radial expansion of the whole ring, for which u_2 is constant and u_1, u_3 and θ vanish. In both cases, the vibration modes can be exactly represented in the finite element space for any mesh. This is the reason why the computed results are exact, even for the coarser meshes.

Figures 1.15–1.17 show some of the vibration modes.

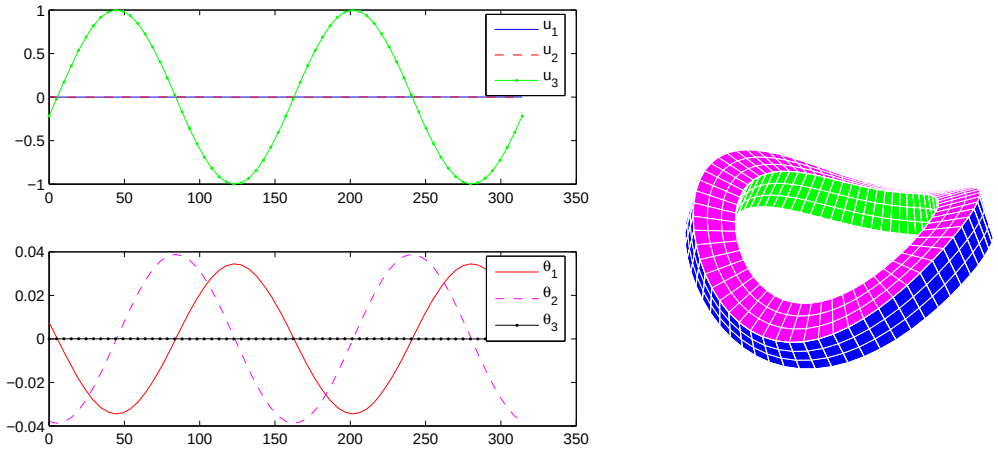

Figure 1.15: Free ring. Vibration mode of frequency ω_1. Displacements and rotations (left). Deformed rod (right).

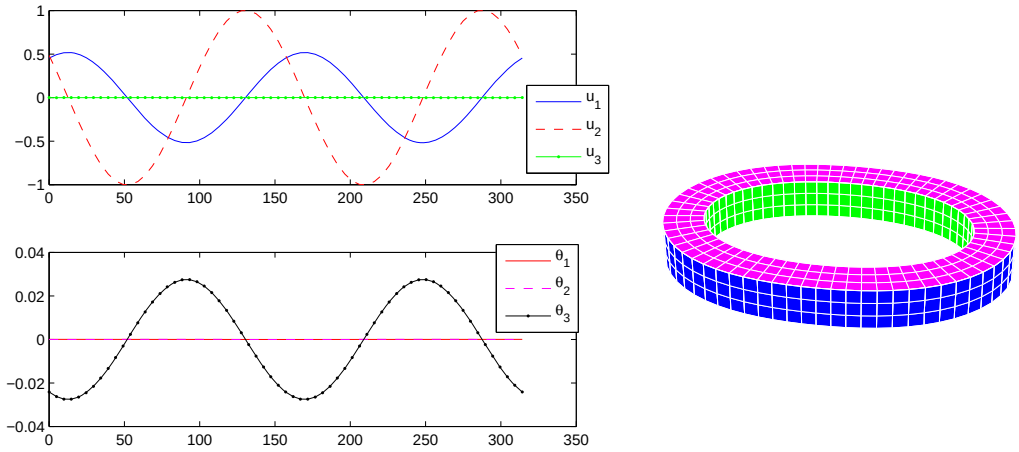

Figure 1.16: Free ring. Vibration mode of frequency ω_2. Displacements and rotations (left). Deformed rod (right).

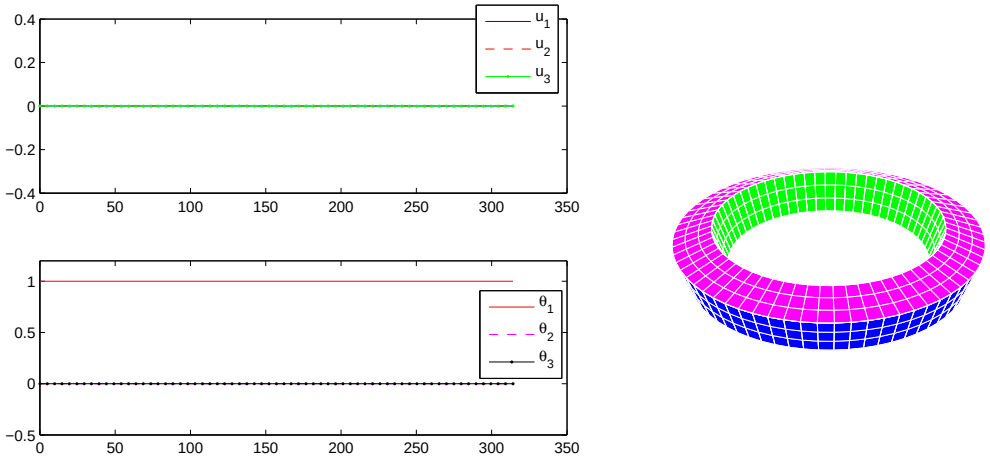

Figure 1.17: Free ring. Vibration mode of frequency ω_5. Displacements and rotations (left). Deformed rod (right).

1.4.5 Test 5: assessing the locking-free property of the method

The aim of this final test is to assess the performance of the finite element method as the non-dimensional thickness parameter d approaches 0. With this purpose, we have computed the lowest-frequency vibration modes for several rods, all with identical geometrical parameters, except for d which takes different values approaching 0.

We have considered again a helix clamped at both ends. The centroids line is given by 1.43, now with $A = 100$ cm and $C = 100$ cm (curvature: $\kappa = A/n^2$; torsion: $\tau = C/n^2$). The length of the helix has been taken $L = \pi n$, which corresponds to half a turn. The section is a square of side-length chosen so that the parameter d varies from 10^{-1} to 10^{-4}. Figure 1.18 shows the undeformed helix for $d = 0.02$.

Tables 1.5 and 1.6 show the lowest computed rescaled eigenvalues $\lambda_h^{(j)} := \left(\omega_j^h\right)^2 \rho/d^2$ ($j = 1$ and 2, respectively) for different values of d and successively refined meshes. According to Lemma 1.2.2 and Theorem 1.3.3, as d and h go to zero, $\lambda_h^{(j)}$ should converge to the corresponding rescaled eigenvalues of the limit problem. This can be clearly observed in both tables. The tables also includes the computed orders of convergence t and the 'exact' rescaled eigenvalue λ_{ex} obtained by means of a least squares fitting of the model

$$\lambda_h^{(j)} \approx \lambda_{\text{ex}} + Ch^t.$$

We also include in these tables the fitted value of the constant C, in order to show that it does not deteriorate as the thickness parameter becomes small (indeed, clearly C also converges as d goes to 0). This confirms that the method is locking-free.

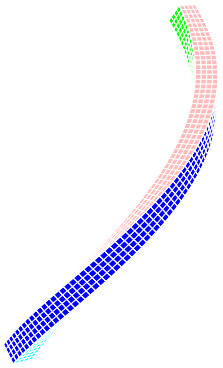

Figure 1.18: Undeformed helical rod.

Table 1.5: Lowest rescaled eigenvalue $\lambda_h^{(1)} \times 10^{-6}$ for helical rods of different thickness

d	$N=32$	$N=64$	$N=96$	$N=128$	order	$\lambda_{\text{ex}} \times 10^{-6}$	C
10^{-1}	1.2706	1.2618	1.2602	1.2596	2.00	1.2589	60.76
10^{-2}	2.0568	2.0374	2.0339	2.0326	2.01	2.0310	130.34
10^{-3}	2.0702	2.0506	2.0470	2.0457	2.01	2.0442	131.32
10^{-4}	2.0704	2.0508	2.0472	2.0459	2.01	2.0443	131.32

Table 1.6: Second lowest rescaled eigenvalue $\lambda_h^{(2)} \times 10^{-6}$ for helical rods of different thickness

d	$N=32$	$N=64$	$N=96$	$N=128$	order	$\lambda_{\text{ex}} \times 10^{-6}$	C
10^{-1}	3.5180	3.4862	3.4803	3.4783	2.00	3.4756	219.5
10^{-2}	13.8379	13.5438	13.4900	13.4712	2.02	13.4475	1920.8
10^{-3}	14.1715	13.8673	13.8116	13.7922	2.02	13.7677	1987.4
10^{-4}	14.1749	13.8706	13.8149	13.7954	2.02	13.7709	1988.4

1.5 Conclusions

We have analyzed the problem of computing the vibration modes and frequencies of a Timoshenko rod of arbitrary geometry. With this purpose, we have considered a finite element mixed method of arbitrary order based on that proposed by Arunakirinathar

and Reddy for the corresponding load problem. The geometrical assumptions for our analysis are slightly more general; in particular, we have not assumed that the Frenet basis determined by the centroids line of the rod is a set of principal axes.

We have proved optimal order of convergence for displacements, rotations and shear stresses of the eigenfunctions, as well as a double-order for the vibration frequencies. We have also proved that the method is locking-free; namely, the convergence does not deteriorate as the thickness of the rod becomes small

We have implemented the lowest-order method and reported several numerical experiments, which allow us to assess the performance and robustness of this approach. In all cases the theoretically predicted optimal order of convergence ($\mathscr{O}(h^2)$ for the vibration frequencies) has been attained. This happens even in cases of boundary conditions not covered by the theoretical analysis. Moreover the experiments show that the method is thoroughly locking-free.

Chapter 2

Computation of the vibration modes of a Reissner-Mindlin laminated plate

This paper deals with the finite element approximation of the vibration modes of a laminated plate modeled by the Reissner-Mindlin equations; DL3 elements are used for the bending terms and standard piecewise linear continuous elements for the in-plane displacements. An *a priori* estimate of the regularity of the solution, independent of the plate thickness, is proved for the corresponding load problem. This allows using the abstract approximation theory for spectral problems to study the convergence of the proposed finite element method. Thus, optimal order error estimates including a double order for the vibration frequencies are obtained under appropriate assumptions. These estimates are independent of the plate thickness, which leads to the conclusion that the method is locking-free. Numerical tests are reported to assess the performance of the method.

2.1 Introduction

The laminated plates are widely used in engineering practice, for instance in automobile, space, and civil applications. The main motivation for this interest is related to the improved ratio between performances and weight of this kind of plates with respect to homogeneous ones. Several different models of these plates have been proposed. The simplest one is the *Classical Laminated Plate Theory* (CLPT) [39], which is based on the Kirchhoff hypotheses. However, other models arising from the Reissner-Mindlin assumptions are often preferred; they are called *First-order Shear-Deformation Theory* (FSDT) [5].

Locking is a very well known phenomenon in the numerical computation of plate problems. It consists in that very unsatisfactory results are obtained when the thickness is small with respect to the other dimensions of the structure. From the point of view of

the numerical analysis, locking reveals itself in that the *a priori* estimates depend on the thickness of the structure in such a way that they degenerate when this parameter becomes small. Several methods based on reduced integration or mixed formulations have been devised to avoid locking in the load plate problem (see [10], for instance). Some of them have been analyzed for the plate vibration problem, as well. For instance, the DL3 and the MITC elements (which were introduced for load problems in [22] and [9], respectively) have been analyzed for vibration problems in [20] and [21], respectively.

Locking-free methods for load problems of laminated plates with several layers all of the same thickness have been analyzed in [4] in a general context. In the present paper we address the corresponding vibration problem. For simplicity, we present the analysis in the case of only two layers. We use the DL3 elements introduced in [22] for the bending terms and standard triangular finite elements for the in-plane displacements. The analysis is made in the framework of the abstract spectral approximation theory for compact operators as stated, for instance, in [6, Section 7]. The goal is to prove optimal order convergence in L^2 and H^1 norms for the eigenfunctions and a double order for the eigenvalues. Moreover, to ensure that the method is locking-free, it has to be proved that the error estimates do not deteriorate as the plate thickness becomes small.

The present analysis is based on the results for load problems for laminated plates from [4] and for the vibration problem for homogeneous plates from [20]. The main difficulty is the need for additional regularity of the solution of the load problem for a Reissner-Mindlin laminated plate. This is the reason why we had to prove new *a priori* estimates for this problem, with constants independent of the plate thickness. This result is interesting by itself, since the error of any numerical method for laminated plates will rely on such an estimate. To the best of the authors knowledge, the obtained estimate had not been proved before. Moreover, the proof of the analogous estimate known for classical Reissner-Mindlin plates (see [2]) does not extend directly to this case. In fact, to extend it, we had to resort to more recent regularity results for formally positive elliptic systems from [34].

The outline of the paper is as follows. In Section 2.2, we present the mathematical setting of the vibration problem for a laminated plate. The resulting spectral problem is shown to be well posed. The eigenvalues and eigenfunctions are shown to converge to the corresponding ones of the limit problem as the thickness of the laminated plate goes to zero, which corresponds to a Kirchhoff laminated plate. The finite element discretization is introduced in Section 2.3 and optimal orders of convergence are proved. These estimates are proved to be independent of the plate thickness and this allows us to conclude that the method is locking-free. In Section 2.4, we report several numerical tests confirming the theoretical results and showing the good performance of the method. The experiments include some cases not covered by the theoretical analysis, where optimal

orders of convergence are also attained. Finally, we prove in an Appendix a thickness-independent *a priori* estimate for the regularity of the solution of the corresponding load problem.

Throughout the paper, we will use standard notation for Sobolev and Lebesgue spaces. Moreover, $\|\cdot\|_0$ will denote the standard norm of $L^2(\Omega)$ (or $L^2(\Omega)^n$, as corresponds). Analogously, $\|\cdot\|_k$ will denote the norm of $H^k(\Omega)$ (or $H^k(\Omega)^n$). Finally, C will denote a generic constant, not necessarily the same at each occurrence, but always independent of the plate thickness t, the particular functions involved, and, in Section 2.3, also independent of the mesh-size.

2.2 Reissner-Mindlin laminated plate equations

Consider an elastic plate of thickness t with reference configuration $\Omega \times \left(-\frac{t}{2}, \frac{t}{2}\right)$, where $\Omega \subset \mathbb{R}^2$ is a convex polygonal domain. The plate is made of two different materials, one occupying the subdomain $\Omega \times \left(-\frac{t}{2}, 0\right)$ and the other one $\Omega \times \left(0, \frac{t}{2}\right)$.

According to the Reissner-Mindlin model, the plate deformation is described by means of the in-plane and transverse displacements, $u^* = (u_1^*, u_2^*)$ and w^*, respectively, and the rotations $\beta^* = (\beta_1^*, \beta_2^*)$ of its mid-surface Ω. For the forthcoming analysis, we assume that the plate is clamped on its whole boundary $\partial\Omega$.

The vibration problem for such a plate can be formally obtained from the three-dimensional linear elasticity equations as follows: According to the Reissner-Mindlin hypotheses, the admissible displacements at each point are given by

$$(u^*(x) - x_3\beta^*(x), w^*(x)), \qquad x := (x_1, x_2) \in \Omega, \quad x_3 \in \left(-\tfrac{t}{2}, \tfrac{t}{2}\right).$$

Test and trial displacements of this form are taken in the variational formulation of the linear elasticity equations for the vibration problem of the three-dimensional plate. By integrating over the thickness and multiplying the shear term by a correcting factor, one arrives at the following problem (see [44]):

Find $\omega > 0$ and non trivial $(u^*, \beta^*, w^*) \in V$ satisfying

$$\begin{aligned} & t\,(\mathscr{A}\varepsilon(u^*), \varepsilon(v)) + t^2\,[(\mathscr{B}\varepsilon(u^*), \varepsilon(\eta)) + (\mathscr{B}\varepsilon(\beta^*), \varepsilon(v))] \\ & + t^3\,(\mathscr{D}\varepsilon(\beta^*), \varepsilon(\eta)) + t\kappa(\beta^* - \nabla w^*, \eta - \nabla z) \\ & \quad = \omega^2 \left\{ \frac{t}{2}\,(\rho_1 + \rho_2)\,(u^*, v) + \frac{t^3}{24}\,(\rho_1 + \rho_2)\,(\beta^*, \eta) \right. \\ & \qquad \left. + \frac{t}{2}\,(\rho_1 + \rho_2)\,(w^*, z) + \frac{t^2}{8}\,(\rho_1 - \rho_2)\,[(\beta^*, v) + (u^*, \eta)] \right\} \quad \forall (v, \eta, z) \in V, \end{aligned}$$

where

$$V := H_0^1(\Omega)^2 \times H_0^1(\Omega)^2 \times H_0^1(\Omega).$$

In the equation above ω is the angular vibration frequency, $(\cdot,\cdot)$ denotes the standard $L^2(\Omega)$ inner product of scalar, vector or tensor fields, as corresponds, and ε is the linear strain tensor defined by $\varepsilon_{ij}(v) := \frac{1}{2}\left(\partial v_i/\partial x_j + \partial v_j/\partial x_i\right)$, $i,j = 1,2$. Moreover, $\mathscr{A}$, $\mathscr{B}$, and $\mathscr{D}$ are fourth order tensors defined by

$$\mathscr{A}(\tau) := \frac{1}{2}(\mathscr{C}_1 + \mathscr{C}_2)\,\tau, \quad \mathscr{B}(\tau) := \frac{1}{8}(\mathscr{C}_1 - \mathscr{C}_2)\,\tau, \quad \text{and} \quad \mathscr{D}(\tau) := \frac{1}{24}(\mathscr{C}_1 + \mathscr{C}_2)\,\tau,$$

where $\mathscr{C}_1$ and $\mathscr{C}_2$ are the linear elasticity operators on each medium,

$$\mathscr{C}_i\tau := \lambda_i \operatorname{tr}(\tau) I + 2\mu_i\tau, \qquad i = 1,2,$$

with plane stress Lamé coefficients $\lambda_i := E_i\nu_i/\left(1-\nu_i^2\right)$ and $\mu_i := E_i/\left[2\left(1+\nu_i\right)\right]$, E_i being the Young modulus and ν_i the Poisson ratio of each material. Finally $\kappa := k(\mu_1+\mu_2)/2$ is the shear modulus of the laminated plate, with k a correction factor usually taken as $5/6$, and ρ_i is the density of each material.

We rescale the problem using new variables

$$u := u^*/t, \quad \beta := \beta^*, \quad w =: w^*, \quad \text{and} \quad \lambda_t := \frac{\rho_1+\rho_2}{2}\frac{\omega^2}{t^2}.$$

The reason for this is that the rescaled variables attain finite non-zero limits as t goes to zero, as will be shown below (cf. Lemma 2.2.2). We also introduce the scaled shear stress

$$\gamma := \frac{\kappa}{t^2}(\beta - \nabla w)$$

and the bilinear forms

$$a((u,\beta),(v,\eta)) := (\mathscr{A}\varepsilon(u),\varepsilon(v)) + (\mathscr{B}\varepsilon(u),\varepsilon(\eta)) + (\mathscr{B}\varepsilon(v),\varepsilon(\beta)) + (\mathscr{D}\varepsilon(\beta),\varepsilon(\eta))$$

and

$$b_t((u,\beta,w),(v,\eta,z)) := (w,z) + t^2(u,v) + \frac{t^2}{12}(\beta,\eta) + \frac{\rho_1-\rho_2}{4(\rho_1+\rho_2)}t^2\left[(\beta,v)+(u,\eta)\right].$$

Thus, the plate vibration problem can be rewritten as follows:

Find $\lambda_t > 0$ and non trivial $(u,\beta,w) \in V$ such that

$$\begin{cases} a((u,\beta),(v,\eta)) + (\gamma,\eta-\nabla z) = \lambda_t b_t((u,\beta,w),(v,\eta,z)) \quad \forall (v,\eta,z)\in V, \\ \gamma = \dfrac{\kappa}{t^2}(\beta-\nabla w). \end{cases} \tag{2.1}$$

All the eigenvalues λ_t of this problem are strictly positive, because of the symmetry of both bilinear forms, the ellipticity of a, which has been proved in [4, Proposition 2.1], and the positiveness of b_t, which can be proved by straightforward computations.

To analyze the approximation of this eigenvalue problem, we introduce the operator

$$T_t : H \longrightarrow H,$$

where

$$H := L^2(\Omega)^2 \times L^2(\Omega)^2 \times L^2(\Omega),$$

defined for $(f,m,g) \in H$ by $T_t(f,m,g) := (u,\beta,w)$, with $(u,\beta,w) \in V$ being the solution to

$$\begin{cases} a((u,\beta),(v,\eta)) + (\gamma, \eta - \nabla z) = b_t((f,m,g),(v,\eta,z)) \quad \forall (v,\eta,z) \in V, \\ \gamma = \dfrac{\kappa}{t^2}(\beta - \nabla w). \end{cases} \tag{2.2}$$

This is the load problem for the Reissner-Mindlin laminated clamped plate. It is a well posed problem; in fact, the existence and uniqueness of the solution for all $t > 0$ follows from [4, Proposition 2.1].

Because of the symmetry of the bilinear forms a and b_t, the operator T_t is self-adjoint in H endowed with the inner-product $b_t(\cdot,\cdot)$. The norm induced by this inner product is equivalent to the weighted L^2 norm

$$|(v,\eta,z)|_t^2 := t^2 \|v\|_0^2 + t^2 \|\eta\|_0^2 + \|z\|_0^2, \qquad (v,\eta,z) \in H,$$

with equivalence constants independent of t. On the other hand, because of the compact embedding $H_0^1(\Omega) \hookrightarrow L^2(\Omega)$, T_t is a compact operator. Then, apart from 0, its spectrum consists of a sequence of finite multiplicity real eigenvalues converging to zero. Note that λ_t is an eigenvalue of Problem (2.1) if and only if $\mu_t := 1/\lambda_t$ is an eigenvalue of T_t, with the same multiplicity and corresponding eigenfunctions.

The solution of the load problem (2.2) satisfies the following additional regularity result, which is systematically used in the proofs that follow: $u, \beta \in H^2(\Omega)^2$, $w \in H^2(\Omega)$, $\gamma \in H^1(\Omega)^2$, and there exists a constant $C > 0$, independent of t and (f,m,g), such that

$$\|u\|_2 + \|\beta\|_2 + \|w\|_2 + \|\gamma\|_0 + t\|\gamma\|_1 \leq C\left(t^2\|f\|_0 + t^2\|m\|_0 + \|g\|_0\right). \tag{2.3}$$

The proof of this *a priori* estimate is far from being straightforward. In fact, although it is proved by extending similar arguments used for classical homogeneous plates in [2, Theorem 7.1], it needs of some preliminary results. Thus, for the sake of clarity, we postpone this analysis to the Appendix. In particular, the estimate (2.3) is a consequence of Theorem 2.6.1 from this Appendix (cf. Corollary 2.6.2).

On the other hand, as a consequence of [15, Theorem 1], it can be shown as in [4, Proposition 2.2] that, when $t \to 0$, the solution (u,β,w) to (2.2) converges to $(u_0, \nabla w_0, w_0)$, where $(u_0, w_0) \in H_0^1(\Omega)^2 \times H_0^2(\Omega)$ satisfies

$$a((u_0, \nabla w_0),(v, \nabla z)) = (g,z) \qquad \forall (v,z) \in H_0^1(\Omega)^2 \times H_0^2(\Omega).$$

This limit problem is well posed and corresponds to the bending of a clamped Kirchhoff-type laminated plate subjected to a (rescaled) transverse load g. The arguments from [10, Section VII.3.1] can be easily adapted to prove that the limit problem above is equivalent to finding $(u_0,\beta_0,w_0)\in V$ such that there exists $\gamma_0\in H_0(\mathrm{rot},\Omega)'$ satisfying

$$\begin{cases} a((u_0,\beta_0),(v,\eta))+\langle\gamma_0,\eta-\nabla z\rangle = b_0\left((f,m,g),(v,\eta,z)\right)\equiv(g,z) \\ \qquad\qquad\qquad\qquad\qquad\qquad\qquad\qquad\qquad\qquad \forall (v,\eta,z)\in V, \\ \beta_0-\nabla w_0=0, \end{cases} \tag{2.4}$$

where $\langle\cdot,\cdot\rangle$ stands for the duality pairing in

$$H_0(\mathrm{rot},\Omega):=\left\{\psi\in L^2(\Omega)^2:\ \mathrm{rot}\,\psi\in L^2(\Omega)\text{ and }\psi\cdot\tau=0\text{ on }\partial\Omega\right\},$$

with $\mathrm{rot}\,\psi:=\partial_1\psi_2-\partial_2\psi_1$ and τ being a unit vector tangent to $\partial\Omega$. Moreover, the arguments from [10] can also be adapted to prove that this is a well posed mixed problem. Thus, we are allowed to introduce the operator

$$T_0: H\longrightarrow H,$$

defined for $(f,m,g)\in H$ by $T_0(f,m,g):=(u_0,\beta_0,w_0)$, with (u_0,β_0,w_0) being the solution to problem (2.4).

An *a priori* estimate similar to (2.3) holds for the limit problem (2.4), as well; namely, $u_0,\beta_0\in H^2(\Omega)^2$, $w_0\in H^2(\Omega)$, $\gamma_0\in L^2(\Omega)^2$, and

$$\|u_0\|_2+\|\beta_0\|_2+\|w_0\|_2+\|\gamma_0\|_0\le C\,\|g\|_0\,. \tag{2.5}$$

The proof of this estimate is a consequence of Lemma 2.6.2 from the Appendix (cf. Corollary 2.6.1).

Now, we may proceed as in [20] to prove an estimate for the convergence of the solution to (2.2) to that to (2.4) as t goes to zero. In fact we have the following result.

Lemma 2.2.1 *There exists a constant $C>0$, independent of t, such that*

$$\|(T_t-T_0)(f,m,g)\|_1\le Ct\,|(f,m,g)|_t\qquad\forall(f,m,g)\in H.$$

Proof. Repeating the arguments of the proof of Lemma 2.6.3 from the Appendix we arrive at

$$\|u-u_0\|_1+\|\beta-\beta_0\|_1\le Ct\,\|(f,m,g)\|_0$$

(cf. (2.19)). Next, subtracting the second equation in (2.4) from that in (2.2), we have

$$\gamma=\frac{\kappa}{t^2}\left(\beta-\beta_0-\nabla(w-w_0)\right).$$

Hence, the estimate above and (2.3) yield

$$\|w - w_0\|_1 \leq \frac{t^2}{\kappa}\|\gamma\|_0 + \|\beta - \beta_0\|_0 \leq Ct\,|(f,m,g)|_{b_t}\,.$$

Thus, we conclude the proof. □

As a consequence of this lemma, the operator $T_t|_V$ converges in norm to $T_0|_V$. Then, standard properties of separation of isolated parts of the spectrum (see for instance [32]) yield the following result.

Lemma 2.2.2 *Let $\mu_0 > 0$ be an eigenvalue of T_0 of multiplicity m. Let D be any disc in the complex plane centered at μ_0 and containing no other element of the spectrum of T_0. Then, for t small enough, D contains exactly m eigenvalues of T_t (repeated according to their respective multiplicities). Consequently, each eigenvalue $\mu_0 > 0$ of T_0 is a limit of eigenvalues μ_t of T_t, as t goes to zero.*

2.3 Finite-element discretization

We restrict our analysis to the DL3 elements introduced in [22], although other finite elements can be analyzed in this same framework. We consider a regular family of triangulations $\{\mathscr{T}_h\}$; as usual, h denotes the mesh-size.

To discretize the rotations, we use standard piecewise linear functions augmented in such a way that they have quadratic tangential components on the boundary of each element. More precisely, for each $T \in \mathscr{T}_h$, let α_i^T, $i = 1,2,3$, be its barycentric coordinates and τ_i^T a unit vector tangent to the edge $\alpha_i^T = 0$. Consider the edge-bubble vector fields $\varphi_i^T := \alpha_j^T \alpha_k^T \tau_i^T$, $i,j,k = 1,2,3$, all different. The finite element space for the rotations is defined by

$$X_h := \left\{\eta_h \in H_0^1(\Omega)^2 :\ \eta_h|_T \in \mathscr{P}_1^2 \oplus \langle \varphi_1^T, \varphi_2^T, \varphi_3^T\rangle \quad \forall T \in \mathscr{T}_h\right\}.$$

We use standard piecewise linear elements for the displacements; namely,

$$W_h := \{z_h \in H_0^1(\Omega) :\ z_h|_T \in \mathscr{P}_1,\ \forall T \in \mathscr{T}_h\}$$

for the transverse displacements and

$$U_h := W_h^2$$

for the in-plane displacements. Thus, the finite element discretization of the space V is defined by

$$V_h := U_h \times X_h \times W_h.$$

For the numerical method, we also need the so called *reduction operator*

$$R : H^1(\Omega)^2 \cap H_0(\mathrm{rot},\Omega) \longrightarrow \Gamma_h,$$

where Γ_h is the lowest-order rotated Raviart-Thomas space (see [41])

$$\Gamma_h := \left\{ \psi_h \in H_0(\mathrm{rot},\Omega) : \ \psi_h|_T \in \mathscr{P}_0^2 \oplus (-x_2,x_1)\mathscr{P}_0 \quad \forall T \in \mathscr{T}_h \right\}.$$

This reduction operator is uniquely determined by

$$\int_\ell R\psi \cdot \tau_\ell = \int_\ell \psi \cdot \tau_\ell, \qquad \psi \in H^1(\Omega)^2 \cap H_0(\mathrm{rot},\Omega),$$

for every edge ℓ of the triangulation (τ_ℓ being a unit tangent vector along ℓ).

Now we are in a position to write the finite element approximation of the plate vibration problem (2.1):

Find $\lambda_{th} > 0$ and non trivial $(u_h,\beta_h,w_h) \in V_h$ such that

$$\left\{ \begin{array}{l} a((u_h,\beta_h),(v_h,\eta_h)) + (\gamma_h, R\eta_h - \nabla v_h) \\ \qquad\qquad = \lambda_{th} b_t((u_h,\beta_h,w_h),(v_h,\eta_h,z_h)) \quad \forall (v_h,\eta_h,z_h) \in V_h, \\ \gamma_h = \dfrac{\kappa}{t^2}(R\beta_h - \nabla w_h). \end{array} \right. \tag{2.1}$$

Notice that the method is non conforming since consistency terms arise because of the reduction operator.

As in the continuous case, we introduce the operator

$$T_{th} : H \longrightarrow H,$$

defined for $(f,m,g) \in H$ by $T_{th}(f,m,g) := (u_h,\beta_h,w_h)$, with $(u_h,\beta_h,w_h) \in V_h$ being the solution to the corresponding finite element discretization of the load problem (2.2), namely,

$$\left\{ \begin{array}{l} a((u_h,\beta_h),(v_h,\eta_h)) + (\gamma_h, R\eta_h - \nabla z_h) = b_t((f,m,g),(v_h,\eta_h,z_h)) \\ \qquad\qquad\qquad\qquad\qquad\qquad\qquad\qquad \forall (v_h,\eta_h,z_h) \in V_h, \\ \gamma_h = \dfrac{\kappa}{t^2}(R\beta_h - \nabla w_h). \end{array} \right.$$

The existence and uniqueness of the solution to this problem follows easily from the ellipticity of a. Once more λ_{th} is an eigenvalue of problem (2.1) if and only if $\mu_{th} := 1/\lambda_{th}$ is a strictly positive eigenvalue of T_{th} with the same multiplicity and corresponding eigenfunctions.

For $t > 0$ fixed, the spectral approximation theory for compact operators (cf. [6]) can be readily applied to prove convergence of the eigenpairs of T_{th} to those of T_t. However, further considerations are needed to show that the error estimates do not deteriorate as t becomes small. With this goal, we will make use of the following result, which will lead to optimal error estimates in the H^1 norm for displacements and rotations.

Lemma 2.3.1 *There exists a constant C, independent of t and h, such that*

$$\|(T_t - T_{th})(f,m,g)\|_1 \le Ch\,|(f,m,g)|_t \qquad \forall (f,m,g) \in H.$$

Proof. Let $(f,m,g) \in H$, $(u,\beta,w) := T_t(f,m,g)$, and $(u_h,\beta_h,w_h) := T_{th}(f,m,g)$. The arguments given in the proof of [4, Proposition 3.2] for pure transverse loads (i.e., $f = 0$ and $m = 0$) extend easily to our case yielding

$$\begin{aligned}\|u-u_h\|_1 + \|\beta-\beta_h\|_1 + \|w-w_h\|_1 + t\,\|\gamma-\gamma_h\|_0 \\ \le Ch\,(\|u\|_2 + \|\beta\|_2 + \|\gamma\|_0 + t\,\|\gamma\|_1)\,.\end{aligned}$$

Thus, the lemma follows from this inequality and (2.3). □

As a consequence of this lemma, $T_{th}|_V$ converges in norm to $T_t|_V$. In fact, for any fixed $t \in (0, t_{\max})$, we have $|\cdot|_t \le t_{\max}\,\|\cdot\|_1$ and hence the lemma yields

$$\|(T_t - T_{th})(f,m,g)\|_1 \le Ch\,\|(f,m,g)\|_1 \qquad \forall (f,m,g) \in V. \tag{2.2}$$

Consequently, if μ_t is an eigenvalue of T_t with multiplicity m, then exactly m eigenvalues of T_{th} (repeated according to their respective multiplicities) converge to μ_t as h goes to zero (see [32]). The following theorem shows that, under mild assumptions, optimal t-independent error estimates in the H^1 norm are valid for the eigenfunctions.

Theorem 2.3.1 *Let μ_t be an eigenvalue of T_t converging to a simple eigenvalue μ_0 of T_0, as t goes to zero. Let μ_{th} be the eigenvalue of T_{th} that converges to μ_t as h goes to zero. Let (u,β,w) and (u_h,β_h,w_h) be the corresponding eigenfunctions conveniently normalized. Then, for t and h small enough,*

$$\|(u,\beta,w) - (u_h,\beta_h,w_h)\|_1 \le Ch,$$

with a constant C independent of t and h.

Proof. The inequality of the theorem is a direct consequence of the estimate (2.2) and [6, Theorem 7.1], with a constant C depending on the constant in (2.2) (which is independent of t) and on the inverse of the distance of μ_t to the rest of the spectrum of T_t. Now, according to Lemma 2.2.2, for t small enough, this distance can be bounded below in terms of the distance of μ_0 to the rest of the spectrum of T_0, which obviously does not depend on t. Thus, we conclude the proof. □

The following lemma is the basic tool to prove a double order of convergence for the eigenvalues.

Lemma 2.3.2 *There exists a constant C, independent of t and h, such that*

$$\|(T_t - T_{th})(f,m,g)\|_0 \leq Ch^2 |(f,m,g)|_t \qquad \forall (f,m,g) \in H.$$

Proof. We do not include it, since it is a straightforward modification of the proof of [20, Lemma 3.4]. □

Theorem 2.3.2 *Let μ_t and μ_{th} be as in Theorem 2.3.1. Then, for t and h small enough,*

$$|\mu_t - \mu_{th}| \leq Ch^2,$$

with a constant C independent of t and h.

Proof. Let (u,β,w) be an eigenfunction corresponding to μ_t normalized in the norm induced by b_t. Applying [6, Theorem 7.3] and taking into account that T and T_h are self-adjoint with respect to b_t, we have

$$|\mu_t - \mu_{th}| \leq C \left[b_t((T_t - T_{th})(u,\beta,w),(u,\beta,w)) + |(T_t - T_{th})(u,\beta,w)|_t^2 \right], \tag{2.3}$$

with a constant C depending on the inverse of the distance of μ_t to the rest of the spectrum of T_t. By repeating the arguments in the proof of Theorem 2.3.1 we observe that, for t small enough, this constant can be chosen independent of t. Thus, since $|\cdot|_t \leq C\|\cdot\|_0$, using the estimate from Lemma 2.3.2 in (2.3), we conclude the proof. □

Another consequence of Lemma 2.3.2 is a double order of convergence for the eigenfunctions in the L^2-norm.

Theorem 2.3.3 *Let μ_t, μ_{th}, (u,β,w) and (u_h,β_h,w_h) be as in Theorem 2.3.1. Then, for t and h small enough,*

$$\|(u,\beta,w) - (u_h,\beta_h,w_h)\|_0 \leq Ch^2,$$

with a constant C independent of t and h.

Proof. Since $|\cdot|_t \leq C\|\cdot\|_0$, the arguments in the proof of Theorem 2.3.1 can be repeated using $\|\cdot\|_0$ instead of $\|\cdot\|_1$ and the estimate from Lemma 2.3.2 instead of (2.2). □

2.4 Numerical experiments

We report in this section some numerical results obtained with a code which implements the method analyzed above. The aim of this numerical experimentation is two-fold: to confirm the theoretical results and to assess the performance of the method.

2.4.1 Test 1: A simply supported rectangular plate with a known analytical solution. Validation

The aim of this first test is to validate the computer code and to corroborate the error estimates proved in the previous section. With this purpose, we applied the method to a problem with a known analytical solution: a rectangular simple supported plate (see [43, 44]). This test allowed us to calculate the error of the different quantities computed with our code. Moreover, it shows that the method is able to deal with other kind of boundary conditions, although the theoretical analysis has been made just for clamped plates.

If the domain of the simply supported plate is the rectangle $\Omega := (0,a)\times(0,b)$, then the eigenfunctions are given by

$$u = \begin{bmatrix} \hat{u}_1 \cos\frac{k\pi x}{a}\sin\frac{l\pi y}{b} \\ \hat{u}_2 \sin\frac{k\pi x}{a}\cos\frac{l\pi y}{b} \end{bmatrix}, \quad w = \hat{w}\sin\frac{k\pi x}{a}\sin\frac{l\pi y}{b}, \quad \beta = \begin{bmatrix} \hat{\beta}_1 \cos\frac{k\pi x}{a}\sin\frac{l\pi y}{b} \\ \hat{\beta}_2 \sin\frac{k\pi x}{a}\cos\frac{l\pi y}{b} \end{bmatrix}, \tag{2.1}$$

$k,l \in \mathbb{N}$. The constants $\hat{u}_1$, $\hat{u}_2$, $\hat{w}$, $\hat{\beta}_1$, and $\hat{\beta}_2$, as well as the corresponding eigenvalues, can be obtained as follows: For each pair $(k,l) \in \mathbb{N}^2$, the terms (2.1) must be plugged into (2.1), written in strong form. This leads to a 5×5 generalized eigenvalue problem whose eigenvectors are $(\hat{u}_1,\hat{u}_2,\hat{w},\hat{\beta}_1,\hat{\beta}_2)^{\mathrm{t}}$ and whose eigenvalues are the ones we are looking for.

We applied the method to a plate of length $a = 6\,\mathrm{m}$, width $b = 4\,\mathrm{m}$, and thickness $t = 0.1\,\mathrm{m}$. We used the following physical parameters:

$$\begin{aligned} E_1 &= 1.440\times 10^{11}\,\mathrm{N/m^2}, & \nu_1 &= 0.35, & \rho_1 &= 7700\,\mathrm{kg/m^3}, \\ E_2 &= 0.144\times 10^{11}\,\mathrm{N/m^2}, & \nu_2 &= 0.30, & \rho_2 &= 770\,\mathrm{kg/m^3}. \end{aligned}$$

Finally, we took $\kappa = 5/6$ as correction factor for this and all the other tests.

We used uniform meshes obtained by refining the coarse one shown in Figure 2.1. The refinement parameter N is the number of layers of elements through the width of the plate.

Table 2.1 shows the six lowest vibration frequencies computed with the method on four successively refined meshes. The table also includes the corresponding exact values obtained from the analytical solution and the computed order of convergence for each one.

A quadratic order of convergence can be clearly observed for all the vibration frequencies, which corresponds to an optimal double order according to the degree of the finite elements used.

Figure 2.2 shows the error curves in L^2 norm and H^1 seminorm of the in-plane and the transverse displacements, u and w, respectively, for the eigenfunction corresponding to the lowest vibration frequency ω_1.

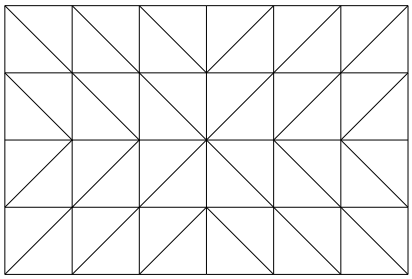

Figure 2.1: Rectangular plate. Finite element coarse mesh ($N = 4$).

Table 2.1: Test 1: Lowest vibration frequencies of a simply supported laminated rectangular plate.

Mode	$N = 8$	$N = 16$	$N = 32$	$N = 64$	Exact	Order
ω_1	84.605	83.368	83.066	82.992	82.967	2.02
ω_2	166.169	161.063	159.829	159.527	159.427	2.03
ω_3	272.770	259.194	255.911	255.102	254.834	2.02
ω_4	308.314	291.870	287.894	286.918	286.595	2.02
ω_5	361.027	338.177	332.772	331.458	331.026	2.04
ω_6	514.209	471.247	461.043	458.564	457.749	2.04

A quadratic order in L^2 and a linear order in H^1 can be clearly observed for both displacements. Once more, this corresponds to the optimal orders according to the degree of the finite elements.

2.4.2 Test 2: A clamped rectangular plate. Testing the locking-free character of the method

The main goal of this test is to confirm experimentally that the method is locking-free, as was proved in the previous section. With this purpose, we chose a problem lying in the theoretical framework: a plate clamped on its whole boundary.

We used a rectangular plate with the same dimensions and physical parameters as in the previous test. We also used the same meshes.

First, we computed the lowest vibration frequencies of the plate on each mesh. Since no analytical solution is available in this case, for each vibration mode, we extrapolated a more accurate approximation of the frequency and estimated the order of convergence by

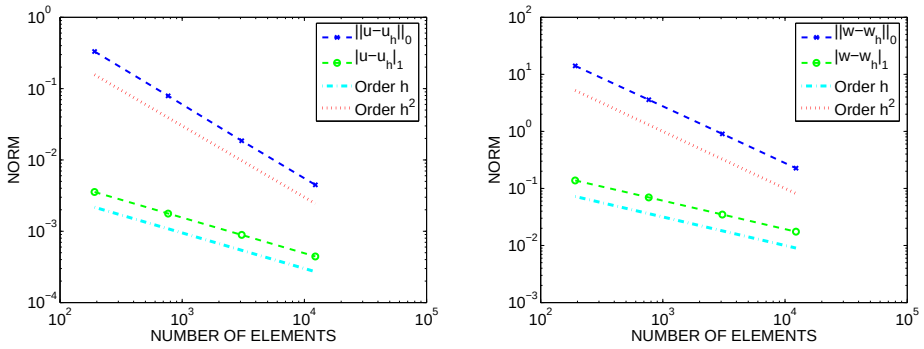

Figure 2.2: Test 1: Error curves for in-plane displacements (left) and transverse displacements (right); log-log plots of the corresponding norms versus the number of elements.

means of a least square fitting.

Table 2.2 shows the six lowest vibration frequencies computed on different meshes, the estimated order of convergence and the extrapolated more accurate value of each frequency.

Table 2.2: Test 2: Lowest vibration frequencies of a clamped laminated rectangular plate.

Mode	$N=8$	$N=16$	$N=32$	$N=64$	Order	Extrapolated
ω_1	161.136	157.902	157.095	156.898	2.01	156.831
ω_2	255.847	245.336	242.757	242.128	2.03	241.924
ω_3	418.592	391.593	384.980	383.358	2.03	382.835
ω_4	419.684	393.806	387.352	385.762	2.01	385.237
ω_5	518.006	475.120	464.831	462.331	2.06	461.574
ω_6	667.968	603.579	587.688	583.781	2.02	582.499

Once more, a double order of convergence can be readily observed for all the vibration frequencies.

Next, we tested whether the method remains locking-free as the thickness becomes small. For this test, we took clamped plates with the same physical parameters and dimensions as above, except for the thickness for which we used different values ranging from $t = 0.1\,\mathrm{m}$ to $0.1\,\mathrm{mm}$.

To allow for comparison, we report normalized frequencies $\hat{\omega} := \omega/t$. Table 2.3 shows the computed lowest vibration frequency of clamped rectangular laminated plates with decreasing values of the thickness. Once more, the table includes the estimated orders of convergence and extrapolated frequencies. We also report on the last row the extrapolated limit values corresponding to $t = 0$ (i.e., the Kirchhoff model).

Table 2.3: Test 2: Normalized lowest frequency $\hat{\omega}_1$ of clamped laminated rectangular plates with varying thickness.

Thickness	$N = 8$	$N = 16$	$N = 24$	$N = 32$	Order	Extrapolated
$t = 0.1\,\mathrm{m}$	1611.365	1579.017	1573.019	1570.948	2.00	1568.239
$t = 0.01\,\mathrm{m}$	1616.810	1584.050	1577.875	1575.707	1.97	1572.859
$t = 0.001\,\mathrm{m}$	1616.866	1584.103	1577.928	1575.759	1.97	1572.883
$t = 0.0001\,\mathrm{m}$	1616.865	1584.103	1577.926	1575.762	1.97	1572.883
$t = 0$ (extr.)	1616.866	1584.103	1577.927	1575.761	1.97	1572.883

We observe that the method is perfectly locking-free, and that the quadratic order of convergence is preserved even for extremely small values of the thickness.

2.4.3 Test 3: A clamped circular plate. Robustness of the plate model and the finite element method

The aim of this test is to assess the efficiency of the Reissner-Mindlin laminated plate model by comparing their results with those obtained from the 3D elasticity equations. In particular, we are interested in exhibiting the robustness of the model, as well as that of the proposed finite element method, when applied to laminates with very different physical parameters. With this purpose, we applied the method to a problem whose corresponding 3D equations can be accurately solved. This is the reason why we chose a circular plate, whose axisymmetric vibration modes can be efficiently computed from the corresponding equations in cylindrical coordinates.

We used a clamped circular plate with diameter $d = 2\,\mathrm{m}$ and thickness $t = 0.1\,\mathrm{m}$. First, we took the same physical parameters as in the other experiments. We used quasiuniform meshes as that shown in Figure 2.3. The refinement parameter N is in this case the number of elements on each quarter of the circle.

On the other hand, by taking advantage of the cylindrical symmetry, the 3D problem reduces to a two-dimensional one posed on a meridional section of the plate. Thus, we also computed the axisymmetric vibration modes by means of another code based on a standard finite element discretization of the 3D elasticity equations in cylindrical coordinates. Also in this case we used successively refined meshes and obtained a very accurate approximation of the vibrations frequencies by extrapolation.

We report in Table 2.4 the results for a couple of axisymmetric modes, which, for this plate, correspond to the lowest and the sixth vibration frequencies. The table includes again the extrapolated values of the frequencies and the estimated orders of convergence,

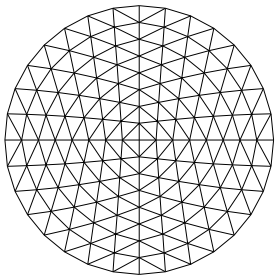

Figure 2.3: Circular plate. Finite element mesh ($N = 8$).

as well. It also includes on the last column the values obtained with the axisymmetric 3D code.

Table 2.4: Test 3: Lowest vibration frequencies of axisymmetric modes of a clamped laminated circular plate; Young moduli ratio $E_1/E_2 = 10$.

Mode	$N = 4$	$N = 8$	$N = 16$	$N = 32$	Order	Extrapolated	3D
ω_1	968.270	945.923	940.395	939.020	2.01	938.571	935.748
ω_6	3908.732	3628.509	3559.984	3543.051	2.03	3537.664	3489.815

It can be seen from this table that the disparity between both extrapolated values is very small indeed, which is merely a confirmation of the accuracy of the Reissner-Mindlin laminated plate model.

Next, we tested the robustness of the model applied to laminates with physical parameters of very different scales. With this aim, we computed the vibration modes of a plate identical to the previous one, except for the fact that the Young modulus of the second material is now $E_2 = 0.144 \times 10^8\,\mathrm{N/m^2}$. Therefore, the ratio between the Young moduli of each material is 10^4.

We report in Table 2.5 the results for this plate analogous to those of the previous table.

Once more, an excellent agreement between both models can be clearly observed, despite the disparity of the Young modulus of each material. Other non reported tests demonstrate the robustness of the method for the Reissner-Mindlin laminated plate model with respect to the remaining physical parameters.

Finally, Figures 2.4 and 2.5 show the transverse displacement fields computed with the Reissner-Mindlin plate model for the two vibration modes reported in Table 2.5. The

Table 2.5: Test 3: Lowest vibration frequencies of axisymmetric modes of a clamped laminated circular plate; Young moduli ratio $E_1/E_2 = 10^4$.

Mode	$N = 4$	$N = 8$	$N = 16$	$N = 32$	Order	Extrapolated	3D
ω_1	671.490	650.794	645.813	644.582	2.05	644.206	645.057
ω_2	2810.616	2540.776	2478.636	2463.491	2.11	2459.352	2425.412

figures also show the corresponding meridional plate sections of each mode computed with the axisymmetric 3D code.

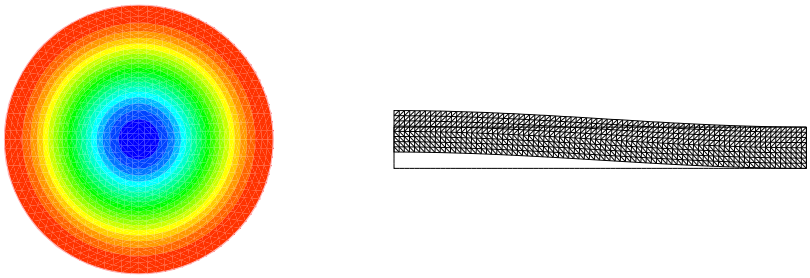

Figure 2.4: Test 3: Lowest axisymmetric vibration mode ω_1 of a clamped laminated circular plate with Young moduli ratio $E_1/E_2 = 10^4$; transverse displacement field (left) and meridional cross section (right).

2.5 Conclusions

We analyzed the problem of computing the vibration modes of a clamped laminated plate modeled by Reissner-Mindlin equations. We considered a finite-element method based on DL3 elements for the bending terms and standard triangular piecewise linear elements for the in-plane displacements. We proved optimal order of convergence in H^1 and L^2 for displacements and rotations, as well as a double order for the eigenvalues. We also proved that the error estimates do not deteriorate as the thickness becomes small, which imply that the method is locking-free. The keypoint of the proof is an *a priori* estimate for the regularity of the solution of the corresponding load problem.

We reported numerical experiments confirming the theoretical results. Moreover, these experiments show the robustness with respect to the physical parameters of both, the Reissner-Mindlin laminated plate model and the proposed method. Finally, the experiments also show that the method works for more general boundary conditions.

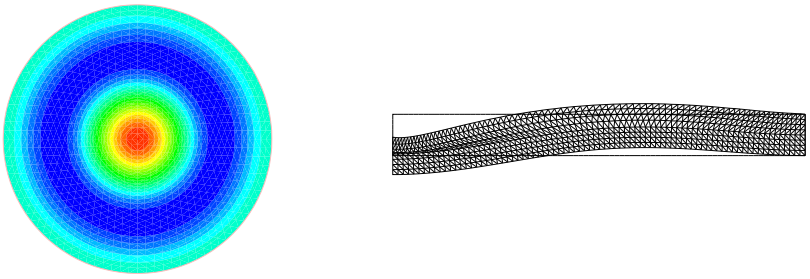

Figure 2.5: Test 3: Second lowest axisymmetric vibration mode ω_6 of a clamped laminated circular plate with Young moduli ratio $E_1/E_2 = 10^4$; transverse displacement field (left) and meridional cross section (right).

2.6 Appendix

In this Appendix we will obtain an *a priori* estimate for the solution of the load problem (2.2) similar to the one valid for classical homogeneous Reissner-Mindlin plates. With this purpose, first we prove the following auxiliary result.

Lemma 2.6.1 *Let Ω be a convex polygonal domain in the plane. Given $F, G \in L^2(\Omega)^2$, let $(u,\beta) \in H_0^1(\Omega)^2 \times H_0^1(\Omega)^2$ be the unique solution of*

$$a((u,\beta),(v,\eta)) = (F,v) + (G,\eta) \qquad \forall (v,\eta) \in H_0^1(\Omega)^2 \times H_0^1(\Omega)^2. \tag{2.1}$$

Then, $(u,\beta) \in H^2(\Omega)^2 \times H^2(\Omega)^2$ and

$$\|u\|_2 + \|\beta\|_2 \leq C\left(\|F\|_0 + \|G\|_0\right),$$

with a constant C independent of F ad G.

Proof. We will resort to additional regularity results from [34, Section 8.6] regarding Dirichlet problems for elliptic systems. In this reference it is proved that the strip of the complex plane $|\mathrm{Re}\,\lambda| \leq 1$ is free of eigenvalues of the Mellin symbol, which implies H^2 regularity for L^2 right hand sides, provided the elliptic system (2.1) is *formally positive*.

Let us recall that *formally positiveness* means in our case that if the bilinear form of the elliptic system is written as follows,

$$a((u,\beta),(v,\eta)) = \sum_{i,j=1}^{2} A_{ij}\,\partial_i U\,\partial_j V, \tag{2.2}$$

with

$$U := \begin{bmatrix} u \\ \beta \end{bmatrix} : \Omega \longrightarrow \mathbb{R}^4, \qquad V := \begin{bmatrix} v \\ \eta \end{bmatrix} : \Omega \longrightarrow \mathbb{R}^4,$$

and $A_{ij} \in \mathbb{R}^{4\times 4}$, then

$$A := \begin{bmatrix} A_{11} & A_{12} \\ A_{21} & A_{12} \end{bmatrix} \in \mathbb{R}^{8\times 8}$$

is a symmetric positive definite matrix.

In our case

$$\begin{aligned} a((u,\beta),(v,\eta)) = {} & \bar{\lambda}_1 (\operatorname{tr}\varepsilon(u), \operatorname{tr}\varepsilon(v)) + 2\bar{\mu}_1 (\varepsilon(u), \varepsilon(v)) \\ & + \bar{\lambda}_2 (\operatorname{tr}\varepsilon(u), \operatorname{tr}\varepsilon(\eta)) + 2\bar{\mu}_2 (\varepsilon(u), \varepsilon(\eta)) \\ & + \bar{\lambda}_2 (\operatorname{tr}\varepsilon(v), \operatorname{tr}\varepsilon(\beta)) + 2\bar{\mu}_2 (\varepsilon(v), \varepsilon(\beta)) \\ & + \bar{\lambda}_3 (\operatorname{tr}\varepsilon(\beta), \operatorname{tr}\varepsilon(\eta)) + 2\bar{\mu}_3 (\varepsilon(\beta), \varepsilon(\eta)), \end{aligned} \tag{2.3}$$

with

$$\begin{aligned} \bar{\lambda}_1 &= \frac{\lambda_1 + \lambda_2}{2}, \qquad \bar{\lambda}_2 = \frac{\lambda_1 - \lambda_2}{8}, \qquad \bar{\lambda}_3 = \frac{\lambda_1 + \lambda_2}{24}, \\ \bar{\mu}_1 &= \frac{\mu_1 + \mu_2}{2}, \qquad \bar{\mu}_2 = \frac{\mu_1 - \mu_2}{8}, \qquad \bar{\mu}_3 = \frac{\mu_1 + \mu_2}{24}. \end{aligned} \tag{2.4}$$

If (2.3) is directly written in the form (2.2), the resulting matrix A is not positive definite. However, using the fact that

$$\begin{aligned} &\int_\Omega \partial_2 u_1 \, \partial_1 \eta_2 = \int_\Omega \partial_1 u_1 \, \partial_2 \eta_2, && \int_\Omega \partial_1 u_2 \, \partial_2 \eta_1 = \int_\Omega \partial_2 u_2 \, \partial_1 \eta_1, \\ &\int_\Omega \partial_2 \beta_1 \, \partial_1 v_2 = \int_\Omega \partial_1 \beta_1 \, \partial_2 v_2, \qquad \text{and} && \int_\Omega \partial_1 \beta_2 \, \partial_2 v_1 = \int_\Omega \partial_2 \beta_2 \, \partial_1 v_1 \end{aligned}$$

(which is proved by a double integration by parts), (2.3) can also be written in the form (2.2) with

$$A_{11} = \begin{bmatrix} \bar{\lambda}_1 + 2\bar{\mu}_1 & 0 & \bar{\lambda}_2 + 2\bar{\mu}_2 & 0 \\ 0 & \bar{\mu}_1 & 0 & \bar{\mu}_2 \\ \bar{\lambda}_2 + 2\bar{\mu}_2 & 0 & \bar{\lambda}_3 + 2\bar{\mu}_3 & 0 \\ 0 & \bar{\mu}_2 & 0 & \bar{\mu}_3 \end{bmatrix}, \quad A_{22} = \begin{bmatrix} \bar{\mu}_1 & 0 & \bar{\mu}_2 & 0 \\ 0 & \bar{\lambda}_1 + 2\bar{\mu}_1 & 0 & \bar{\lambda}_2 + 2\bar{\mu}_2 \\ \bar{\mu}_2 & 0 & \bar{\mu}_3 & 0 \\ 0 & \bar{\lambda}_2 + 2\bar{\mu}_2 & 0 & \bar{\lambda}_3 + 2\bar{\mu}_3 \end{bmatrix},$$

and

$$A_{12} = A_{21}^{\mathrm{t}} = \begin{bmatrix} 0 & \bar{\lambda}_1 + \bar{\mu}_1 & 0 & \bar{\lambda}_2 + \bar{\mu}_2 \\ 0 & 0 & 0 & 0 \\ 0 & \bar{\lambda}_2 + \bar{\mu}_2 & 0 & \bar{\lambda}_3 + \bar{\mu}_3 \\ 0 & 0 & 0 & 0 \end{bmatrix}.$$

There only remains to prove that A is positive definite. With this purpose, we write $A = B_1 + B_2$ with

$$B_1 := \begin{bmatrix} 2\bar{\mu}_1 & 0 & 2\bar{\mu}_2 & 0 & 0 & \bar{\mu}_1 & 0 & \bar{\mu}_2 \\ 0 & \bar{\mu}_1 & 0 & \bar{\mu}_2 & 0 & 0 & 0 & 0 \\ 2\bar{\mu}_2 & 0 & 2\bar{\mu}_3 & 0 & 0 & \bar{\mu}_2 & 0 & \bar{\mu}_3 \\ 0 & \bar{\mu}_2 & 0 & \bar{\mu}_3 & 0 & 0 & 0 & 0 \\ 0 & 0 & 0 & 0 & \bar{\mu}_1 & 0 & \bar{\mu}_2 & 0 \\ \bar{\mu}_1 & 0 & \bar{\mu}_2 & 0 & 0 & 2\bar{\mu}_1 & 0 & 2\bar{\mu}_2 \\ 0 & 0 & 0 & 0 & \bar{\mu}_2 & 0 & \bar{\mu}_3 & 0 \\ \bar{\mu}_2 & 0 & \bar{\mu}_3 & 0 & 0 & 2\bar{\mu}_2 & 0 & 2\bar{\mu}_3 \end{bmatrix}$$

and

$$B_2 := \begin{bmatrix} \bar{\lambda}_1 & 0 & \bar{\lambda}_2 & 0 & 0 & \bar{\lambda}_1 & 0 & \bar{\lambda}_2 \\ 0 & 0 & 0 & 0 & 0 & 0 & 0 & 0 \\ \bar{\lambda}_2 & 0 & \bar{\lambda}_3 & 0 & 0 & \bar{\lambda}_2 & 0 & \bar{\lambda}_3 \\ 0 & 0 & 0 & 0 & 0 & 0 & 0 & 0 \\ 0 & 0 & 0 & 0 & 0 & 0 & 0 & 0 \\ \bar{\lambda}_1 & 0 & \bar{\lambda}_2 & 0 & 0 & \bar{\lambda}_1 & 0 & \bar{\lambda}_2 \\ 0 & 0 & 0 & 0 & 0 & 0 & 0 & 0 \\ \bar{\lambda}_2 & 0 & \bar{\lambda}_3 & 0 & 0 & \bar{\lambda}_2 & 0 & \bar{\lambda}_3 \end{bmatrix}.$$

We observe that B_1 is positive definite. In fact, reordering rows and columns of B_1, we obtain the block diagonal matrix

$$\widehat{B}_1 := \begin{bmatrix} C_1 & O \\ O & C_2 \end{bmatrix},$$

with

$$C_1 := \begin{bmatrix} 2D_1 & D_1 \\ D_1 & 2D_1 \end{bmatrix}, \qquad C_2 := \begin{bmatrix} D_1 & O \\ O & D_1 \end{bmatrix}, \qquad \text{and} \qquad D_1 := \begin{bmatrix} \bar{\mu}_1 & \bar{\mu}_2 \\ \bar{\mu}_2 & \bar{\mu}_3 \end{bmatrix}.$$

Using (2.4), it is simple to show that $\bar{\mu}_1\bar{\mu}_3 - \bar{\mu}_2^2 > 0$. Hence, D_1 is positive definite. Therefore, elementary computations show that C_1, C_2, and consequently $\widehat{B}_1$ and B_1, are positive definite, too.

On the other hand, B_2 is positive semi-definite. In fact, reordering rows and columns of B_2, we obtain

$$\widehat{B}_2 = \begin{bmatrix} C_3 & O \\ O & O \end{bmatrix}, \qquad \text{with} \qquad C_3 := \begin{bmatrix} D_2 & D_2 \\ D_2 & D_2 \end{bmatrix} \qquad \text{and} \qquad D_2 := \begin{bmatrix} \bar{\lambda}_1 & \bar{\lambda}_2 \\ \bar{\lambda}_2 & \bar{\lambda}_3 \end{bmatrix}.$$

The matrix D_2 is positive definite because, using again (2.4), we have $\overline{\lambda}_1\overline{\lambda}_3 - \overline{\lambda}_2^2 > 0$. Therefore, C_3 and consequently $\widehat{B}_2$ and B_2 are positive semi-definite, too. Thus, $A = B_1 + B_2$ is positive definite and we conclude the proof. □

Now we are in a position to prove that the solutions of the load problems for laminated and classical homogeneous Reissner-Mindlin clamped plates have the same regularity. With this aim, we adapt the arguments from the proof of [2, Theorem 7.1].

For any $t > 0$ and $(f,m,g) \in H$, let $(u,\beta,w) \in V$ and $\gamma \in L^2(\Omega)$ be the solution to

$$\begin{cases} a((u,\beta),(v,\eta)) + (\gamma, \eta - \nabla z) = (f,v) + (m,\eta) + (g,z) \quad \forall (v,\eta,z) \in V, \\ \gamma = \dfrac{\kappa}{t^2}(\beta - \nabla w). \end{cases} \tag{2.5}$$

Consider the Helmholtz decomposition of the shear term $\gamma \in H_0(\mathrm{rot},\Omega)$:

$$\gamma = \nabla r + \mathrm{curl}\, p. \tag{2.6}$$

with $r \in H_0^1(\Omega)$ and $p \in H^1(\Omega)/\mathbb{R}$. Using this decomposition in (2.5), this problem turns out equivalent to finding $r, w \in H_0^1(\Omega)$, $u, \beta \in H_0^1(\Omega)^2$, and $p \in H^1(\Omega)/\mathbb{R}$ such that

$$-(\nabla r, \nabla z) = (g,z) \qquad \forall z \in H_0^1(\Omega), \tag{2.7}$$

$$a((u,\beta),(v,\eta)) + (\mathrm{curl}\, p, \eta) = (f,v) + (m,\eta) - (\nabla r, \eta) \qquad \forall (v,\eta) \in H_0^1(\Omega)^2 \times H_0^1(\Omega)^2, \tag{2.8}$$

$$(\beta, \mathrm{curl}\, q) - \frac{t^2}{\kappa}(\mathrm{curl}\, p, \mathrm{curl}\, q) = 0 \qquad \forall q \in H^1(\Omega)/\mathbb{R}, \tag{2.9}$$

$$(\nabla w, \nabla s) = (\beta, \nabla s) - \frac{t^2}{\kappa}(\nabla r, \nabla s) \qquad \forall s \in H_0^1(\Omega). \tag{2.10}$$

This is a well posed problem. In fact, first, r is the unique solution to the Dirichlet problem (2.7). Then, subtracting (2.9) from (2.8), since $t > 0$, existence and uniqueness of (u,β) and p follows from Lax-Milgram lemma. Finally, w is the solution to the well posed problem (2.10).

For $t = 0$, equations (2.7)–(2.10) also make sense, but the terms $(\mathrm{curl}\, p, \eta)$ from (2.8) and $(\beta, \mathrm{curl}\, q)$ from (2.9) must be understood weakly. Thus, in this case, we are led to finding $r_0, w_0 \in H_0^1(\Omega)$, $u_0, \beta_0 \in H_0^1(\Omega)^2$, and $p_0 \in L^2(\Omega)/\mathbb{R}$ such that

$$-(\nabla r_0, \nabla z) = (g,z) \qquad \forall z \in H_0^1(\Omega), \tag{2.11}$$

$$a((u_0,\beta_0),(v,\eta)) + (p_0, \mathrm{rot}\, \eta) = (f,v) + (m,\eta) - (\nabla r_0, \eta) \qquad \forall (v,\eta) \in H_0^1(\Omega)^2 \times H_0^1(\Omega)^2, \tag{2.12}$$

$$(\mathrm{rot}\, \beta_0, q) = 0 \qquad \forall q \in L^2(\Omega)/\mathbb{R}. \tag{2.13}$$

$$(\nabla w_0, \nabla s) = (\beta_0, \nabla s) \qquad \forall s \in H_0^1(\Omega). \tag{2.14}$$

This is a well posed problem, too. In fact, equations (2.11) and (2.7) are the same, so that $r_0 = r$, as well. Existence and uniqueness of (u_0, β_0) and p_0 follows from the fact that (2.12)–(2.13) is a well posed mixed problem (a is elliptic in the whole space and the *inf-sup* condition is essentially the same as that of the Stokes problem). Finally w_0 is the solution of the Dirichlet problem (2.14). Moreover the following additional regularity holds.

Lemma 2.6.2 *Let $(r_0, u_0, \beta_0, p_0, w_0)$ be the solution to problem (2.11)–(2.14). Then, we have that $r_0, w_0 \in H^2(\Omega)$, $u_0, \beta_0 \in H^2(\Omega)^2$, $p_0 \in H^1(\Omega)$, and*

$$\|r_0\|_2 + \|u_0\|_2 + \|\beta_0\|_2 + \|p_0\|_1 + \|w_0\|_2 \leq C \|(f, m, g)\|_0 , \tag{2.15}$$

with a constant C independent of f, m, and g.

Proof. The standard *a priori* estimate for the Poisson equation on a convex domain, implies that $r_0 \in H^2(\Omega)$ and

$$\|r_0\|_2 \leq C \|g\|_0 . \tag{2.16}$$

Next, we write (2.12)–(2.13) in the distributional sense:

$$\begin{cases} -\bar{\mu}_1 \Delta u_0 - \left(\bar{\lambda}_1 + \bar{\mu}_1\right) \nabla (\operatorname{div} u_0) - \bar{\mu}_2 \Delta \beta_0 - \left(\bar{\lambda}_2 + \bar{\mu}_2\right) \nabla (\operatorname{div} \beta_0) = f, \\ -\bar{\mu}_2 \Delta u_0 - \left(\bar{\lambda}_2 + \bar{\mu}_2\right) \nabla (\operatorname{div} u_0) - \bar{\mu}_3 \Delta \beta_0 - \left(\bar{\lambda}_3 + \bar{\mu}_3\right) \nabla (\operatorname{div} \beta_0) \\ \qquad\qquad + \operatorname{curl} p_0 = m - \nabla r_0, \\ \operatorname{rot} \beta_0 = 0, \end{cases}$$

with Dirichlet homogeneous boundary conditions for u_0 and β_0 and the coefficients $\bar{\lambda}_i$ and $\bar{\mu}_i$, $i = 1, 2, 3$, as defined in (2.4).

The third equation above implies that $\beta_0 = \nabla \varphi$, with $\varphi \in H_0^1(\Omega)$ such that $\frac{\partial \varphi}{\partial n} = 0$ on $\partial\Omega$. Using this in the first and second equations, we obtain

$$-\bar{\mu}_1 \Delta u_0 - \left(\bar{\lambda}_1 + \bar{\mu}_1\right) \nabla (\operatorname{div} u_0) - \left(\bar{\lambda}_2 + 2\bar{\mu}_2\right) \Delta (\nabla \varphi) = f, \tag{2.17}$$

$$-\bar{\mu}_2 \Delta u_0 - \left(\bar{\lambda}_2 + \bar{\mu}_2\right) \nabla (\operatorname{div} u_0) - \left(\bar{\lambda}_3 + 2\bar{\mu}_3\right) \Delta (\nabla \varphi) + \operatorname{curl} p_0 = m - \nabla r_0, \tag{2.18}$$

with homogeneous boundary conditions $u_0 = 0$, $\beta_0 = 0$, $\varphi = 0$ and $\frac{\partial \varphi}{\partial n} = 0$ on $\partial\Omega$.

Taking divergence in the first two equations, we have

$$\begin{aligned} -\left(\bar{\lambda}_1 + 2\bar{\mu}_1\right) \operatorname{div} (\Delta u_0) - \left(\bar{\lambda}_2 + 2\bar{\mu}_2\right) \Delta^2 \varphi &= \operatorname{div} f, \\ -\left(\bar{\lambda}_2 + 2\bar{\mu}_2\right) \operatorname{div} (\Delta u_0) - \left(\bar{\lambda}_3 + 2\bar{\mu}_3\right) \Delta^2 \varphi &= \operatorname{div} m - \Delta r_0. \end{aligned}$$

Eliminating u_0 we arrive at the following problem for φ:

$$\begin{cases} K\Delta^2\varphi = \left(\bar{\lambda}_2 + 2\bar{\mu}_2\right) \operatorname{div} f - \left(\bar{\lambda}_1 + 2\bar{\mu}_1\right) (\operatorname{div} m - \Delta r_0) \in H^{-1}(\Omega), \\ \varphi = \dfrac{\partial \varphi}{\partial n} = 0 \quad \text{on } \partial\Omega. \end{cases}$$

with $K := \left(2\bar{\mu}_1 + \bar{\lambda}_1\right)\left(2\bar{\mu}_3 + \bar{\lambda}_3\right) - \left(2\bar{\mu}_2 + \bar{\lambda}_2\right)^2$, which can be shown to be strictly positive by using (2.4) and a little algebra. Therefore, from the standard *a priori* estimate for the biharmonic equation in convex domains, we know that $\varphi \in H^3(\Omega)$ and

$$\|\varphi\|_3 \leq C \left(\|\operatorname{div} f\|_{-1} + \|\operatorname{div} m\|_{-1} + \|\Delta r_0\|_0 \right) \leq C \|(f, m, g)\|_0 ,$$

where we have used (2.16) for the last inequality. Therefore $\beta_0 = \nabla\varphi \in H^2(\Omega)^2$.

Next, using the last inequality in (2.17), we obtain from the usual *a priori* estimate for the elasticity problem in a polygonal convex domain that $u_0 \in H^2(\Omega)^2$ and

$$\|u_0\|_2 \leq C \|(f, m, g)\|_0 .$$

Now, from this inequality and (2.18), we obtain that $p_0 \in H^1(\Omega)$ and the corresponding estimate. Finally, the regularity of w_0 follows again from the standard *a priori* estimate for the Poisson equation on a convex domain applied to (2.14). Thus we conclude the proof. □

Corollary 2.6.1 *The solution of the limit problem (2.4) satisfies $u_0, \beta_0 \in H^2(\Omega)^2$, $w_0 \in H^2(\Omega)$, $\gamma_0 \in L^2(\Omega)^2$, and the a priori estimate (2.5) holds true.*

Proof. In this case, the Helmholtz decomposition (2.6) holds in a distributional sense (cf. [10, Proposition 3.4]):

$$\gamma_0 = \nabla r_0 + \operatorname{curl} p_0,$$

with $r_0 \in H_0^1(\Omega)$ and $p_0 \in L^2(\Omega)/\mathbb{R}$. Then, problem (2.4) is equivalent to (2.11)–(2.14), with $f = m = 0$. Hence, the additional regularity result follows from Lemma 2.6.2 and the above equation. □

Now we are ready to prove the *a priori* estimate for the solution to problem (2.7)–(2.10) and, consequently, to that of problem (2.5), which is the main goal of this Appendix.

Lemma 2.6.3 *For any $t > 0$, let (r, u, β, p, w) be the solution to problem (2.7)–(2.10). Then, $r, w, p \in H^2(\Omega)$, $u, \beta \in H^2(\Omega)^2$, and*

$$\|r\|_2 + \|u\|_2 + \|\beta\|_2 + \|p\|_1 + t\,\|p\|_2 + \|w\|_2 \leq C \left(\|f\|_0 + \|m\|_0 + \|g\|_0 \right),$$

with a constant C independent of t, f, m, and g.

Proof. Let $(r_0, u_0, \beta_0, p_0, w_0)$ be the solution to problem (2.11)–(2.14). Recall that $r = r_0$, so that we have already proved in Lemma 2.6.2 the estimate for r (cf. (2.16)).

Now, since according to Lemma 2.6.2, $p_0 \in H^1(\Omega)$, from (2.8)–(2.9) and (2.12)–(2.13), we obtain

$$a((u-u_0, \beta-\beta_0), (v, \eta)) + (\operatorname{curl}(p-p_0), \eta) - (\beta-\beta_0, \operatorname{curl} q) + \frac{t^2}{\kappa}(\operatorname{curl}(p-p_0), \operatorname{curl} q) = -\frac{t^2}{\kappa}(\operatorname{curl} p_0, \operatorname{curl} q)$$

for all $v, \eta \in H_0^1(\Omega)^2$ and all $q \in H^1(\Omega)/\mathbb{R}$. Testing this equation with $v := u - u_0$, $\eta := \beta - \beta_0$, and $q =: p - p_0$ and using the ellipticity of a, we have

$$\|u-u_0\|_1^2 + \|\beta-\beta_0\|_1^2 + t^2\|p-p_0\|_1^2 \le Ct^2\|p_0\|_1\|p-p_0\|_1$$

and, from this estimate and (2.15), we arrive at

$$\|u-u_0\|_1 + \|\beta-\beta_0\|_1 + t\|p-p_0\|_1 \le Ct\|(f,m,g)\|_0. \tag{2.19}$$

Hence also

$$\|p\|_1 \le \|p-p_0\|_1 + \|p_0\|_1 \le C\|(f,m,g)\|_0. \tag{2.20}$$

Next, we apply Lemma 2.6.1 to (2.8) with $F := f$ and $G := m - \nabla r - \operatorname{curl} p$, to show that $u, \beta \in H^2(\Omega)^2$ and

$$\|u\|_2 + \|\beta\|_2 \le C\|(f,m,g)\|_0,$$

where we have used (2.16) and (2.20).

On the other hand, from (2.9) and (2.13), we have that

$$(\operatorname{curl} p, \operatorname{curl} q) = \frac{\kappa}{t^2}(\beta-\beta_0, \operatorname{curl} q) = (\operatorname{rot}(\beta-\beta_0), q) \qquad \forall q \in H^1(\Omega).$$

Therefore, p is the solution of the Neumann problem

$$\begin{cases} \Delta p = \dfrac{\kappa}{t^2}\operatorname{rot}(\beta-\beta_0) & \text{in } \Omega, \\ \dfrac{\partial p}{\partial n} = 0 & \text{on } \partial\Omega. \end{cases}$$

Hence, since Ω is convex we have

$$\|p\|_2 \le Ct^{-2}\|\beta-\beta_0\|_1 \le Ct^{-1}\|(f,m,g)\|_0,$$

the last inequality because of (2.19).

Finally, (2.10) is a Poisson equation, for which there holds the *a priori* estimate

$$\|w\|_2 \le C\left(\|\beta\|_1 + t^2\|r\|_2\right) \le C\|(f,m,g)\|_0,$$

where we have used (2.16) once more. Thus we end the proof. □

We conclude with the main result of this Appendix.

Theorem 2.6.1 *Let Ω be a convex polygonal domain in the plane. For any $t > 0$ and $(f,m,g) \in H$, let $(u,\beta,w) \in V$ and $\gamma \in L^2(\Omega)$ be the solution to problem (2.5). Then, $u,\beta \in H^2(\Omega)^2$, $w \in H^2(\Omega)$, $\gamma \in H^1(\Omega)^2$, and there exists a constant C, independent of t and (f,m,g), such that*

$$\|u\|_2 + \|\beta\|_2 + \|w\|_2 + \|\gamma\|_0 + t\,\|\gamma\|_1 \leq C\,(\|f\|_0 + \|m\|_0 + \|g\|_0)\,.$$

Proof. This is an immediate consequence of Lemma 2.6.3 and the equivalence between problems (2.5) and (2.7)–(2.10), through (2.6). □

Corollary 2.6.2 *The solution of the load problem (2.2) satisfies $u,\beta \in H^2(\Omega)^2$, $w \in H^2(\Omega)$, $\gamma \in H^1(\Omega)^2$, and the a priori estimate (2.3) holds true.*

Proof. It is a direct application of the previous theorem to the particular right hand side of the first equation from (2.2). □

Chapter 3

A finite element method for a stiffened plate problem

The aim of this paper is to analyze a low order mixed finite element method for a stiffened plate modeled by the Reissner-Mindlin equations. The plate is modeled by Reissner Mindlin equations and the stiffener by Timoshenko beams equations. The resulting problem is shown to be well posed. In the case of concentric stiffeners it decouples into two problems, one for the in-plane plate deformation and the other for the bending of the plate. The analysis and discretization of the first one is straightforward. The second one is shown to attain a solution bounded above and below independently of the thickness of the plate. A discretization based on DL3 finite elements combined with *ad-hoc* elements for the stiffener is proposed. Optimal order error estimates are proved for displacements, rotations and shear stresses for the plate and the stiffener. Numerical tests are reported in order to assess the performance of the method. These numerical computations demonstrate that the error estimates are independent of the thickness, providing a numerical evidence that the method is locking free.

3.1 Introduction

A stiffened plates is a plate reinforced with ribs to increase it capacity to resist loads. Such plates are applied usually in buildings, hulls of ships, aircraft and many other applications in the structural engineering.

Different models of stiffeners plates have been used. See for instance [28] for a discussion of several simple engineering models and further references.

A different approach has been proposed in [40]. It consists of coupling Kirchhoff-Love equations for the plate with Navier-Bernoulli equations for the stiffener. The constraint between both structures are imposed by means of Lagrange multipliers. A particular finite

element method is proposed. Numerical experiments demonstrate the effectivity of this approach although no analysis is given.

The same problem has been analyzed in [19] based in a model proposed in [30]. In this case HCT $\mathscr{C}^1$ elements are proposed for the plate combined with $\mathscr{P}_2 - \mathscr{P}_3$ elements for the beam. A domain decomposition technique is proposed for the solution of the resulting algebraic problem. An alternative modeling approach consist of using Reissner-Mindlin equation for the plate and Timoshenko beam equations for the stiffener. This model has been considered in [38], where an elementary finite element method is proposed. However this method is shown to suffer from locking.

Locking consists in that very unsatisfactory results are obtained when the thickness is small with respect to the other dimension of the structure. From the point of view of the numerical analysis, locking reveals itself in that the *a priori* estimates depends on the thickness of the structure in a such way that they degenerate when this parameter become small.

Several finite element have been proposed to avoid locking in Reissner-Mindlin equations (See [11] for a review on this subject).

A typical locking-free finite element method MITC9 ([8]) is proposed in [28] to discretize the stiffened plate equations. These elements are combined with standard quadratic element for the stiffener. Once more, only numerical evidence of the performance of the method is reported.

In the present paper we use the same model , based on Reissner-Mindlin equations for the plate and Timoshenko equations for the stiffener. We introduce the constraint between both structures by means of Lagrange multipliers. We prove existence and uniqueness of solution to the resulting problem.

The case that the mid-line of the stiffener lies on the mid-surface of the plate is known as *concentrically* stiffened. In this case the problem decomposes into two simpler as it happens for unstiffened plates: *in-plane* and *bending* plate problems. The analysis of the former is quite simpler since it leads to equation independent of the plate thickness. This is not the case for the stiffened plate bending problem.

In this case we consider a family of problems parameterized by the plate thickness t. We show that the mechanical coefficients of the stiffener must be taken as proportional to $1/t$ to obtain a significant limit problem as t goes to zero. We show that the solution of the stiffened plate bending problem is bounded above and below far from zero independent of t. We also prove additional regularity of the solution although not independently of t.

For the discretization of the in-plane stiffened plate we use standard linear elements, and the analysis is straightforward. For the stiffened plate bending problem we use a low order plate finite element, DL3 ([22]), combined with $\mathscr{P}_2 - \mathscr{P}_1$ element for the stiffener. The choice of this hybrid element for the rod allow us to impose the constraints in an

simpler way.

We prove optimal order error estimates depending on higher order norms of the solution. These higher order norms are the same that appear in the case of uncoupled plates and rods. In such case they are bounded independently of t.

For the stiffened plate bending problem these higher norms have been proved to be finite, but not bounded independently of t. Therefore, we have made a thorough numerical experimentation to assess the locking-free character of the method.

The outline of the paper is as follows. In Section 3.2 we present the mathematical setting of the load problem and prove existence and uniqueness. In Section 3.3 we analyze for the *concentrically* stiffened plate, the stability results, the latter independent of the plate thickness for the in-plane and bending plate problems. In section 3.4 we present the finite element discretization, and the existence and uniqueness of the solution for the in-plane and bending plate problems. In the section 3.5 we prove error estimates of the numerical solution. In section 3.6 we report numerical results to assess the performance of the proposed method. First to validate our codes, we have applied it to a vibration problem which was also solved in [28]. Secondly we have applied our method to a couple of problems whose limit behavior as the thickness becomes small is known. Finally we apply the proposed method to a family of problems which allow us to demonstrate that it is locking-free.

3.2 The Problem of the Stiffened Plate

We consider a plate entirely crossed by a rod which act as a stiffener. We restrict our attention to plates with constant thickness and rods with uniform cross section. If the mid-line of the rod lies on the mid surface of the plate we call it a *concentrically stiffened plate*. Otherwise it is called an *eccentrically stiffened plate* (see Figure 3.1). Most of this

Figure 3.1: Transverse sections of concentrically (left) and eccentrically (right) stiffened plates.

paper is devoted to concentrically stiffened plates except for the present section which is valid for eccentrically stiffened plates too. We consider a coordinate system such that the plate occupies the domain $\Omega \times (-t/2, t/2)$, where $t > 0$ is the plate thickness. The two-dimensional domain is the mid surface of the plate and is assumed polygonal. Moreover

we assume that the coordinate system is such that the mid-line of the rod lies on the plane $y = 0$. We denote $\Gamma := \{(x,y) \in \Omega : y = 0\}$ and $r > 0$ the distance between the rod mid-line and the plate mid surface ($r = 0$ for concentrically stiffened plates). We denote also

$$\Omega_1 := \{(x,y) \in \Omega : y > 0\}, \qquad \Omega_2 := \{(x,y) \in \Omega : y < 0\}. \tag{3.1}$$

We illustrate these definitions in Figure 3.2. We restrict our analysis to the case of a plate modeled by Reissner-Mindlin equations and completely clamped by its lateral boundary $\partial\Omega$. We denote by $u = (u_1, u_2)$, w and $\beta = (\beta_1, \beta_2)$ the mid surface in-plane plate dis-

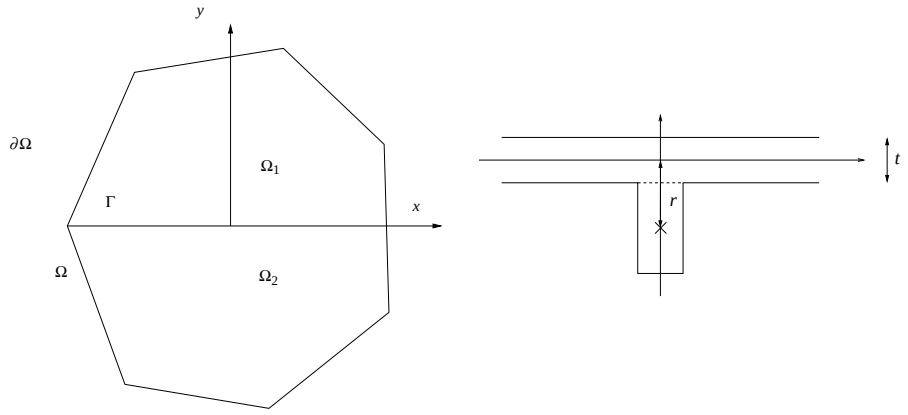

Figure 3.2: Geometry of stiffened plate

placements, transversal displacements and rotations, respectively. In its turn, also u^s, v^s, w^s denote the stiffener displacements in each coordinate direction and, θ_x^s, θ_y^s and θ_z^s the stiffener rotations with respect to each axis.

To derive the equations of the stiffened plate we will obtain first an expression for its total energy. With this aim, we add the corresponding energies of the plate and the stiffener. However, for the latter, the shear and bending terms in the plane of the plate are typically neglected. (see [28]). We consider a load acting on the plate, and denote by f its in-plane component, and by g the transverse one. Therefore the total energy including the works of the loads reads:

$$\begin{aligned} E_t := \frac{t}{2} a_1(u,u) + \frac{t^3}{2} a_2(\beta,\beta) + t\int_\Omega \kappa\mu\,(\nabla w - \beta)^2 + \int_\Gamma E^s A \left(\frac{du^s}{dx}\right)^2 \\ + \int_\Gamma \kappa^s \mu^s A \left(\frac{dw^s}{dx} + \theta_y^s\right)^2 + \int_\Gamma E^s I_{yy} \left(\frac{d\theta_y^s}{dx}\right)^2 + \int_\Gamma \mu^s J \left(\frac{d\theta_x^s}{dx}\right)^2 \\ - t\int_\Omega f \cdot u - \int_\Omega g w. \end{aligned}$$

In the above equation

$$a_1(u,v) := \int_\Omega \frac{E\nu}{(1+\nu)(1-2\nu)} \operatorname{div} u \ \operatorname{div} v + \int_\Omega \frac{E}{1+\nu} \varepsilon(u) : \varepsilon(v)$$

and

$$a_2(\beta,\eta) := \frac{1}{12}\left\{ \int_\Omega \frac{E\nu}{1-\nu^2} \operatorname{div}\beta \ \operatorname{div}\eta + \int_\Omega \frac{E}{1+\nu} \varepsilon(\beta) : \varepsilon(\eta) \right\}$$

are the plane strain and plane stress bilinear forms, respectively. The operator $\varepsilon(v) := \frac{1}{2}(Dv + Dv^t)$, the coefficients E and ν are the Young and Poisson moduli. Moreover $\mu := \frac{E}{2(1+\nu)}$ is the shear modulus of the plate. In its turn, A is the area of the stiffener section, I_{yy} and I_{zz} are the second moments of area with respect to y- and z-axes, respectively, $J := I_{yy} + I_{zz}$, E^{s} and ν^{s} the Young and Poisson moduli of the stiffener and $\mu^{\mathrm{s}} := \frac{E^{\mathrm{s}}}{2(1+\nu)}$ the shear modulus. Finally κ and κ^{s} are the shear correction factors for the plate and the rod, respectively . All the parameters are strictly positive constants. In the case of the stiffener this corresponds to a rod of arbitrary section, the same for all $(x,0) \in \Gamma$. Notice that, since the bending and shear energy of the stiffener have been neglected, the variables v^{s} and θ_z do not appear in the expression for the total energy.

The appropriate functional spaces for displacements and rotations are the following. $u, \beta \in H_0^1(\Omega)^2$; $w \in H_0^1(\Omega)$; $u^{\mathrm{s}}, w^{\mathrm{s}}, \theta_x^{\mathrm{s}}, \theta_y^{\mathrm{s}} \in H_0^1(\Gamma)$. For the loads we consider $f \in L^2(\Omega)^2$ and $g \in L^2(\Omega)$.

The stiffened plate problem is obtained by minimizing the total energy subject to the following kinematic constraints:

$$u_1 = u^{\mathrm{s}} - r\beta_1, \tag{3.2}$$

$$w = w^{\mathrm{s}}, \tag{3.3}$$

$$\beta_2 = \theta_x^{\mathrm{s}}, \tag{3.4}$$

$$\beta_1 = -\theta_y^{\mathrm{s}}. \tag{3.5}$$

Let us recall that r in the first constraint denotes the transverse distance between the mid surface of the plate the mid-line of the stiffener. The constraint (3.3) comes from the fact that the plate end the rod are joint monolithically. Moreover the rotations of the plate and the stiffener are the same in this model, which leads to (3.4) and (3.5). Finally (3.2) can be easily deduced from the previous constraints. In fact, using the notation from Figure 3.3, we have that

$$\frac{u_1}{r+e} = \frac{u^{\mathrm{s}}}{e}.$$

Therefore approximating $-\beta_1$ by $\frac{u^{\mathrm{s}}}{e}$, straightforward computations lead to (3.2). For the

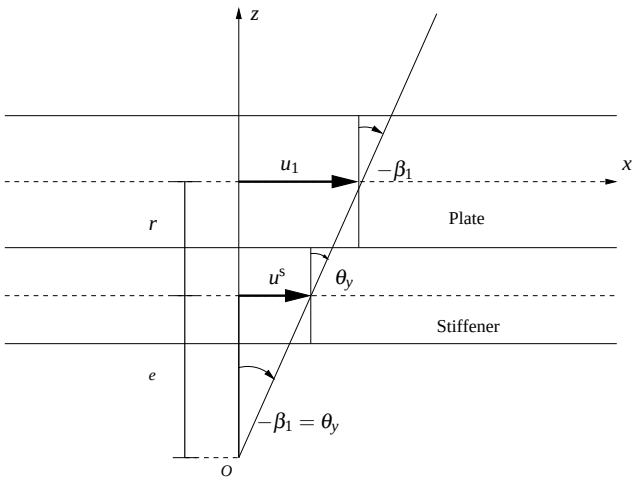

Figure 3.3: Geometric illustration of (3.6)

analysis, we introduce these constraints by means of Lagrange multipliers as follows:

$$\int_\Gamma \lambda_1 \left(u_1 - u^s + r\beta_1\right) = 0, \tag{3.6}$$

$$\int_\Gamma \lambda_2 \left(w - w^s\right) = 0, \tag{3.7}$$

$$\int_\Gamma \lambda_3 \left(\beta_2 - \theta_x^s\right) = 0, \tag{3.8}$$

$$\int_\Gamma \lambda_4 \left(\beta_1 + \theta_y^s\right) = 0. \tag{3.9}$$

In the expressions above and throughout the paper, to simplify the notation, we write:

$$\int_\Gamma \lambda\, \eta := \langle \lambda, \eta \rangle_{H^{-1/2}(\Gamma) \times H_{00}^{1/2}(\Gamma)},$$

where in this case $H_{00}^{1/2}(\Gamma) := \left\{ v|_\Gamma : v \in H_0^1(\Omega) \right\}$ endowed with the intrinsic norm of $H^{1/2}(\Gamma)$ (see ([26]) and $H^{-1/2}(\Gamma) := H_{00}^{1/2}(\Gamma)'$, with $L^2(\Gamma)$ as pivot space.

Therefore, by minimizing E_t subject to the constraints (3.2)-(3.5), we arrive at the following *clamped stiffened plate problem*:

Find $(U, \lambda) \in \mathscr{H} \times \mathscr{Q}$, such that

$$\mathscr{A}(U,V) + \mathscr{B}(V,\lambda) = \mathscr{F}(V) \qquad \forall V \in \mathscr{H}, \tag{3.10}$$

$$\mathscr{B}(U,\chi) = 0 \qquad \forall \chi \in \mathscr{Q}, \tag{3.11}$$

where

$$\begin{aligned}
&\mathscr{H} := H_0^1(\Omega)^2 \times H_0^1(\Omega)^2 \times H_0^1(\Omega) \times H_0^1(\Gamma)^4,\ \mathscr{Q} := H^{-1/2}(\Gamma)^4,\\
&U := \left(u, \beta, w, u^{\mathrm{s}}, w^{\mathrm{s}}, \theta_x^{\mathrm{s}}, \theta_y^{\mathrm{s}}\right),\ V := \left(v, \eta, z, z^{\mathrm{s}}, v^{\mathrm{s}}, \varphi_x^{\mathrm{s}}, \varphi_y^{\mathrm{s}}\right) \in \mathscr{H}\\
&\lambda := (\lambda_1, \lambda_2, \lambda_3, \lambda_4),\ \chi := (\chi_1, \chi_2, \chi_3, \chi_4) \in \mathscr{Q}.
\end{aligned}$$

$$\begin{aligned}
\mathscr{A}(U,V) :=\ & t a_1(u,v) + t^3 a_2(\beta,\eta) + t\int_\Omega \kappa\mu\,(\nabla w - \beta)\cdot(\nabla z - \eta)\\
&+ \int_\Gamma E^{\mathrm{s}} A \frac{du^{\mathrm{s}}}{dx}\frac{dv^{\mathrm{s}}}{dx} + \kappa^{\mathrm{s}}\mu^{\mathrm{s}}\int_\Gamma A\left(\frac{dw^{\mathrm{s}}}{dx} + \theta_y^{\mathrm{s}}\right)\left(\frac{dz^{\mathrm{s}}}{dx} + \varphi_y^{\mathrm{s}}\right)\\
&+ \int_\Gamma E^{\mathrm{s}} I_{yy}\frac{d\theta_y^{\mathrm{s}}}{dx}\frac{d\varphi_y^{\mathrm{s}}}{dx} + \mu^{\mathrm{s}}\int_\Gamma J\frac{d\theta_x^{\mathrm{s}}}{dx}\frac{d\varphi_x^{\mathrm{s}}}{dx},\\
\mathscr{B}(U,\lambda) :=\ & \int_\Gamma \lambda_1(u_1 - u^{\mathrm{s}} + r\beta_1) + \int_\Gamma \lambda_2(w - w^{\mathrm{s}}) + \int_\Gamma \lambda_3(\beta_2 - \theta_x^{\mathrm{s}})\\
&+ \int_\Gamma \lambda_4\left(\beta_1 + \theta_y^{\mathrm{s}}\right),\\
\mathscr{F}(V) :=\ & t\int_\Omega f\cdot v + t\int_\Omega g z.
\end{aligned}$$

It is well known that the standard finite element methods applied to plates or rods are subject to "numerical locking". This means they lead to unacceptable poor results for thin structures, unless the mesh size is excessively small. The standard methodology to deal with locking-free methods is to consider a family of problems depending on a small parameter: the plate thickness t. A method will be locking-free if the error estimates do not deteriorate as the thickness becomes small. In our case, to avoid dealing with more than one parameter, we restrict our attention to a stiffener such that

$$A = t^2\tilde{A}, \qquad I_{yy} = t^4\tilde{I}_{yy} \qquad \text{and} \qquad J = t^4\tilde{J}, \tag{3.12}$$

where $\tilde{A}$, $\tilde{I}_{yy}$ and $\tilde{J}$ are constants. This corresponds to a rod section with width and height proportional to t.

The stiffening effect of such a rod tends to disappear as t tends to zero. To avoid this and obtaining a proper limit problem, we assume that the physical parameters of the rod increase as t tends to zero. More precisely we assume that

$$E^{\mathrm{s}} = \frac{\tilde{E}^{\mathrm{s}}}{t}, \tag{3.13}$$

where $\tilde{E}^{\mathrm{s}}$ is a fixed constant. See [19] for a similar choice in the case of Kirchhoff stiffened plates.

Scalings (3.12) and (3.13) ensure that if the loads are scaled as usual for plates, then the solution of problem (3.10)-(3.11) attains a limit as t tends to zero and that, in the limit

problem, the rod remains as a stiffener. This will be clearly seen in the numerical examples of Section 3.6, where different scalings of the physical parameters are considered. It is shown therein that (3.13) leads to a stiffened limit problem (Test 4) whereas other scalings lead either to a vanishing or to a perfectly rigid stiffener (Section 3.6.2). Using these scalings we write the bilinear form $\mathscr{A}$ as follows:

$$\begin{aligned}\mathscr{A}(U,V) = {} & t a_1(u,v) + t^3 a_2(\beta,\eta) + t\int_\Omega \kappa\mu\,(\nabla w-\beta)\cdot(\nabla z-\eta) \\ & + t\int_\Gamma \tilde{E}^s\tilde{A}\frac{du^s}{dx}\frac{dv^s}{dx} + t\int_\Gamma \kappa^s\tilde{\mu}^s\tilde{A}\left(\frac{dw^s}{dx}+\theta_y^s\right)\left(\frac{dz^s}{dx}+\varphi_y^s\right) \\ & + t^3\int_\Gamma \tilde{E}^s\tilde{I}_{yy}\frac{d\theta_y^s}{dx}\frac{d\varphi_y^s}{dx} + t^3\int_\Gamma \tilde{\mu}^s\tilde{J}\frac{d\theta_x^s}{dx}\frac{d\varphi_x^s}{dx} \end{aligned} \tag{3.14}$$

We are interested in showing the existence and uniqueness of the solution to the problem defined by (3.10) and (3.11). For this purpose we will show the ellipticity of $\mathscr{A}(\cdot,\cdot)$ in whole the space $\mathscr{H}$ and the inf-sup condition for $\mathscr{B}(\cdot,\cdot)$ in the appropriates spaces. The ellipticity of $\mathscr{A}(\cdot,\cdot)$ will depend on t.

Throughout the paper, C will denote a strictly positive constant, not necessarily the same at each occurrence, but always independent of t and the mesh-size h, which will be introduced in the next section.

For the existence and uniqueness, we consider the continuous problem (3.10)-(3.11) with $0 < t \leq 1$ fixed. The bilinear form $\mathscr{A}(\cdot,\cdot)$ is elliptic in $\mathscr{H}$, with an ellipticity constant depending of t:

$$\begin{aligned}\mathscr{A}(V,V) \geq {} & Ct^3\left\{\|\eta\|_{1,\Omega}^2 + \|z\|_{1,\Omega}^2 + \left\|\varphi_y^s\right\|_{1,\Omega}^2 + \|z^s\|_{1,\Omega}^2 + \|\varphi_x^s\|_{1,\Gamma}^2\right\} \\ & + Ct\left\{\|v\|_{1,\Omega}^2 + \|v^s\|_{1,\Gamma}^2\right\}.\end{aligned}$$

In fact, the inequality above follows from

$$ta_1(v,v) \geq Ct\|v\|^2_{1,\Omega} \qquad \forall v \in H^1_0(\Omega)^2, \tag{3.15}$$

$$a_2(\eta,\eta) \geq C\|\eta\|^2_{1,\Omega} \qquad \forall \eta \in H^1_0(\Omega)^2, \tag{3.16}$$

$$t^3 a_2(\eta,\eta) + \kappa\mu t \int_\Omega \kappa\mu\,|\nabla z - \eta|^2 \geq Ct^3\left\{\|\eta\|^2_{1,\Omega} + \|z\|^2_{1,\Omega}\right\}$$
$$\forall \eta \in H^1_0(\Omega)^2, z \in H^1_0(\Omega), \tag{3.17}$$

$$t\int_\Gamma \tilde{E}^s\tilde{A}\left(\frac{dv^s}{dx}\right)^2 \geq Ct\|v^s\|^2_{1,\Gamma} \qquad \forall v^s \in H^1_0(\Gamma), \tag{3.18}$$

$$t^3\int_\Gamma \tilde{\mu}^s\tilde{J}\left(\frac{d\varphi^s_x}{dx}\right)^2 \geq Ct^3\|\varphi^s_x\|^2_{1,\Gamma} \qquad \forall \varphi^s_x \in H^1_0(\Gamma), \tag{3.19}$$

$$t^3\int_\Gamma \tilde{E}^s\tilde{I}_{yy}\left(\frac{d\varphi^s_y}{dx}\right)^2 + t\int_\Gamma \kappa^s\tilde{\mu}^s\tilde{A}\left|\frac{dz^s}{dx} + \varphi^s_y\right|^2 \geq Ct^3\left\{\|z^s\|^2_{1,\Gamma} + \left\|\varphi^s_y\right\|^2_{1,\Gamma}\right\}$$
$$\forall \varphi^s_y, z^s \in H^1_0(\Gamma). \tag{3.20}$$

The inequalities (3.15) and (3.16) are consequences of Korn's inequalities, whereas (3.17) is a classical result, (see [10]). In its turn (3.18)-(3.20) follow from the scalings (3.12)-(3.13), Poincaré inequality and a straightforward computation for $\int_\Gamma \left|\frac{dz^s}{dx} + \varphi^s_y\right|^2$ (see [1]).

On the other hand, $\mathscr{B}(\cdot,\cdot)$ satisfies an inf-sup condition: There exist $C > 0$, independent of t, such that,

$$S := \sup_{0\neq V\in\mathscr{H}} \frac{\mathscr{B}(V,\chi)}{\|V\|_{\mathscr{H}}} \geq C\|\chi\|_Q \qquad \forall \chi \in \mathscr{Q}.$$

To prove this, we consider separately each component of χ. For the first one, we take $v_1 \in H^1_0(\Omega)$ arbitrary and the remaining components of V^* set equal to zero to write

$$S \geq \sup_{0\neq v_1\in H^1_0(\Omega)} \frac{\int_\Gamma \chi_1 v_1}{\|v_1\|_{1,\Omega}} \geq C_1 \sup_{0\neq\psi\in H^{1/2}_{00}(\Gamma)} \frac{\int_\Gamma \chi_1\psi}{\|\psi\|_{1/2,\Gamma}} = C\|\chi_1\|_{-1/2,\Gamma}. \tag{3.21}$$

For the second inequality, we have used the equivalence between the intrinsic norm of $H^{1/2}_{00}(\Gamma)$ and the norm $\inf\left\{\|v\|_{1,\Omega},\ v \in H^1_0(\Omega) :\ v|_\Gamma = \psi\right\}$ (see [26]). The same arguments allow us to prove that

$$S \geq C\|\chi_2\|_{-1/2,\Gamma} \qquad \text{and} \quad S \geq C\|\chi_3\|_{-1/2,\Gamma}. \tag{3.22}$$

Finally, taking $\eta_1 \in H^1_0(\Omega)$ arbitrary and the remaining components of V set equal to zero and using (3.21), we have

$$C\|\chi_4\|_{-1/2,\Gamma} \leq S + C'r\|\chi_1\|_{-1/2,\Gamma} \leq \left(1 + \frac{C'}{C}r\right)S,$$

which, since r is bounded above, leads to

$$S \geq C'' \|\chi_4\|_{-1/2,\Gamma}.$$

The inequality above together with (3.22) and (3.21) allow us to prove inf-sup condition for $\mathscr{B}$. This condition and the global ellipticity of $\mathscr{A}$ allow us to use the standard theory for mixed problems (see [10]) to conclude the following theorem:

Theorem 3.2.1 *For any $t > 0$ fixed, problem (3.10)-(3.11) has a unique solution $(U, \lambda) \in \mathscr{H} \times \mathscr{Q}$.*

3.3 Concentrically stiffened plates

From now on, we restrict our attention to concentrically stiffened plates (i.e, $r = 0$, see Figure 3.2). The reason for this is that, in this case, the plate problem decomposes into two uncoupled ones: the in-plane and the bending stiffened plate problems, as it happens for non stiffened plates.

In fact, the in-plane displacements of the model u and u^s relate with the remaining variables only through equation (3.6) which is part of (3.11) and this happen only if $r \neq 0$. For $r = 0$ we are led to the following two uncoupled problems, the first one for the in-plane terms and the second one for the bending terms.

Find $(u, u^s) \in H_0^1(\Omega)^2 \times H_0^1(\Gamma)$ and $\lambda_1 \in H^{-1/2}(\Gamma)$, such that

$$ta_1(u,v) + t\int_\Gamma \tilde{E}^s \tilde{A} \frac{du^s}{dx}\frac{dv^s}{dx} + \int_\Gamma \lambda_1 (v_1 - v^s) = t\int_\Omega f \cdot v \qquad \forall\, (v, v^s) \in H_0^1(\Omega)^2 \times H_0^1(\Gamma), \tag{3.23}$$

$$\int_\Gamma \chi_1 (u_1 - u^s) = 0 \qquad \forall \chi_1 \in H^{-1/2}(\Gamma). \tag{3.24}$$

Find $\left(\beta, w, w^s, \theta_x^s, \theta_y^s\right) \in H_0^1(\Omega)^2 \times H_0^1(\Omega) \times H_0^1(\Gamma)^3$ and $(\lambda_2, \lambda_3, \lambda_4) \in H^{-1/2}(\Gamma)^3$,

such that

$$t^3 a_2(\beta,\eta) + t\int_\Omega \kappa\mu\,(\nabla w-\beta)\cdot(\nabla z-\eta) + t^3\int_\Gamma \tilde{E}^{\rm s}\tilde{I}_{yy}\frac{d\theta_y^{\rm s}}{dx}\frac{d\varphi_y^{\rm s}}{dx}$$
$$+t^3\int_\Gamma \tilde{\mu}^{\rm s}\tilde{J}\frac{d\theta_x^{\rm s}}{dx}\frac{d\varphi_x^{\rm s}}{dx} + t\int_\Gamma \kappa^{\rm s}\tilde{\mu}^{\rm s}\tilde{A}\left(\frac{dw^{\rm s}}{dx}+\theta_y^{\rm s}\right)\left(\frac{dz^{\rm s}}{dx}+\varphi_y^{\rm s}\right) + \int_\Gamma \lambda_2\,(z-z^{\rm s})$$
$$+\int_\Gamma \lambda_3\,(\eta_2-\varphi_x^{\rm s}) + \int_\Gamma \lambda_4\left(\eta_1+\varphi_y^{\rm s}\right) = t\int_\Omega gz$$
$$\forall\left(\eta,z,z^{\rm s},\varphi_x^{\rm s},\varphi_y^{\rm s}\right)\in H_0^1(\Omega)^2\times H_0^1(\Omega)\times H_0^1(\Gamma)^3, \qquad (3.25)$$

$$\int_\Gamma \chi_2\,(w-w^{\rm s}) + \int_\Gamma \chi_3\,(\beta_2-\theta_x^{\rm s}) + \int_\Gamma \chi_4\left(\beta_1+\theta_y^{\rm s}\right) = 0$$
$$\forall(\chi_2,\chi_3,\chi_4)\in H^{-1/2}(\Gamma)^3. \qquad (3.26)$$

From now on, to simplify a bit the notation, we set all the constants in (3.14) equal to one. Since these constants have been assumed to be independent of t, this does not affect any subsequent asymptotic analysis. Moreover to obtain a family of problems uniformly stable with respect to t, we consider a transverse load proportional to t^2, namely

$$g = \tilde{g}t^2 \qquad (3.27)$$

with $\tilde{g}$ independent of t. Finally, it is also convenient for the analysis to rescale the Lagrange multipliers according to the scales of the different problems in which they appear:

$$\lambda_1 = \tilde{\lambda}_1 t \qquad \text{and} \qquad \lambda_i = \tilde{\lambda}_i t^3,\ i=2,3,4. \qquad (3.28)$$

In what follows we analyze the resulting rescaled problems.

3.3.1 Stiffened in-plane plate problem

Using the scaling (3.28) in (3.23)-(3.24) and setting all the constants equal to one we obtain the following rescaled problem, in which we omit the tildes in $\tilde{\lambda}_1$ to simplify the notation.

Find $(u,u^{\rm s})\in H_0^1(\Omega)^2\times H_0^1(\Gamma)$ and $\lambda_1\in H^{-1/2}(\Gamma)$, such that

$$a_1(u,v) + \int_\Gamma \frac{du^{\rm s}}{dx}\frac{dv^{\rm s}}{dx} + \int_\Gamma \lambda_1\,(v_1-v^{\rm s}) = \int_\Omega f\cdot v$$
$$\forall\,(v,v^{\rm s})\in H_0^1(\Omega)^2\times H_0^1(\Gamma), \qquad (3.29)$$

$$\int_\Gamma \chi_1\,(u_1-u^{\rm s}) = 0 \qquad \forall\chi_1\in H^{-1/2}(\Gamma). \qquad (3.30)$$

This is a well posed problem completely independent of the thickness t. In fact, all the bilinear forms in this problem are continuous and the following ellipticity result holds

$$a_1(v,v) + \int_\Gamma\left(\frac{dv^{\rm s}}{dx}\right)^2 \geq C\left\{\|v\|_{1,\Omega}^2 + \|v^{\rm s}\|_{1,\Gamma}^2\right\} \qquad \forall(v,v^{\rm s})\in H_0^1(\Gamma)\times H_0^1(\Omega)^2. \quad (3.31)$$

Moreover, the arguments leading to (3.21) show that there exist $C>0$, independent of t, such that

$$\sup_{0\neq(v,v^s)\in H_0^1(\Omega)^2\times H_0^1(\Gamma)} \frac{\int_\Gamma \chi_1\,(v_1-v^s)}{\|v\|_{1,\Omega}+\|v^s\|_{1,\Gamma}} \geq C\,\|\chi_1\|_{-1/2,\Gamma} \quad \forall\,\chi_1\in H^{-1/2}(\Gamma)\,.$$

Thus, using Babuška-Brezzi theory (see [10]), we have the *a-priori* estimate

$$\|u\|_{1,\Omega}+\|u^s\|_{1,\Gamma}+\|\lambda_1\|_{-1/2,\Gamma}\leq C\,\|f\|_{0,\Omega}\,.$$

3.3.2 Stiffened bending plate problem

In this case we use the scalings (3.27) and (3.28) in (3.25)-(3.26). Thus if we denote

$$H:=H_0^1(\Omega)^2\times H_0^1(\Omega)\times H_0^1(\Gamma)^3 \qquad \text{and} \qquad Q:=H^{-1/2}(\Gamma)^3\,,$$

and we set all the constants equal to one again, then we arrive at the following rescaled problem, in which we omit the tildes in $\tilde{\lambda}_i$ $i=2,3,4$ and $\tilde{g}$

Find $(\beta,w,w^s,\theta_x^s,\theta_y^s)\in H$ and $(\lambda_2,\lambda_3,\lambda_4)\in Q$, such that

$$\begin{aligned}
&a_2(\beta,\eta)+\frac{1}{t^2}\int_\Omega(\nabla w-\beta)\cdot(\nabla z-\eta)+\int_\Gamma\frac{d\theta_x^s}{dx}\frac{d\varphi_x^s}{dx}+\int_\Gamma\frac{d\theta_y^s}{dx}\frac{d\varphi_y^s}{dx}\\
&\quad+\frac{1}{t^2}\int_\Gamma\left(\frac{dw^s}{dx}+\theta_y^s\right)\left(\frac{dz^s}{dx}+\varphi_y^s\right)+\int_\Gamma\lambda_2\,(z-z^s)+\int_\Gamma\lambda_3\,(\eta_2-\varphi_x^s)\\
&\quad+\int_\Gamma\lambda_4\left(\eta_1+\varphi_y^s\right)=\int_\Omega gz \qquad \forall\,(\eta,z,z^s,\varphi_x^s,\varphi_y^s)\in H, \qquad (3.32)\\
&\int_\Gamma\chi_2\,(w-w^s)+\int_\Gamma\chi_3\,(\beta_2-\theta_x^s)+\int_\Gamma\chi_4\left(\beta_1+\theta_y^s\right)=0 \quad \forall\,(\chi_2,\chi_3,\chi_4)\in Q. \qquad (3.33)
\end{aligned}$$

This problem has a unique solution. In fact, this is a consequence of Theorem 3.2.1 and the equivalence of problems (3.10)-(3.11) and (3.29)-(3.33) in the case $r=0$. Our next goal is to prove that, for a non vanishing g, the solution of problem (3.32)-(3.33) is bounded above and below far from zero uniformly with respect to t. More precisely, we will prove that there exist strictly positive constants C_1 and C_2 such that the solution of this problem satisfies

$$C_1\leq\|\beta\|_{1,\Omega}+\|w\|_{1,\Omega}+\|w^s\|_{1,\Gamma}+\|\theta_x^s\|_{1,\Gamma}+\left\|\theta_y^s\right\|_{1,\Gamma}\leq C_2, \qquad (3.34)$$

for all $t\in(0,1]$.

With this aim we consider the space

$$W:=\left\{(\eta,z)\in H_0^1(\Omega)^2\times H_0^1(\Omega):\frac{d\eta_1}{dx},\frac{d\eta_2}{dx},\frac{dz}{dx}\in L^2(\Gamma)\right\},$$

endowed with the norm

$$\|(\eta,z)\|_W^2 := \|\eta\|_{1,\Omega}^2 + \|z\|_{1,\Omega}^2 + \|\eta_1\|_{1,\Gamma}^2 + \|\eta_2\|_{1,\Gamma}^2 + \|z\|_{1,\Gamma}^2, \quad (\eta,z) \in W.$$

Equation (3.33) is equivalent to.

$$w^s = w, \qquad \theta_x^s = \beta_2 \qquad \text{and} \qquad \theta_y^s = -\beta_1 \quad \text{on } \Gamma, \tag{3.35}$$

which in its turn implies that $(\beta,w) \in W$. Using this and testing (3.32) with functions satisfying the same constraints we arrive at

$$\begin{aligned} &a_2(\beta,\eta) + \frac{1}{t^2}\int_\Omega (\nabla w - \beta)\cdot(\nabla z - \eta) + \int_\Gamma \frac{\partial \beta_1}{\partial x}\frac{\partial \eta_1}{\partial x} \\ &\quad + \int_\Gamma \frac{\partial \beta_2}{\partial x}\frac{\partial \eta_2}{\partial x} + \frac{1}{t^2}\int_\Gamma \left(\frac{\partial w}{\partial x} - \beta_1\right)\left(\frac{\partial z}{\partial x} - \eta_1\right) = \int_\Omega gz \qquad \forall\,(\eta,z) \in W. \end{aligned} \tag{3.36}$$

Testing the above problem with $(\eta,z) = (\beta,w)$ we obtain

$$\begin{aligned} a_2(\beta,\beta) + \frac{1}{t^2}\int_\Omega (\nabla w - \beta)^2 + \int_\Gamma \left(\frac{\partial \beta_1}{\partial x}\right)^2 + \int_\Gamma \left(\frac{\partial \beta_1}{\partial x}\right)^2 \\ + \frac{1}{t^2}\int_\Gamma \left(\frac{\partial w}{\partial x} - \beta_1\right)^2 = \int_\Omega gw. \end{aligned} \tag{3.37}$$

On the other hand from (3.17), we have that

$$\|\beta\|_{1,\Omega}^2 + \|w\|_{1,\Omega}^2 \le C\left\{\frac{1}{t^2}\|\nabla w - \beta\|_{0,\Omega}^2 + a_2(\beta,\beta)\right\}, \tag{3.38}$$

whereas from (3.18) and (3.20), we have:

$$\begin{aligned} \|w\|_{1,\Gamma}^2 + \|\beta_1\|_{1,\Gamma}^2 + \|\beta_2\|_{1,\Gamma}^2 \le C\left\{\frac{1}{t^2}\left\|\frac{\partial w}{\partial x} - \beta_1\right\|_{0,\Gamma}^2 + \int_\Gamma \left(\frac{\partial \beta_1}{\partial x}\right)^2 \right. \\ \left. + \int_\Gamma \left(\frac{\partial \beta_2}{\partial x}\right)^2\right\}. \end{aligned} \tag{3.39}$$

Therefore, adding (3.38) and (3.39) and using (3.37), we obtain

$$\|\beta\|_{1,\Omega}^2 + \|w\|_{1,\Omega}^2 + \|w\|_{1,\Gamma}^2 + \|\beta_1\|_{1,\Gamma}^2 + \|\beta_2\|_{1,\Gamma}^2 \le C\int_\Omega gw,$$

from which it follows that

$$\|\beta\|_{1,\Omega} + \|w\|_{1,\Omega} + \|w\|_{1,\Gamma} + \|\beta_1\|_{1,\Gamma} + \|\beta_2\|_{1,\Gamma} \le C_2. \tag{3.40}$$

To prove the other estimate in (3.34), we observe that the solution $(\beta, w) \in W$ to problem (3.36) is the minimum in W of the energy functional $E_t(\eta, z)$ defined by:

$$E_t(\eta,z) := \frac{1}{2}\left\{ a_2(\eta,\eta) + \frac{1}{t^2}\int_\Omega (\nabla z - \eta)^2 + \int_\Gamma \left(\frac{\partial \eta_1}{\partial x}\right)^2 + \int_\Gamma \left(\frac{\partial \eta_2}{\partial x}\right)^2 + \frac{1}{t^2}\int_\Gamma \left(\frac{\partial z}{\partial x} - \eta_1\right)^2 \right\} - \int_\Omega gz. \tag{3.41}$$

Consider the following closed subspace of W:

$$W_0 := \{(\eta,z) \in W : \nabla z = \eta\} = \left\{ (\nabla z, z), z \in H_0^2(\Omega) : \frac{\partial^2 z}{\partial x \partial y}, \frac{\partial^2 z}{\partial x^2} \in L^2(\Gamma) \right\}.$$

Notice that for $(\eta, z) \in W_0$, the associated energy reads

$$E_t(\eta,z) := \frac{1}{2}\left\{ a_2(\nabla z, \nabla z) + \int_\Gamma \left(\frac{\partial^2 z}{\partial x^2}\right)^2 + \int_\Gamma \left(\frac{\partial^2 z}{\partial x \partial y}\right)^2 \right\} - \int_\Omega gz. \tag{3.42}$$

We note that

$$\min_W E_t \leq \min_{W_0} E_t < 0.$$

In fact, the first inequality is clear, and for the second one, we observe that the minimum of E_t in W_0 is attained at $(\eta, z) = (\nabla z_0, z_0) \in W_0$ with z_0 satisfying

$$a_2(\nabla z_0, \nabla z) + \int_\Gamma \frac{\partial^2 z_0}{\partial x^2}\frac{\partial^2 z}{\partial x^2} + \int_\Gamma \frac{\partial^2 z_0}{\partial x \partial y}\frac{\partial^2 z}{\partial x \partial y} = \int_\Omega gz \quad \forall (\nabla z, z) \in W_0. \tag{3.43}$$

The bilinear form on the left hand side is bounded and elliptic in W_0, the latter because of (3.15). Hence, from the Lax-Milgram Theorem there exists a unique $(\nabla z_0, z_0) \in W_0$ solution of (3.43) and $\|(\nabla z_0, z_0)\|_W \leq C\|g\|_{0,\Omega}$. Therefore, for $g \neq 0$, replacing (3.43) in (3.42), we have

$$\begin{aligned} \min_{(\eta,z)\in W} E_t(\eta,z) &\leq \min_{(\eta,z)\in W_0} E_t(\eta,z) \\ &= -\frac{1}{2}\left\{ a_2(\nabla z_0, \nabla z_0) + \int_\Gamma \left(\frac{\partial^2 z_0}{\partial x^2}\right)^2 + \int_\Gamma \left(\frac{\partial^2 z_0}{\partial x \partial y}\right)^2 \right\} \\ &=: -C_0 < 0. \end{aligned} \tag{3.44}$$

Since $\min_W E_t(\eta, z)$ is attained in the solution (β, w) of problem (3.36), we use this equation in (3.41) and (3.44) to write

$$a_2(\beta,\beta) + \frac{1}{t^2}\int_\Omega (\nabla w - \beta)^2 + \int_\Gamma \left(\frac{\partial \beta_1}{\partial x}\right)^2 + \int_\Gamma \left(\frac{\partial \beta_2}{\partial x}\right)^2 + \frac{1}{t^2}\int_\Gamma \left(\frac{\partial w}{\partial x} - \beta_1\right)^2 \geq 2C_0. \tag{3.45}$$

On the other hand, testing (3.36) with $(\eta, z) = (\beta, w)$, we have

$$\begin{aligned}\frac{1}{t^2}\int_\Omega (\nabla w - \beta)^2 + \frac{1}{t^2}\int_\Gamma \left(\frac{\partial w}{\partial x} - \beta_1\right)^2 \\ &= \int_\Omega gw - a_2(\beta,\beta) - \int_\Gamma \left(\frac{\partial \beta_1}{\partial x}\right)^2 - \int_\Gamma \left(\frac{\partial \beta_2}{\partial x}\right)^2 \\ &\leq \int_\Omega gw \leq \frac{\varepsilon}{2}\|g\|^2_{0,\Omega} + \frac{1}{2\varepsilon}\|w\|^2_{0,\Omega} \qquad \forall \varepsilon > 0. \end{aligned} \tag{3.46}$$

Substituting (3.46) in (3.45) choosing an adequate value of ε and using the boundedness of $a_2(\cdot,\cdot)$, we arrive at

$$\|\beta\|_{1,\Omega} + \|w\|_{1,\Omega} + \|w\|_{1,\Gamma} + \|\beta_1\|_{1,\Gamma} + \|\beta_2\|_{1,\Gamma} \geq C_1. \tag{3.47}$$

Therefore, recalling (3.35), we obtain the following result as a consequence of (3.40) and (3.47)

Proposition 1 *Given a non vanishing $g \in L^2(\Omega)$, let $\left(\beta, w, w^s, \theta^s_x, \theta^s_y\right) \in H$ be the solution of (3.32)-(3.33). There exists strictly positive constants C_1, C_2 independent of $t \in (0,1]$ such that*

$$C_1 \leq \|\beta\|_{1,\Omega} + \|w\|_{1,\Omega} + \|w^s\|_{1,\Gamma} + \|\theta^s_x\|_{1,\Gamma} + \left\|\theta^s_y\right\|_{1,\Gamma} \leq C_2.$$

In what follows we present some regularity results associated to the stiffened bending plate problem. First,we define the shear terms in the plate and the stiffener as follows:

$$\gamma := \frac{1}{t^2}(\nabla w - \beta), \tag{3.48}$$

$$\alpha := \frac{1}{t^2}\left(\frac{dw^s}{dx} + \theta^s_y\right). \tag{3.49}$$

Proposition 2 *The solution of (3.32)-(3.33) satisfies $\beta|_{\Omega_i} \in H^2(\Omega_i)^2$, $w|_{\Omega_i} \in H^2(\Omega_i)^2$, $i = 1,2$ and θ^s_x, θ^s_y, $w^s \in H^{5/2}(\Gamma)$. Moreover, $\gamma|_{\Omega_i} \in H^1(\Omega_i)^2$, $i = 1,2$ and $\alpha \in H^{3/2}(\Gamma)$.*

Proof. Testing in (3.32) with $\varphi^s_x \in H^1_0(\Gamma)$ and setting to zero all the other test functions, we have

$$-\frac{d^2\theta^s_x}{dx^2} = \lambda_3 \in H^{-1/2}(\Gamma) \tag{3.50}$$

and hence $\theta^s_x \in H^{3/2}(\Gamma)$. In a similar way, testing in (3.32) with $z^s \neq 0$ and $\varphi^s_y \neq 0$, respectively, we obtain that $\theta^s_y \in H^{3/2}(\Gamma)$, $\alpha \in H^{1/2}(\Gamma)$ and, consequently, (3.49) yields $w^s \in H^{3/2}(\Gamma)$. next we extend w^s to the whole domain Ω in such a way that the extension

belongs to H^2 of each subdomain Ω_i. More precisely, let $w_0 \in H_0^1(\Omega)$ be such that $w_0|_{\Omega_i} \in H^2(\Omega_i)$, $i = 1,2$ (see [27, Theorem 1.5.2.8]) and

$$w_0|_\Gamma = w^s. \tag{3.51}$$

Analogously, let $\beta_0 \in H_0^1(\Omega)^2$: $\beta_0|_{\Omega_i} \in H^2(\Omega_i)$, $i = 1,2$, and

$$\beta_0|_\Gamma = \left(-\theta_y^s, \theta_x^s\right). \tag{3.52}$$

Let $\tilde{\beta} \in H_0^1(\Omega)^2$ and $\tilde{w} \in H_0^1(\Omega)$ be defined by

$$\beta = \tilde{\beta} + \beta_0 \qquad \text{and} \qquad w = \tilde{w} + w_0. \tag{3.53}$$

Since $\beta|_\Gamma = \beta_0|_\Gamma$ and $w|_\Gamma = w_0|_\Gamma$, we have that $\tilde{\beta}|_{\Omega_i} \in H_0^1(\Omega_i)^2$ and $\tilde{w}|_{\Omega_i} \in H_0^1(\Omega_i)$, $i = 1,2$. Our next goal is to show that $(\tilde{\beta}|_{\Omega_i}, \tilde{w}|_{\Omega_i})$ is the solution of a plate problem for which an additional regularity result holds. With this aim, we take $\eta \in H_0^1(\Omega_i)^2$ and $z \in H_0^1(\Omega_i)$ and extend them by zero to Ω. These extensions that we also denote η and z clearly satisfy $\eta \in H_0^1(\Omega)^2$ and $z \in H_0^1(\Omega)$. If we take such η and z with vanishing z^s, φ_x^s and φ_y^s in (3.32), we obtain that

$$a_2^i(\beta,\eta) + \frac{1}{t^2}\int_{\Omega_i}(\nabla w - \beta)\cdot(\nabla z - \eta) = \int_{\Omega_i} gz \qquad \forall\,(\eta,z) \in H_0^1(\Omega_i)^2 \times H_0^1(\Omega_i), \tag{3.54}$$

with

$$a_2^i(\beta,\eta) := \frac{1}{12}\left\{\int_{\Omega_i}\frac{E\nu}{1-\nu^2}\operatorname{div}\beta\ \operatorname{div}\eta + \int_{\Omega_i}\frac{E}{1+\nu}\varepsilon(\beta):\varepsilon(\eta)\right\}.$$

Therefore using (3.53) we have that $\tilde{\beta}|_{\Omega_i} \in H_0^1(\Omega_i)^2$ and $\tilde{w}|_{\Omega_i} \in H_0^1(\Omega_i)$ are the solution of the following problem:

$$\begin{aligned} a_2^i\left(\tilde{\beta},\eta\right) &+ \frac{1}{t^2}\int_{\Omega_i}\left(\nabla\tilde{w} - \tilde{\beta}\right)\cdot(\nabla z - \eta) \\ &= -a_2^i(\beta_0,\eta) - \frac{1}{t^2}\int_{\Omega_i}(\nabla w_0 - \beta_0)\cdot(\nabla z - \eta) + \int_{\Omega_i} gz \\ &= \int_{\Omega_i} F\cdot\eta + \int_{\Omega_i} Gz \qquad \forall\,(\eta,z) \in H_0^1(\Omega_i)^2 \times H_0^1(\Omega_i). \end{aligned}$$

Notice that $F \in L^2(\Omega)^2$ and $G \in L^2(\Omega)$, because $\beta_0|_{\Omega_i} \in H^2(\Omega_i)^2$ and $w_0|_{\Omega_i} \in H^2(\Omega_i)$. Hence, using the regularity results of ([2, Theorem 2.1]) we have that $(\tilde{\beta},\tilde{w}) \in H^2(\Omega_i)^2 \times H^2(\Omega_i)$, which using (3.53) yields the regularity for β.

The next step is to prove additional regularity for γ and α. With this aim, we observe first that by using the definition of γ in (3.48) and the regularity of β and w we have that $\gamma|_{\Omega_i} \in H^1(\Omega_i)^2$, $i = 1,2$.

On the other hand, testing problem (3.54) with $z \in H_0^1(\Omega_i)$ and $\eta = 0$, we obtain that

$$-\operatorname{div}\gamma = g \qquad \text{in } \Omega_i.$$

Therefore, testing (3.32) with $z \in H_0^1(\Omega)$ and all the other variables set to zero, integrating by parts in each subdomain Ω_i and using the equation above, we have that

$$\int_\Gamma [\![\gamma \cdot n]\!]\, z + \int_\Gamma \lambda_2 z = 0$$

where $[\![\cdot]\!]$ denotes the jump across Γ. Consequently, we obtain $\lambda_2 \in H^{1/2}(\Gamma)$ from the regularity of γ. Therefore, testing (3.32) with $z^s \in H_0^1(\Gamma)$ and all the other variables set to zero we have that $\alpha' = \lambda_2$ and hence $\alpha \in H^{3/2}(\Gamma)$. Moreover, testing (3.54) with $\eta \in H_0^1(\Omega_i)^2$ and $z = 0$, we obtain

$$-\operatorname{div}(\sigma(\beta)) = \gamma \qquad \text{in } \Omega_i,$$

where $\sigma(\beta) := \frac{1}{12}\left\{\frac{E}{1+\nu}\varepsilon(\beta) + \frac{E}{1-\nu^2}\operatorname{div}\beta\right\}$ is the plane strain stress tensor. On the other hand, testing (3.32) with $\eta \in H_0^1(\Omega)^2$ and all the other test functions set to zero, integrating by parts in each subdomain Ω_i and using the above equation we arrive at

$$\int_\Gamma [\![\sigma(\beta)\, n]\!]_\Gamma \cdot \eta + \int_\Gamma \lambda_3 \eta_2 + \lambda_4 \eta_1 = 0.$$

Consequently, since $\beta|_{\Omega_i} \in H^2(\Omega_i)$, $i = 1,2$, we obtain that λ_3, $\lambda_4 \in H^{1/2}(\Gamma)$. Therefore, from (3.50) and the analogous expression for θ_y^s, we obtain that θ_x^s and θ_y^s are in $H^{5/2}(\Gamma)$. Finally from these regularity results, (3.49) and the additional regularity of α, we obtain $w^s \in H^{5/2}(\Gamma)$ and conclude the proof. □

Remark 3.3.1 *According to Proposition 2, the solution of problem (3.32)-(3.33) satisfies additional regularity. However, we have not proved that the corresponding norms are bounded independently of t. Indeed, we have used that λ_2, λ_3 and λ_4 belong to $H^{-1/2}(\Gamma)$, which is true but we do not have bounds of $\|\lambda_2\|_{-1/2,\Gamma}$, $\|\lambda_3\|_{-1/2,\Gamma}$ and $\|\lambda_4\|_{-1/2,\Gamma}$ independent of t. In spite of this, the numerical results in Section 3.6 seem to suggest that such bounds should hold true.*

3.4 The discrete problems

We consider separately the discretization of the stiffened in-plane and bending problems. Let $\{\mathscr{T}_h\}$ be a regular family of triangulations consistent with Γ, in the sense that, for all meshes, Γ is a union of edges of $\mathscr{T}_h$. Let $\mathscr{T}_h^\Gamma$ be the partition induced by $\mathscr{T}_h$ in Γ. We assume that the family $\{\mathscr{T}_h\}$ is such that $\left\{\mathscr{T}_h^\Gamma\right\}$ is quasi uniform.

3.4.1 Stiffened in-plane plate problem

We define:

$$X_h := \left\{ z_h \in H_0^1(\Omega) : z_h|_T \in \mathscr{P}_1 \, \forall T \in \mathscr{T}_h \right\},$$
$$P_{1h}^0 := \left\{ v_h \in H_0^1(\Gamma) : v_h|_\ell \in \mathscr{P}_1 \, \forall \ell \in \mathscr{T}_h^\Gamma \right\}.$$

The discrete analogue to problem (3.29)-(3.30) reads

Find $\left(u_h, u_h^s\right) \in X_h^2 \times P_{0h}^1$ and $\lambda_{1h} \in P_{0h}^1$ such that

$$a_1(u_h, v_h) + \int_\Gamma \frac{du_h^s}{dx}\frac{dv_h^s}{dx} + \int_\Gamma \lambda_{1h}(v_{1h} - v_h^s) = \int_\Omega f \cdot v_h \qquad \forall \left(v_h, v_h^s\right) \in X_h^2 \times P_{1h}^0, \tag{3.55}$$

$$\int_\Gamma \chi_{1h}(u_{1h} - u_h^s) = 0 \qquad \forall \chi_{1h} \in P_{1h}^0. \tag{3.56}$$

Since $X_h^2 \subset H_0^1(\Omega)^2$ and $P_{1h}^0 \subset H_0^1(\Gamma)$, by virtue of (3.31) we only need to prove the following inf-sup condition to be able to apply the classical Babuška-Brezzi theory:

$$\sup_{0 \neq \left(v_h, v_h^s\right) \in X_h \times P_{1h}^0} \frac{\int_\Gamma \chi_h \left(v_{1h} - v_h^s\right)}{\|v_h\|_{1,\Omega} + \left\|v_h^s\right\|_{1,\Gamma}} \geq C \|\chi_h\|_{-1/2,\Gamma}, \qquad \forall \chi_h \in P_{1h}^0.$$

To prove this, we will define a Fortin operator $\overline{\Pi}$. In what follows we define several auxiliary operators that we will use to define $\overline{\Pi}$.

First let $\hat{\pi} : L^2(\Gamma) \to P_{0h}^1$ be the L^2-projection. Clearly we have that

$$\|\hat{\pi} v\|_{0,\Gamma} \leq C \|v\|_{0,\Gamma} \qquad \forall v \in L^2(\Gamma). \tag{3.57}$$

Moreover, it is a classical result (see [25, Lemma 1.131]) that

$$\|v\|_{1,\Gamma} \leq C \|v\|_{1,\Gamma} \qquad \forall v \in H_0^1(\Gamma), \tag{3.58}$$

provided $\left\{\mathscr{T}_h^\Gamma\right\}$ is a quasi-uniform family of meshes. Consequently, using interpolation of Banach Spaces we arrive at

$$\|\hat{\pi} v\|_{1/2,\Gamma} \leq C \|v\|_{1/2,\Gamma}. \tag{3.59}$$

Next, let $I_{SZ} : H_0^1(\Omega) \to X_h$ be a Scott-Zhang interpolation operator (see [46]) such that if $v \in H_0^1(\Omega)$ satisfies $v|_\Gamma \in P_{1h}^0$, then $(I_{SZ} v)|_\Gamma = v|_\Gamma$.

On the other hand let $E : H_{00}^{1/2}(\Gamma) \to H_0^1(\Omega)$ be a continuous right-inverse of the trace operator on Γ. Notice that

$$I_{SZ}(E v_h) = v_h \qquad \forall v_h \in P_{1h}^0. \tag{3.60}$$

Now we are in the a position to define the Fortin operator

$$\overline{\Pi}(v,v^{\mathrm{s}}) := ((I_{\mathrm{SZ}}(E(\hat{\pi}(v_1|_\Gamma))), I_{\mathrm{SZ}}v_2), \hat{\pi}v^{\mathrm{s}}).$$

As a consequence of (3.58), (3.59) and the boundedness of the operators E and I_{SZ} we have

$$\left\|\overline{\Pi}(v,v^{\mathrm{s}})\right\|_{H_0^1(\Omega)^2\times H_0^1(\Gamma)} \leq C\left\{\|v\|_{1,\Omega}+\|v^{\mathrm{s}}\|_{1,\Gamma}\right\} \qquad \forall (v,v^{\mathrm{s}})\in H_0^1(\Omega)^2\times H_0^1(\Gamma).$$

Moreover $\overline{\Pi}$ satisfies the commuting diagram property. In fact, because of (3.60)

$$\int_\Gamma (v_1 - I_{\mathrm{SZ}}(E(\hat{\pi}(v_1|_\Gamma))))\,\chi_h = 0 \qquad \forall (v,v^{\mathrm{s}})\in H_0^1(\Omega)^2\times H_0^1(\Gamma),\ \chi_h\in P_{1h}^0.$$

Therefore $\overline{\Pi}$ satisfies the assumptions of the Fortin lemma ([25]). Consequently we have that the Babuška-Brezzi theory (see for instance [10]) allows us to prove the next theorem.

Theorem 3.4.1 *Problem (3.55)-(3.56) has a unique solution* $\left(u_h,u_h^{\mathrm{s}}\right)\in X_h^2\times P_{1h}^0$, $\lambda_{1h}\in P_{1h}^0$ *and there exists a positive constant C such that, if* (u,u^{s}) *is the solution to problem (3.29)-(3.30), then*

$$\begin{aligned}&\|u-u_h\|_{1,\Omega}+\|u^{\mathrm{s}}-u_h^{\mathrm{s}}\|_{1,\Gamma}+\|\lambda_1-\lambda_{1h}\|_{-1/2,\Gamma}\\ &\leq C\left\{\inf_{v_h\in X_h^2}\|u-v_h\|_{1,\Omega}+\inf_{v_h^{\mathrm{s}}\in P_{1h}^0}\|u^{\mathrm{s}}-v_h^{\mathrm{s}}\|_{1,\Gamma}+\inf_{\chi_{1h}\in P_{1h}^0}\|\lambda_1-\chi_{1h}\|_{-1/2,\Gamma}\right\}.\end{aligned}$$

The error estimate above depends as usual on some additional regularity of the solution to the continuous problem (3.29)-(3.30). In what follows we derive a simpler form of this problem. By testing (3.29) with $v^{\mathrm{s}}\in H_0^1(\Gamma)$ and setting the other variables to zero we have

$$-\frac{d^2u^{\mathrm{s}}}{dx^2} = \lambda_1 \in H^{-1/2}(\Gamma) \tag{3.61}$$

and hence, $u^{\mathrm{s}}\in H^{3/2}(\Gamma)$. Moreover, from (3.30), $u_1 = u^{\mathrm{s}}$ on Γ. On the other hand, using different test functions in (3.29) it can be shown that

$$[\![\sigma(u)n]\!]_\Gamma = \begin{bmatrix}\lambda_1\\ 0\end{bmatrix} \tag{3.62}$$

where $\sigma(u) := \frac{E}{1+\nu}\varepsilon(u)+\frac{E\nu}{(1+\nu)(1-2\nu)}(\mathrm{div}\,u)\,I_b$ is the plane stress tensor. Therefore, $u\in H_0^1(\Omega)^2$ is the solution to the following problem:

$$\begin{aligned}-\mathrm{div}(\sigma(u)) = f\in L^2(\Omega_i) \qquad & i=1,2,\\ u_1 = u^{\mathrm{s}}\in H_{00}^{1/2}(\Gamma)\cap H^{3/2}(\Gamma),&\\ \left[\!\left[\frac{\partial u_2}{\partial n}\right]\!\right] = 0 \qquad \text{on } \Gamma.&\end{aligned}$$

Moreover , $\lambda_1 = \frac{E}{2(1+\nu)}\left[\!\left[\frac{\partial u_1}{\partial y}+\frac{\partial u_2}{\partial x}\right]\!\right]$.

3.4.2 The stiffened bending plate problem

To discretize this problem we consider the DL3 element introduced in [22]. For each $T \in \mathscr{T}_h$, let μ_1, μ_2, μ_3 be its barycentric coordinates. We denote by τ_i a unit tangent vector to the edge $\mu_i = 0$ and define

$$\mathbf{p}_1 = \mu_2\mu_3\tau_1, \quad \mathbf{p}_2 = \mu_1\mu_3\tau_2, \quad \mathbf{p}_3 = \mu_1\mu_2\tau_3. \tag{3.63}$$

Let

$$\begin{aligned}
Y_h &:= \left\{\eta \in H_0^1(\Omega)^2 : \eta|_T \in \mathscr{P}_1 \oplus \langle \mathbf{p}_1, \mathbf{p}_2, \mathbf{p}_3\rangle \quad \forall T \in \mathscr{T}_h\right\},\\
W_h &:= \left\{v \in H_0^1(\Omega) : v|_T \in \mathscr{P}_1 \quad \forall T \in \mathscr{T}_h\right\},\\
P_{kh}^0 &:= \left\{\varphi \in H_0^1(\Gamma) : \varphi|_\ell \in \mathscr{P}_k \quad \forall \ell \in \mathscr{T}_h^\Gamma\right\}, \quad k = 1, 2,\\
P_{0h}^d &:= \left\{\varphi \in L^2(\Gamma) : \varphi|_\ell \in \mathscr{P}_0 \quad \forall \ell \in \mathscr{T}_h^\Gamma\right\},\\
\Gamma_h &:= \left\{\eta_h \in H_0(\mathrm{rot}, \Omega) : \eta_h|_T \in \mathscr{P}_0^2 \oplus \mathscr{P}_0 \begin{pmatrix} -x_2 \\ x_1 \end{pmatrix} \quad \forall T \in \mathscr{T}_h\right\},
\end{aligned}$$

the latter being the rotated Raviart-Tomas space (see [41]). Let Π be the rotated Raviart-Thomas interpolant on this space (see [41] again). This operator is well defined in $H^1(\Omega)^2$. Moreover for $\eta \in H^1(\Omega)^2 \cap H_0(\mathrm{rot}, \Omega)$, $\Pi\eta \in \Gamma_h$ and there holds

$$\|\eta - \Pi\eta\|_{0,\Omega} \leq Ch\|\eta\|_{1,\Omega}, \tag{3.64}$$

Let $\pi : L^2(\Gamma) \to P_{0h}^d$ be the orthogonal projection onto P_{0h}^d. It is well known that

$$\|v - \pi v\|_{0,\Gamma} \leq Ch\|v\|_{1,\Gamma} \qquad \forall v \in H^1(\Gamma). \tag{3.65}$$

Let $\tilde{\pi} : L^2(\Gamma) \to P_{2h}^0$ be the orthogonal projection onto P_{2h}^0.

Finally, let

$$H_h := Y_h \times W_h \times P_{1h}^0 \times P_{1h}^0 \times P_{2h}^0 \qquad \text{and} \qquad Q_h := P_{1h}^0 \times P_{1h}^0 \times P_{2h}^0$$

The discrete problem is defined as follows:

Find $\left(\beta_h, w_h, w_h^s, \theta_{xh}^s, \theta_{yh}^s\right) \in H_h$ and $(\lambda_{2h}, \lambda_{3h}, \lambda_{4h}) \in Q_h$ such that

$$\begin{aligned}
&a_2(\beta_h, \eta_h) + \frac{1}{t^2}\int_\Omega (\nabla w_h - \Pi\beta_h)\cdot(\nabla z_h - \Pi\eta_h) + \int_\Gamma \frac{\partial\theta_{xh}^s}{\partial x}\frac{\partial\varphi_{xh}^s}{\partial x} + \int_\Gamma \frac{\partial\theta_{yh}^s}{\partial x}, \frac{\partial\varphi_{yh}^s}{\partial x}\\
&\quad + \frac{1}{t^2}\int_\Gamma \left(\frac{\partial z_h^s}{\partial x} + \pi\theta_{yh}^s\right)\left(\frac{\partial z_h^s}{\partial x} + \pi\varphi_{yh}^s\right) + \int_\Gamma \lambda_{2h}(z_h - z_h^s) + \int_\Gamma \lambda_{3h}(\eta_{2h} - \varphi_{xh}^s)\\
&\quad + \int_\Gamma \lambda_{4h}\left(\eta_{1h} - \varphi_{yh}^s\right) = \int_\Omega g z_h \qquad \forall \left(\eta_h, z_h, z^s, \varphi_{xh}^s, \varphi_{yh}^s\right) \in H_h,
\end{aligned} \tag{3.66}$$

$$\int_\Gamma \chi_{2h}(w_h - w_h^s) + \int_\Gamma \chi_{3h}(\beta_{2h} - \theta_{xh}^s) + \int_\Gamma \chi_{4h}\left(\beta_{1h} + \theta_{yh}^s\right) = 0$$

$$\forall (\chi_{2h}, \chi_{3h}, \chi_{4h}) \in Q_h. \tag{3.67}$$

The existence and uniqueness of the solution to(3.66)-(3.67) is obtained using the Babuška-Brezzi theory. The ellipticity condition

$$a_2(\eta_h,\eta_h)+\frac{1}{t^2}\int_\Omega|\nabla z_h-\Pi\eta_h|^2+\frac{1}{t^2}\int_\Gamma\left(\frac{\partial z_h^s}{\partial x}+\pi\varphi_{yh}^s\right)^2+\int_\Gamma\left|\frac{\partial\varphi_{xh}^s}{\partial x}\right|^2+\int_\Gamma\left|\frac{\partial\varphi_{yh}^s}{\partial x}\right|^2$$
$$\geq C\left\{\|\eta_h\|_{1,\Omega}^2+\|z_h\|_{1,\Omega}^2+\|z_h^s\|_{1,\Gamma}^2+\|\varphi_{xh}^s\|_{1,\Gamma}^2+\left\|\varphi_{yh}^s\right\|_{1,\Gamma}^2\right\}$$
$$\forall\left(\eta_h,z_h,z^s,\varphi_{xh}^s,\varphi_{yh}^s\right)\in H_h,$$

is attained from the ellipticities of the discrete unstiffened plate problem (see for instance [22]) and the discrete beam problem (see for instance [1]) and Poincaré inequality in $H_0^1(\Gamma)$.

On the other hand, it is simple to show that the discrete inf-sup condition holds true (with a positive constant in principle depending of h) if and only if

$$\sup_{0\neq\left(\eta,z_h,z_h^s,\varphi_{xh}^s,\varphi_{yh}^s\right)\in H_h}\int_\Gamma\chi_{2h}(z_h-z_h^s)+\chi_{3h}(\eta_{2h}-\varphi_{xh}^s)+\chi_{4h}\left(\eta_{1h}+\varphi_{yh}^s\right)>0$$
$$\forall(\chi_{2h},\chi_{3h},\chi_{4h})\in Q_h.$$

The latter can be proved to hold by taking $\chi_{2h}=z_h|_\Gamma-z_h^s$, $\chi_{3h}=\eta_{2h}|_\Gamma-\varphi_{xh}^s$ and $\chi_{4h}=\eta_{1h}|_\Gamma+\varphi_{yh}^s$. Thus we arrive at the following lemma.

Lemma 3.4.1 *Problem (3.66)-(3.67) has a unique solution.*

3.5 Error estimate

Let us introduce the discrete shear terms approximating (3.48) and (3.49) as follows:

$$\gamma_h:=\frac{1}{t^2}(\nabla w_h-\Pi\beta_h),\tag{3.68}$$
$$\alpha_h:=\frac{1}{t^2}\left(\frac{\partial z_h^s}{\partial x}+\pi\theta_{yh}^s\right).\tag{3.69}$$

The first step to obtain the estimates is to write an error error equation.

With this aim, we test the continuous problem (3.32)-(3.33) and the discrete problem

(3.66)-(3.67) with $\left(\eta_h, z_h, z_h^{\mathrm{s}}, \varphi_{xh}^{\mathrm{s}}, \varphi_{yh}^{\mathrm{s}}\right) \in H_h$ and obtain

$$
\begin{aligned}
&a_2(\beta-\beta_h,\eta_h)+\int_\Omega(\gamma-\gamma_h)\cdot(\nabla z_h-\Pi\eta_h)+\int_\Gamma(\alpha-\alpha_h)\left(\frac{\partial z^{\mathrm{s}}}{\partial x}+\pi\varphi_y^{\mathrm{s}}\right)\\
&\quad+\int_\Gamma\left(\frac{\partial\theta_y^{\mathrm{s}}}{\partial x}-\frac{\partial\theta_{yh}^{\mathrm{s}}}{\partial x}\right)\frac{\partial\varphi_y^{\mathrm{s}}}{\partial x}+\int_\Gamma\left(\frac{\partial\theta_x^{\mathrm{s}}}{\partial x}-\frac{\partial\theta_{xh}^{\mathrm{s}}}{\partial x}\right)\frac{\partial\varphi_x^{\mathrm{s}}}{\partial x}+\int_\Gamma(\lambda_2-\lambda_{2h})(z-z^{\mathrm{s}})\\
&\quad+\int_\Gamma(\lambda_3-\lambda_{3h})(\eta_2-\varphi_x^{\mathrm{s}})+\int_\Gamma(\lambda_4-\lambda_{4h})(\eta_1-\varphi_y^{\mathrm{s}})\\
&\quad=\int_\Omega\gamma\cdot(\eta_h-\Pi\eta_h)+\int_\Gamma\alpha\left(\pi\varphi_{yh}^{\mathrm{s}}-\varphi_{yh}^{\mathrm{s}}\right)\qquad\forall\left(\eta_h,z_h,z_h^{\mathrm{s}},\varphi_{xh}^{\mathrm{s}},\varphi_{yh}^{\mathrm{s}}\right)\in H_h, \quad (3.70)\\
&\int_\Gamma\chi_{2h}(w-w_h-(w^{\mathrm{s}}-w_h^{\mathrm{s}}))+\int_\Gamma\chi_{3h}(\beta_2-\beta_{2h}-(\theta_x^{\mathrm{s}}-\theta_{xh}^{\mathrm{s}}))\\
&\quad+\int_\Gamma\chi_{4h}\left(\beta_1-\beta_{1h}+\theta_y^{\mathrm{s}}-\theta_{yh}^{\mathrm{s}}\right)=0\qquad\forall(\chi_{2h},\chi_{3h},\chi_{4h})\in Q_h. \quad (3.71)
\end{aligned}
$$

The following lemma well be used to prove the error estimates.

Lemma 3.5.1 *Given $\hat{\beta}\in Y_h$, $\hat{w}\in W_h$, let*

$$
\begin{aligned}
\hat{\gamma}&:=t^{-2}\left(\nabla\hat{w}-\Pi\hat{\beta}\right)\in\Gamma_h,\\
\hat{\theta}_x^{\mathrm{s}}&:=\hat{\beta}_2\Big|_\Gamma\in P_{1h}^0,\\
\hat{\theta}_y^{\mathrm{s}}&:=-\hat{\beta}_1\Big|_\Gamma\in P_{2h}^0,\\
\hat{w}^{\mathrm{s}}&:=\hat{w}|_\Gamma\in P_{1h}^0,\\
\hat{\alpha}&:=t^{-2}\left(\frac{d\hat{w}^{\mathrm{s}}}{dx}+\pi\hat{\theta}_y^{\mathrm{s}}\right)\in P_0^{dh}.
\end{aligned}
$$

Then, we have

$$
\begin{aligned}
&\left\|\hat{\beta}-\beta_h\right\|_{1,\Omega}+t\,\|\hat{\gamma}-\gamma_h\|_{0,\Omega}+t\,\|\hat{\alpha}-\alpha_h\|_{0,\Gamma}+\left\|\hat{\theta}_x^{\mathrm{s}}-\theta_{xh}^{\mathrm{s}}\right\|_{1,\Gamma}+\left\|\hat{\theta}_y^{\mathrm{s}}-\theta_{yh}^{\mathrm{s}}\right\|_{1,\Gamma}\\
&\qquad\le C\left\{\left\|\hat{\beta}-\beta\right\|_{1,\Omega}+t\,\|\hat{\gamma}-\gamma\|_{0,\Omega}+t\,\|\hat{\alpha}-\alpha\|_{0,\Gamma}+\left\|\hat{\theta}_x^{\mathrm{s}}-\theta_x^{\mathrm{s}}\right\|_{1,\Gamma}\right.\\
&\qquad\qquad\left.+\left\|\hat{\theta}_y^{\mathrm{s}}-\theta_y^{\mathrm{s}}\right\|_{1,\Gamma}+h\,\|\gamma\|_{0,\Omega}+h\,\|\alpha\|_{0,\Gamma}\right\}. \quad (3.72)
\end{aligned}
$$

Proof. Let $\hat{R}: H^{-1/2}(\Gamma)\to P_{1h}^0$ and $\tilde{R}: H^{-1/2}(\Gamma)\to P_{2h}^0$ be the projectors respectively defined for any $\lambda\in H^{-1/2}(\Gamma)$ by

$$
\begin{aligned}
\int_\Gamma(\lambda-\hat{R}\lambda)\,\chi_h&=0\qquad\forall\chi_h\in P_{1h}^0,\\
\int_\Gamma(\lambda-\tilde{R}\lambda)\,\chi_h&=0\qquad\forall\chi_h\in P_{2h}^0.
\end{aligned}
$$

Using this in the error equation (3.70) we have

$$
\begin{aligned}
a_2\left(\hat{\beta}-\beta_h,\eta_h\right)+\int_\Omega(\hat{\gamma}-\gamma_h)\cdot(\nabla z_h-\Pi\eta_h)+\int_\Gamma(\hat{\alpha}-\alpha_h)\left(\frac{\partial z_h^{\mathrm{s}}}{\partial x}+\pi\varphi_{yh}^{\mathrm{s}}\right)\\
+\int_\Gamma\left(\frac{\partial\hat{\theta}_x^{\mathrm{s}}}{\partial x}-\frac{\partial\theta_{xh}^{\mathrm{s}}}{\partial x}\right)\frac{\partial\varphi_{xh}^{\mathrm{s}}}{\partial x}+\int_\Gamma\left(\frac{\partial\hat{\theta}_y^{\mathrm{s}}}{\partial x}-\frac{\partial\theta_{yh}^{\mathrm{s}}}{\partial x}\right)\frac{\partial\varphi_{yh}^{\mathrm{s}}}{\partial x}\\
=-\int_\Gamma\left(\hat{R}\lambda_2-\lambda_{2h}\right)(z_h-z_h^{\mathrm{s}})-\int_\Gamma\left(\hat{R}\lambda_3-\lambda_{3h}\right)\left(\eta_{1h}-\varphi_{yh}^{\mathrm{s}}\right)\\
-\int_\Gamma\left(\tilde{R}\lambda_4-\lambda_{4h}\right)(\eta_{2h}+\varphi_{xh}^{\mathrm{s}})+a_2\left(\hat{\beta}-\beta,\eta_h\right)\\
+\int_\Omega(\hat{\gamma}-\gamma)\cdot(\nabla z_h-\Pi\eta_h)+\int_\Gamma(\hat{\alpha}-\alpha)\left(\frac{\partial z_h^{\mathrm{s}}}{\partial x}-\pi\varphi_{yh}^{\mathrm{s}}\right)\\
+\int_\Gamma\left(\frac{\partial\hat{\theta}_x^{\mathrm{s}}}{\partial x}-\frac{d\theta_x^{\mathrm{s}}}{dx}\right)\frac{\partial\varphi_{xh}^{\mathrm{s}}}{\partial x}+\int_\Gamma\left(\frac{\partial\hat{\theta}_y^{\mathrm{s}}}{\partial x}-\frac{d\theta_y^{\mathrm{s}}}{dx}\right)\frac{\partial\varphi_{yh}^{\mathrm{s}}}{\partial x}\\
+\int_\Omega\gamma\cdot(\eta_h-\Pi\eta_h)+\int_\Gamma\alpha\left(\pi\varphi_{yh}^{\mathrm{s}}-\varphi_{yh}^{\mathrm{s}}\right).
\end{aligned}
$$

Now, take $\eta_h:=\hat{\beta}-\beta_h$, $z_h:=\hat{w}-w_h$, $z^{\mathrm{s}}:=\hat{w}^{\mathrm{s}}-w_h^{\mathrm{s}}$, $\varphi_{xh}^{\mathrm{s}}:=\hat{\theta}_x^{\mathrm{s}}-\theta_{xh}^{\mathrm{s}}$ and $\varphi_{yh}^{\mathrm{s}}:=\hat{\theta}_y^{\mathrm{s}}-\theta_{yh}^{\mathrm{s}}$ and use that $\hat{w}^{\mathrm{s}}=\hat{w}|_\Gamma$, $\hat{\theta}_x^{\mathrm{s}}=\hat{\beta}_1\Big|_\Gamma$, $\hat{\theta}_y^{\mathrm{s}}=-\hat{\beta}_2\Big|_\Gamma$ and (3.71), to obtain

$$
\begin{aligned}
\int_\Gamma\left(\hat{R}\lambda_2-\lambda_{2h}\right)(\hat{w}-w_h-(\hat{w}^{\mathrm{s}}-w_h^{\mathrm{s}}))+\int_\Gamma\left(\hat{R}\lambda_3-\lambda_{3h}\right)\left(\hat{\beta}_1-\beta_{1h}-\left(\hat{\theta}_x^{\mathrm{s}}-\theta_{xh}^{\mathrm{s}}\right)\right)\\
+\int_\Gamma\left(\tilde{R}\lambda_4-\lambda_{4h}\right)\left(\hat{\beta}_2-\beta_{2h}+\hat{\theta}_y^{\mathrm{s}}-\theta_{yh}^{\mathrm{s}}\right)=0.
\end{aligned}
$$

Hence, using the ellipticity of a_2 (cf. (3.16)), the definition of $\hat{\gamma}$ and $\hat{\alpha}$, (3.68), (3.69), and a little of algebra we obtain

$$
\begin{aligned}
\left\|\hat{\beta}-\beta_h\right\|_{1,\Omega}^2+t^2\left\|\hat{\gamma}-\gamma_h\right\|_{0,\Omega}^2+t^2\left\|\hat{\alpha}-\alpha_h\right\|_{0,\Gamma}^2+\left\|\hat{\theta}_y^{\mathrm{s}}-\theta_{yh}^{\mathrm{s}}\right\|_{1,\Gamma}^2+\left\|\hat{\theta}_x^{\mathrm{s}}-\theta_{xh}^{\mathrm{s}}\right\|_{1,\Gamma}^2\\
\leq C\left\{\left\|\hat{\beta}-\beta\right\|_{1,\Omega}^2+t^2\left\|\hat{\gamma}-\gamma\right\|_{0,\Omega}^2+t^2\left\|\hat{\alpha}-\alpha\right\|_{0,\Gamma}^2+C_2\left\|\hat{\theta}_y^{\mathrm{s}}-\theta_y^{\mathrm{s}}\right\|_{1,\Gamma}^2\right.\\
\left.+\left\|\hat{\theta}_x^{\mathrm{s}}-\theta_x^{\mathrm{s}}\right\|_{1,\Gamma}^2\right\}+\|\gamma\|_{0,\Omega}\left\|\left(\hat{\beta}-\beta_h\right)-\Pi\left(\hat{\beta}-\beta_h\right)\right\|_{0,\Omega}\\
+\|\alpha\|_{0,\Gamma}\left\|\left(\hat{\theta}_y^{\mathrm{s}}-\theta_{yh}^{\mathrm{s}}\right)-\pi\left(\hat{\theta}_y^{\mathrm{s}}-\theta_{yh}^{\mathrm{s}}\right)\right\|_{0,\Gamma}.
\end{aligned}
$$

where we have used (3.64) and (3.65) to obtain the last two terms. Thus we conclude the lemma. □

Next step consists in defining $\hat{\beta}$ and $\hat{w}$ so that appropriate error estimates hold for the right hand side of (3.72). With this aim we will use the Lagrange interpolant I_{L} of different

functions β_1, β_2, w, θ_x^s, etc. This interpolant is well defined because of the additional regularity proved in Proposition 2. Moreover, for each edge ℓ of the triangulation, let β_ℓ be a unit tangent vector and b_ℓ the piecewise quadratic bubble associated to ℓ, so that $b_\ell\beta_\ell$ is a tangential bubble as defined in (3.63).

To define $\hat{\beta}$ we use the Lagrange interpolant of β enriched with quadratic tangential bubbles so that, for all edges ℓ,

$$\int_\ell \hat{\beta}\cdot\beta_\ell = \int_\ell \beta\cdot\beta_\ell. \tag{3.73}$$

Namely

$$\hat{\beta} := I_{\mathrm{L}}(\beta) + \sum_\ell c_\ell b_\ell \beta_\ell, \tag{3.74}$$

with

$$c_\ell := \frac{6}{|\ell|}\int_\ell (\beta - I_{\mathrm{L}}\beta)\cdot\beta_\ell. \tag{3.75}$$

Based on results from [26], it was shown in [22] that

$$\left\|\beta-\hat{\beta}\right\|_{1,\Omega_i} \le Ch\,\|\beta\|_{2,\Omega_i}, \qquad i=1,2. \tag{3.76}$$

On the other hand, we use the plain Lagrange interpolant of w to define $\hat{w}$:

$$\hat{w} := I_{\mathrm{L}} w. \tag{3.77}$$

Our next goal is to estimate $\|\hat{\gamma}-\gamma\|_{0,\Omega}$. Notice that, in spite of the fact that $\gamma\notin H^1(\Omega)^2$, its rotated Raviart-Thomas interpolant is well defined because $\gamma|_{\Omega_i}\in H^1(\Omega_i)^2$ and the tangential components of $\gamma|_{\Omega_1}$ and $\gamma|_{\Omega_2}$ coincide on Γ (see [41]). Moreover, an error estimate similar to (3.64) also holds in this case; namely,

$$\|\gamma-\Pi\gamma\|_{0,\Omega} \le Ch\left(\|\gamma\|_{1,\Omega_1}+\|\gamma\|_{1,\Omega_2}\right). \tag{3.78}$$

On the other hand another well known property of rotated Raviart-Tomas interpolant is that $\Pi(\nabla w) = \nabla(I_{\mathrm{L}} w) := \nabla\hat{w}$ (see [41] again). Therefore,

$$\hat{\gamma} := \frac{1}{t^2}(\nabla\hat{w}-\Pi\beta) = \frac{1}{t^2}\Pi(\nabla w-\beta) = \Pi\gamma. \tag{3.79}$$

Next, for $\hat{\theta}_x^s$, since $\theta_x^{\mathrm{s}} = \beta_2$ (cf. 3.35), we have that

$$\hat{\theta}_x^{\mathrm{s}} := \hat{\beta}_2\Big|_\Gamma = (I_{\mathrm{L}}\beta_2)|_\Gamma = I_{\mathrm{L}}\theta_x^{\mathrm{s}}$$

and, hence,

$$\left\|\theta_x^{\mathrm{s}}-\hat{\theta}_x^{\mathrm{s}}\right\|_{1,\Gamma} \le Ch\,\|\theta_x^{\mathrm{s}}\|_{2,\Gamma}. \tag{3.80}$$

Analogously, for $\hat{\theta}_y^{\mathrm{s}}$ we have

$$\hat{\theta}_y^{\mathrm{s}} := -\,\hat{\beta}_1\Big|_{\Gamma} = -\,(I_{\mathrm{L}}\beta_1)|_{\Gamma} - \sum_{\ell\in\mathscr{T}_h^{\Gamma}} c_\ell\, b_\ell. \tag{3.81}$$

Since $\theta_y^{\mathrm{s}} = -\beta_1|_{\Gamma}$ (cf. (3.35)), there holds.

$$\left\|\theta_y^{\mathrm{s}} - \hat{\theta}_y^{\mathrm{s}}\right\|_{1,\Gamma} \le \left\|\theta_y^{\mathrm{s}} - I_{\mathrm{L}}\theta_y^{\mathrm{s}}\right\|_{1,\Gamma} + \left\|\sum_{l\in\mathscr{T}_h^{\Gamma}} c_l\, b_l\right\|_{1,\Gamma}. \tag{3.82}$$

The first term on the right hand side above is bounded by the standard estimates for the Lagrange interpolant. For the second one we write

$$\left\|\sum_{\ell\in\mathscr{T}_h^{\Gamma}} c_\ell\, b_\ell\right\|_{1,\Gamma}^2 = \sum_{\ell\in\mathscr{T}_h^{\Gamma}} |c_\ell|^2\, \|b_\ell\|_{1,\ell}^2$$

Straightforward computations show that $\|b_\ell\|_{1,\ell}^2 \le \frac{C}{|\ell|}$. On the other hand, for the coefficients c_ℓ we use that $\beta\cdot\beta_\ell = \beta_1 = -\theta_y^{\mathrm{s}}$ on ℓ. Consequently, $I_{\mathrm{L}}\beta\cdot\beta_\ell = -I_{\mathrm{L}}\theta_y^{\mathrm{s}}$, and we have from (3.75)

$$|c_\ell|^2 \le \frac{36}{|\ell|}\left\|\theta_y^{\mathrm{s}} - I_{\mathrm{L}}\theta_y^{\mathrm{s}}\right\|_{0,\ell}^2 \le C\,|\ell|^3\left\|\theta_y^{\mathrm{s}}\right\|_{2,\ell}^2. \tag{3.83}$$

Altogether, we obtain

$$\left\|\theta_y^{\mathrm{s}} - \hat{\theta}_y^{\mathrm{s}}\right\|_{1,\Gamma} \le Ch\left\|\theta_y^{\mathrm{s}}\right\|_{2,\Gamma}. \tag{3.84}$$

It remains to estimate the term $\|\hat{\alpha}-\alpha\|_{0,\Gamma}$ in (3.72). With this aim we will show that $\hat{\alpha} = \pi\alpha$. First , it is simple to show that

$$\pi\frac{dw^{\mathrm{s}}}{dx} = \frac{d}{dx}\left(I_{\mathrm{L}}w^{\mathrm{s}}\right). \tag{3.85}$$

Hence, from (3.35), (3.77) and the definition of $\hat{w}^{\mathrm{s}}$ from Lemma 3.5.1 we obtain

$$\pi\frac{dw^{\mathrm{s}}}{dx} = \frac{d\hat{w}^{\mathrm{s}}}{dx}.$$

Secondly we will show that

$$\pi\theta_y^{\mathrm{s}} = \pi\hat{\theta}_y^{\mathrm{s}}. \tag{3.86}$$

To prove this, it is enough to show that $\int_\ell \theta_y^{\mathrm{s}} = \int_\ell \hat{\theta}_y^{\mathrm{s}}$ for all $\ell\in\mathscr{T}_h^{\Gamma}$, which follows from (3.35), (3.73) and the definition of $\hat{\theta}_y^{\mathrm{s}}$ in Lemma 3.5.1:

$$\int_\ell \theta_y^{\mathrm{s}} = -\int_\ell \beta_1 = -\int_\ell \hat{\beta}_1 = \int_\ell \hat{\theta}_y^{\mathrm{s}}.$$

Therefore, (3.86) and (3.85) leads to

$$\hat{\alpha} = \frac{1}{t^2}\left(\frac{d\hat{w}^s}{dx} + \pi\hat{\theta}_y^s\right) = \frac{1}{t^2}\pi\left(\frac{dw^s}{dx} + \theta_y^s\right) = \pi\alpha. \tag{3.87}$$

Consequently, from (3.65) we have

$$\|\hat{\alpha} - \alpha\|_{0,\Gamma} \leq Ch\,\|\alpha\|_{1,\Gamma}. \tag{3.88}$$

Now, we are in a position to prove the following theorem.

Theorem 3.5.1 *Let* $\left(\beta, w, w^s, \theta_x^s, \theta_y^s\right)$ *and* $\left(\beta_h, w_h, w_h^s, \theta_{xh}^s, \theta_{yh}^s\right)$ *be the solutions of problems (3.32)-(3.33) and (3.66)-(3.67), respectively. Let* γ, α, γ_h *and* α_h *be as defined in (3.48), (3.49), (3.68) and (3.69), respectively. Then*

$$\begin{aligned}
&\|\beta - \beta_h\|_{1,\Omega} + \|\theta_x^s - \theta_{xh}^s\|_{1,\Gamma} + \left\|\theta_y^s - \theta_{yh}^s\right\|_{1,\Gamma} + t\,\|\gamma - \gamma_h\|_{0,\Omega} + t\,\|\alpha - \alpha_h\|_{0,\Gamma} \\
&\quad \leq Ch\Big\{\|\beta\|_{2,\Omega_1} + \|\beta\|_{2,\Omega_2} + t\,\|\gamma\|_{1,\Omega_1} + t\,\|\gamma\|_{1,\Omega_2} + \|\gamma\|_{0,\Omega} \\
&\qquad\quad + \|\theta_x^s\|_{2,\Gamma} + \left\|\theta_y^s\right\|_{2,\Gamma} + t\,\|\alpha\|_{1,\Gamma} + \|\alpha\|_{0,\Gamma}\Big\}.
\end{aligned} \tag{3.89}$$

Proof. Let $\hat{\beta}$ and $\hat{w}$ be defined as in (3.74) and (3.73), respectively. Let $\hat{\gamma}$, $\hat{\theta}_x^s$, $\hat{\theta}_y^s$ and $\hat{\alpha}$ as in Lemma 3.5.1. Adding and subtracting these terms on the left hand side of (3.89), using triangular inequality, Lemma 3.5.1 and estimates (3.76), (3.78), (3.80), (3.84) and (3.88), we conclude the proof. □

Corollary 3.5.1 *Under the same assumptions as in Theorem 3.5.1, there holds*

$$\begin{aligned}
&\|w - w_h\|_{1,\Omega} + \|w^s - w_h^s\|_{1,\Gamma} \\
&\quad \leq Ch\Big\{\|\beta\|_{2,\Omega_1} + \|\beta\|_{2,\Omega_2} + t\,\|\gamma\|_{1,\Omega_1} + t\,\|\gamma\|_{1,\Omega_2} + \|\gamma\|_{0,\Omega} \\
&\qquad\quad + \|\theta_x^s\|_{2,\Gamma} + \left\|\theta_y^s\right\|_{2,\Gamma} + t\,\|\alpha\|_{1,\Gamma} + \|\alpha\|_{0,\Gamma}\Big\}
\end{aligned} \tag{3.90}$$

Proof. From (3.48) and (3.68), we have

$$\nabla w - \nabla w_h = t^2(\gamma - \gamma_h) + \beta - \Pi\beta_h.$$

Hence,

$$\begin{aligned}
|w - w_h|_{1,\Omega} &\leq t^2\,\|\gamma - \gamma_h\|_{0,\Omega} + \|\beta - \Pi\beta\|_{0,\Omega} + \|\Pi(\beta - \beta_h)\|_{0,\Omega} \\
&\leq t^2\,\|\gamma - \gamma_h\|_{0,\Omega} + \|\beta - \Pi\beta\|_{0,\Omega} + C\,\|\beta - \beta_h\|_{1,\Omega},
\end{aligned} \tag{3.91}$$

The latter because of (3.64). Analogously, from (3.49) and (3.69), we have

$$\frac{dw^s}{dx} - \frac{dw_h^s}{dx} = t^2(\alpha - \alpha_h) + \theta_y^s - \pi\theta_{yh}^s$$

and hence

$$\begin{aligned} |w^s - w_h^s|_{1,\Gamma} &\le t^2 \|\alpha - \alpha_h\|_{0,\Gamma} + \left\|\theta_y^s - \pi\theta_y^s\right\|_{0,\Gamma} + \left\|\pi\left(\theta_y^s - \theta_{yh}^s\right)\right\|_{0,\Gamma} \\ &\le t^2 \|\alpha - \alpha_h\|_{0,\Gamma} + \left\|\theta_y^s - \pi\theta_y^s\right\|_{0,\Gamma} + \left\|\theta_y^s - \theta_{yh}^s\right\|_{0,\Gamma} \end{aligned}$$

Therefore the corollary follows from these estimates (3.64), (3.65) and Theorem 3.5.1. □

3.6 Numerical Experiments

In this section we report some numerical results obtained with a code which implements the method analyzed above. The aim of the numerical experimentation is to assess the performance of the method. The error estimate from Theorem 3.5.1 involves higher order norms of quantities which are known to be bounded (cf. Proposition 2). These bound are independent of the thickness t for uncoupled plates ([2]) and rods ([3]). However analogous thickness independent bounds have not been proved for a stiffened plate. Therefore, one of the goals of the reported numerical experimentation is to test whether the method is actually locking-free.

To solve problem (3.66)-(3.67), first we eliminate the Lagrange multipliers and impose the constraints directly by writing the variables corresponding to the stiffener in terms of those of the plate. In fact, (3.67) implies that

$$w_h^s = w_h, \qquad \theta_{xh}^s = \beta_{2h}, \qquad \theta_{yh}^s = -\beta_{1h} \qquad \text{on } \Gamma.$$

Thus, problem (3.66)-(3.67) turns out to be equivalent to the following one, in which we included again the physical constants that have been set to 1 for the analysis:

$$\begin{aligned} t^3 a_2(\beta_h, \eta_h) + \int_\Omega \kappa\mu t\,(\nabla w_h - \Pi\beta_h)\cdot(\nabla z_h - \Pi\eta_h) + \int_\Gamma E^s I_{yy} \frac{\partial\beta_{1h}}{\partial x}\frac{\partial\eta_{1h}}{\partial x} \\ + \int_\Gamma \kappa^s\mu^s A\left(\frac{\partial z_h}{\partial x} - \pi\beta_{1h}\right)\left(\frac{\partial z_h}{\partial x} - \pi\eta_{1h}\right) + \int_\Gamma \mu^s J \frac{\partial\beta_{2h}}{\partial x}\frac{\partial\eta_{2h}}{\partial x} \\ = t\int_\Omega g z_h, \qquad \forall\,(z_h, \eta_h) \in W_h \times Y_h. \end{aligned} \tag{3.92}$$

Let us remark that the stiffness matrix of the problem can be easily obtained by static condensation from the separate corresponding stiffness matrices of the plate and the rod.

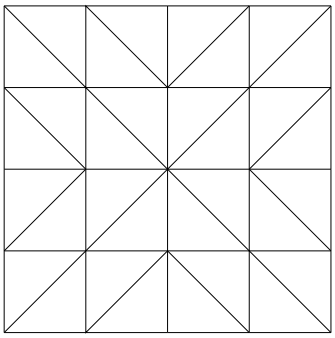

Figure 3.4: Square plate. Finite element mesh ($N = 4$).

In all tests, we considered a square plate of side length 60 cm. The stiffener crosses the plate joining the mid-points of two opposite edges.

We use uniform meshes obtained by refining the coarse one shown in Figure 3.4. The parameter N represents the number of elements on each side of the plate. We took $\kappa = \kappa^{\mathrm{s}} = 1$ as correction factors in the plate and the stiffener, respectively, for all the tests.

3.6.1 Test 1: A free vibration problem for a clamped stiffened plate

Since no analytical solution for the load problem of the stiffened plate is available to compare with, we used a vibration problem solved in [28] by means of MITC9 elements.

For the vibration problem, we have to consider the mass terms of the plate and the stiffener instead of the load terms. Thus, the vibration problem consists in finding $\omega_h > 0$

and $(w_h, \beta_h) \in W_h \times Y_h$ such that

$$\begin{aligned} t^3 a_2(\beta_h, \eta_h) + \int_\Omega \kappa\mu t\,(\nabla w_h - \Pi\beta_h)\cdot(\nabla z_h - \Pi\eta_h) + \int_\Gamma E^{\mathrm{s}} I_{yy} \frac{\partial\beta_{1h}}{\partial x}\frac{\partial\eta_{1h}}{\partial x} \\ + \int_\Gamma \kappa^{\mathrm{s}}\mu^{\mathrm{s}} A\left(\frac{\partial z_h}{\partial x} - \pi\beta_{1h}\right)\left(\frac{\partial z_h}{\partial x} - \pi\eta_{1h}\right) + \int_\Gamma \mu^{\mathrm{s}} J \frac{\partial\beta_{2h}}{\partial x}\frac{\partial\eta_{2h}}{\partial x} \\ = \omega_h^2 \left(t\int_\Omega \rho w_h z_h + \frac{t^3}{12}\int_\Omega \rho\beta_h\cdot\eta_h + \int_\Gamma \rho^{\mathrm{s}} A w_h z_h + \int_\Gamma \rho^{\mathrm{s}} I_{yy}\beta_{1h}\eta_{1h} \right. \\ \left. + \int_\Gamma \rho^{\mathrm{s}} J\beta_{2h}\eta_{2h}\right) \qquad \forall\,(z_h,\eta_h) \in W_h \times Y_h, \end{aligned} \tag{3.93}$$

where ω_h is the unknown vibration frequency and ρ and ρ^{s} are the densities of the plate and the stiffener, respectively. We applied the method to a square clamped stiffened plate of side length 60 cm and thickness 1 mm. We used the same physical parameters as in [28]:

$$\begin{aligned} &E = E^{\mathrm{s}} = 68.85\times 10^9 \text{ Pa},\\ &\nu = \nu^{\mathrm{s}} = 0.34,\\ &\rho = \rho^{\mathrm{s}} = 2780 \text{ kg/m}^3,\\ &A = 67 \text{ mm}^2,\\ &I_{yy} = 2290 \text{ mm}^4,\\ &J = 22.33 \text{ mm}^4. \end{aligned}$$

Table 3.1 shows the six lowest vibration frequencies computed with the method on four successively refined meshes. The table includes extrapolated frequencies and the order of convergence in powers of h estimated by means of a least squares fitting. It also includes the frequencies computed in [28] with MITC9 elements.

Table 3.1: Test 1: Lowest vibration frequencies of a square clamped stiffened plate.

Mode	$N=16$	$N=32$	$N=48$	$N=64$	order	extrapolated	[28]
ω_1	50.919	50.527	50.452	50.426	1.97	50.392	50.36
ω_2	64.266	63.810	63.719	63.687	1.89	63.641	63.65
ω_3	76.221	75.298	75.124	75.063	1.97	74.982	74.95
ω_4	86.656	85.694	85.510	85.445	1.95	85.358	85.36
ω_5	116.762	114.468	114.022	113.865	1.93	113.650	113.63
ω_6	123.714	121.363	120.895	120.729	1.89	120.493	120.52

We observe a good agreement between the values computed with both methods. On the other hand, a quadratic order of convergence can be clearly appreciated. Since typi-

cally the order of convergence of the eigenvalues doubles that of the load problem, this corresponds to $O(h)$ for the latter, which is the optimal one for the elements we have used.

3.6.2 Test 2: Robustness with respect to the stiffener properties

The aim of this test is to assess the robustness of the method with respect to the physical parameters of the stiffener.

We considered two asymptotics with respect to the thickness t. In the first one, the stiffener rigidity increases a t becomes smaller. As discussed above, the proper scaling for attaining a limit as t goes to zero is to take E^{s} proportional to $1/t$ (cf. (3.13)). This is the reason why we used $E^{\mathrm{s}} := E/t^2$ for this experiment. Therefore, in the limit as t goes to zero, this problem corresponds to that of a clamped plate also clamped along its mid-line Γ.

The material and the stiffener cross-sectional properties were taken as follows:

$$\begin{aligned} &A = t^2, \\ &I_{yy} = t^4/12, \\ &J = t^4/6, \\ &E = 68.85 \times 10^9 \text{ Pa}, \\ &\nu = \nu^{\mathrm{s}} = 0.34. \end{aligned}$$

The load was taken as constant on the whole plate:

$$g = 10^6 \text{ N/m}^4 \, t^2.$$

We took various values of the thickness ranging from 10 to 0.01 mm. We compared the transverse displacement w_h and the rotation β_h computed with the present method with those corresponding to the plate clamped along Γ, which were computed by DL3 elements ([22]). We denote the latter by w_h^{c} and β_h^{c}. We measure the deviation between both models by means of the relative differences

$$\frac{\left|w_h - w_h^{\mathrm{c}}\right|_{1,\Omega}}{\left|w_h^{\mathrm{c}}\right|_{1,\Omega}} \qquad \text{and} \qquad \frac{|\beta_h - \beta_h^{\mathrm{c}}|_{1,\Omega}}{|\beta_h^{\mathrm{c}}|_{1,\Omega}}$$

computed on the mesh corresponding to $N = 64$. It can clearly seen that the relative differences decreases linearly with the thickness t.

This experiment shows that the stiffened plate behaves as expected in this limit case.

As a second experiment we took $E^{\mathrm{s}} = E$ and the same values as above for A, I_{yy}, J, E and ν. In this case, as t becomes smaller, the effect of the stiffener tends to disappear. In fact, $A = t^2$ corresponds to a rod section with width and height proportional to t. In the limit as t goes to zero this problem correspond to that of an unstiffened plate. Once

Table 3.2: Test 2: Comparison of stiffened plates with an almost rigid and a perfectly rigid stiffener.

Thickness (m)	$\frac{\lvert w_h - w_h^{\mathrm{c}}\rvert_{1,\Omega}}{\lvert w_h^{\mathrm{c}}\rvert_{1,\Omega}}$	$\frac{\lvert \beta_h - \beta_h^{\mathrm{c}}\rvert_{1,\Omega}}{\lvert \beta_h^{\mathrm{c}}\rvert_{1,\Omega}}$
10^{-2}	2.6914×10^{-2}	1.6122×10^{-2}
10^{-3}	2.8980×10^{-3}	1.6167×10^{-3}
10^{-4}	2.9001×10^{-4}	1.6178×10^{-4}
10^{-5}	2.9351×10^{-5}	1.6279×10^{-5}

more we took values of t ranging from 10 to 0.01mm and we compared the transverse displacements and the rotations computed with the present method with those of the unstiffened plate computed by DL3 elements. We denote the latter by w_h^{f} and β_h^{f}. We report in Table 3.3 the relative differences between both models computed again on the mesh corresponding to $N = 64$.

Table 3.3: Test 2: Comparison of a stiffened plate with a very soft stiffener and plate without a stiffener.

Thickness (m)	$\frac{\lvert w_h - w_h^{\mathrm{f}}\rvert_{1,\Omega}}{\lvert w_h^{\mathrm{f}}\rvert_{1,\Omega}}$	$\frac{\lvert \beta_h - \beta_h^{\mathrm{f}}\rvert_{1,\Omega}}{\lvert \beta_h^{\mathrm{f}}\rvert_{1,\Omega}}$
10^{-2}	1.4452×10^{-2}	1.5399×10^{-2}
10^{-3}	1.4624×10^{-3}	1.5650×10^{-3}
10^{-4}	1.4643×10^{-4}	1.5687×10^{-4}
10^{-5}	1.5688×10^{-5}	1.6183×10^{-5}

Once more, it can be clearly observed a linear decrease with respect to t. Therefore, the behavior of this softly stiffened plates agrees with what expected, too.

On the other hand, Tables 3.2 and 3.3 show that the method is thoroughly robust with respect to the physical parameters of the stiffener. Moreover, in both cases the results do not deteriorate as t becomes smaller, which suggests that the method is locking free.

3.6.3 Test 3: Testing the locking-free character of the method

The main goal of this test is to confirm experimentally that the method is locking free. In this case we took the scaling $E^{\mathrm{s}} := E/t$ which allow us to achieve a well posed limit problem. We computed a very accurate approximation of the solution with the mesh

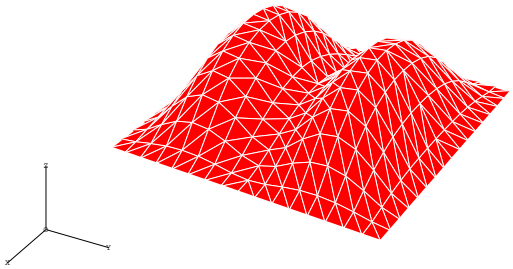

Figure 3.5: Test 4: Transverse displacement field computed with the method proposed ($N = 16$)

corresponding to $N = 64$ and we took it an 'exact' solution. We denote by w^{e} the corresponding transversal displacement. We estimated the error of the numerical solutions computed on coarse meshes ($N = 8, 12, 16$) by means of $|w^{\mathrm{e}} - w_h|_{1,\Omega}$.

We report in Table 3.4 the values of $|w^e - w_h|_{1,\Omega}$ for different meshes and decreasing values of the thickness. We also include the orders of convergence estimated by means of a least squares fitting and, in the last row, the extrapolated limit values corresponding to $t = 0$.

Table 3.4: Test 3: Testing the locking-free character of the method, $|w^e - w_h|_{1,\Omega} \times 10^8$.

Thickness (m)	$N = 8$	$N = 12$	$N = 16$	$N = 20$	order
10^{-2}	0.48539537	0.32111497	0.26220361	0.17661659	1.05
10^{-3}	0.48461630	0.32097671	0.26194608	0.17665166	1.05
10^{-4}	0.48460920	0.32097551	0.26194343	0.17665175	1.05
10^{-5}	0.48460877	0.32097521	0.26194321	0.17665155	1.05
$t = 0$ (extr.)	0.48460875	0.32097512	0.26194319	0.17665121	1.05

We observe that the method is perfectly locking-free and that an order of convergence close to one is attained even for extremely small values of the thickness. Thus, this experiment provides a solid numerical evidence of the locking-free character of the method.

Finally Figure 3.5 show the transverse displacement field of the stiffened plate model

reported in Table 3.4 for $t = 0.001$m and $N = 16$. In this case the relation $E^s/E = 10^4$. The effect of the stiffener can be clearly appreciated in the Figure 3.5.

3.7 Conclusion

We analyzed the load problem of the clamped stiffened plate modeled by Reissner-Mindlin equations. We restrict our analysis to the case of concentrically stiffened plates, in which the mid-line of the stiffener lies on the mid-surface of the plate. In such a case, the problem decouples into two well posed problems: a stiffened in-plate plate problem and a stiffened bending plate problem.

We propose a finite element method based on a standard linear triangular elements for the in-plane problem and DL3 elements for the bending problem. The analysis of the former is straightforward, since it turns out a standard elliptic problem not depending on the plate thickness.

The analysis of the bending problem is more involved. We proved optimal order error estimates for all the quantities in terms of higher order norms of these quantities. We have proved that this higher order norms are bounded, but we could not obtain bounds independent of the plate thickness.

Because of this the main achievement of the numerical experimentation was to assess the locking-free character of the method. The numerical tests also confirmed the optical order of convergence and showed the robustness of the method with respect to the physical parameters of the stiffener.

Chapter 4

Conclusiones y proyecciones

4.1 Conclusiones

- Se analizó el problema de vibraciones libres de una barra empotrada de Timoshenko de geometría arbitraria utilizando hipótesis un poco más generales que las del trabajo de Arunakirinathar & Reddy (en el que se estudió el problema fuente) demostrando un orden de convergencia óptimo para los desplazamientos, rotaciones y esfuerzos de corte asociados a las autofunciones, además de un doble orden de convergencia para las frecuencias de vibración. También se demostró que el método respectivo es libre de bloqueo, es decir, la convergencia del método no se deteriora cuando el espesor característico de la barra se hace pequeño.

- Se estudió también el problema de vibraciones libres de una placa laminada empotrada modelada por las ecuaciones de Reissner-Mindlin. Se consideró un elemento finito de placa DL3 para los términos asociados a la flexión y lineales a trozos y continuos para los desplazamientos en el plano. Se demostró un orden de convergencia óptimo en H^1 y L^2 para los desplazamientos y rotaciones y un doble orden de convergencia para las frecuencias de vibración. Se demostró que el método es libre de bloqueo y se presentaron resultados numéricos que confirman los resultados teóricos, extendiendo la experimentación a condiciones de contorno más generales con resultados satisfactorios.

- Se analizó el problema de cargas de una placa rigidizada modelada por las ecuaciones de Reissner-Mindlin. Restringiendo el análisis al caso de placas rigidizadas concéntricas. Se muestra que en tal caso el problema se descompone en un problema rigidizado en el plano y un problema rigidizado de flexión. Se propuso utilizar elementos lineales a trozos y continuos para el problema en el plano y elementos de placa DL3 para el problema de la placa rigidizada. El análisis del primero es

estándar e inclusive independiente del espesor. En el segundo se demostraron estimaciones del error óptimas para todas las cantidades en término de normas de orden superior de esas cantidades, las cuales se demostró que son finitas, aunque no de manera independiente del espesor. Se llevó a cabo una experimentación numérica adecuada que permitió mostrar el carácter libre de bloqueo de este método de elementos finitos.

4.2 Proyecciones

- En el Capítulo 3 queda abierto el estudio de la regularidad del problema de flexión de placas rigidizadas con regularidad independiente del espesor de la placa.
- Estudiar el problema de placas laminadas rigidizadas combinando los elementos de los Capítulos 2 y 3.
- Estudiar el problema de placas rigidizadas con rigidizadores excéntricos.
- En el Capítulo 3, Estudiar el uso de mallas de elementos finitos que no respeten la dirección del rigidizador.

Bibliography

[1] ARNOLD D. N., *Discretization by finite element of a model parameter dependent problem*, Numer. Math. 37

[2] ARNOLD D.N. AND FALK R.S., *A uniformly accurate finite element method for the Reissner-Mindlin plate*, SIAM J. Numer. Anal., 26 (1989) pp. 1276–1290.

[3] ARUNAKIRINATHAR, K. & REDDY, B.D., *Mixed finite element methods for elastic rods of arbitrary geometry*, Numer. Math. 64 (1993) pp. 13–43.

[4] AURICCHIO F., LOVADINA C., AND SACCO E., *Analysis of mixed finite elements for laminated composite plates* Comput. Methods Appl. Mech. Engrg., 190 (2000) pp. 4767–4783.

[5] AURICCHIO F. AND SACCO E., *A mixed-enhanced finite element for the analysis of laminated composite plates*, Internat. J. Numer. Methods Engrg., 44 (1999) pp. 1481–1504.

[6] I. BABUŠKA AND J. OSBORN, *Eigenvalue problems*, in Handbook of Numerical Analysis, Vol. II, P.G. Ciarlet and J.L. Lions, eds., North-Holland, Amsterdam, 1991, pp. 641–787.

[7] BABUŠKA, I. AND SURI, M. *On locking and robustness in the finite element method*, SIAM J. Numer. Anal., 29 (1992), pp. 1261–1293.

[8] BATHE K.-J., BREZZI F. AND CHO S. W., *The MITC7 and MITC9 plate bendings elements*, in Computers & Structures 32 (1984), pp. 797-814.

[9] BATHE K.J. AND DVORKIN E.N., *A four-node plate bending element based on Mindlin/Reissner plate theory and a mixed interpolation*, Internat. J. Numer. Methods Engrg., 21 (1985), pp. 367–383.

[10] BREZZI F. AND FORTIN M., *Mixed and Hybrid Finite Element Methods*, Springer-Verlag (1991).

[11] BOFFI, D., BREZZI, F., DEMKOWICZ, L.F., DURN, R.G., FALK, R.S., FORTIN, M. *Mixed Finite Elements, Compatibility Conditions, and Applications: Lectures given at the C.I.M.E. Summer School held in Cetraro, Italy June 26-July 1, 2006* Springer-Verlag Berlin Heidelberg.

[12] BOFFI, D., BREZZI, F. AND GASTALDI, L. *On the convergence of eigenvalues for mixed formulations,* Ann. Scuola Norm. Sup. Pisa Cl. Sci. (4), 25 (1998), pp. 131–154.

[13] BOFFI, D., BREZZI, F. & GASTALDI, L. *On the problem of spurious eigenvalues in the approximation of linear elliptic problems in mixed form,* Math. Comp., 69 (2000), pp. 121–140.

[14] CHAPELLE, D. *A locking-free approximation of curved rods by straight beam elements,* Numer. Math., **77** (1997), pp. 299–322.

[15] CHENAIS D. AND PAUMIER J.-C., *On the locking phenomenon for a class of elliptic problems,* Numer. Math. 67 (1994), pp. 427–440.

[16] CLOUGH R.W. AND TOCHER, J. L., *Finite element stiffness matrices for analysis of plate bending,* Proc. of Second. Conf. on Matrix Methods in Struct. Mech. (1965), pp. 515–546.

[17] DEB A. AND BOTTOM M., *Finite element models for stiffened plates under transversal loading,* Computers and Structures 28 (1988), pp. 361–372.

[18] DESTUYNDER F. AND SALAUN M., *Mathematical analysis of thin plate models,* Springer-Verlag, Germany, 1996.

[19] D'HENNEZEL F., *Domain decomposition method and elastic multi-structures: the stiffened plate problem,* Numer. Math. 66 (1993), pp. 181–197.

[20] DURÁN, R., HERVELLA-NIETO, L., LIBERMAN, E., RODRÍGUEZ, R. AND SOLOMIN, J. *Approximation of the vibration modes of a plate by Reissner-Mindlin equations,* Math. Comp., 68 (1999), pp. 1447–1463.

[21] DURÁN, R., HERNÁNDEZ, E., HERVELLA-NIETO, L., LIBERMAN, E. & RODRÍGUEZ, R. *Error estimates for low-order isoparametric quadrilateral finite elements for plates,* SIAM J. Numer. Anal., 41 (2003), pp. 1751–1772.

[22] DURÁN R. G., LIBERMAN E., *On the mixed finite element methods for the Reissner- Mindlin plate model,* in Mathematics of Computation 58 (1992), pp. 561-573.

[23] DURÁN R. G. , RODRÍGUEZ R. AND SANHUEZA F., *Computation of the vibration modes of a Reissner-Mindlin laminated Plate*by to appear

[24] DURÁN R. G., RODRÍGUEZ R. AND SANHUEZA F. *A finite element method for stiffened plates*by to appear

[25] ERN A. AND GUERMOND J-L., *Theory and Practice of Finite Elements*, Springer-Verlag, New York (2004).

[26] GIRAULT V., RAVIART P.A., *Finite element methods for Navier-Stokes equations*, Springer-Verlag, (1986).

[27] GRISVARD P., *Elliptic problems in nonsmooth domains*, Pitman (1985).

[28] HOLOPAINEN T. P., *Finite element free vibration analysis of eccentrically stiffened plates*, in Computers & Structures 56 (1995), pp. 993-1007.

[29] HUANG, T.C. *The effect of rotatory inertia and of shear deformation on the frequency and normal mode equations of uniform beams with simple end conditions*, J. Appl. Mech. 28 (1961), pp. 579–584.

[30] JANOWSKY, V. AND PROCHAKA, *The nonconforming finite element method in the problem of clamped plate with ribs*, Apl. Mat. 21 (1976), pp. 273–289.

[31] KARAMI, G., FARSHAD, M. AND YAZDCHI, M. *Free vibrations of spatial rods – a finite-element analysis*, Comm. Appl. Numer. Methods 6 (1990), pp. 417–428.

[32] KATO, T. Perturbation Theory for Linear Operators. Berlin: Springer Verlag.(1995).

[33] KIKUCHI, F. *Accuracy of some finite element models for arch problems*, Comput. Methods Appl. Mech. Engrg. 35 (1982), pp. 315–345.

[34] KOZLOV V., MAZ'YA V. AND ROSSMANN J., *Spectral Problems Associated with Corner Singularities of Solutions to Elliptic Equations*, Mathematical Surveys and Monographs 85, AMS, Providence, RI, (2001).

[35] LITEWKA, P. AND RAKOWSKI, J. *Free vibrations of shear-flexible and compressible arches by FEM*, Internat. J. Numer. Methods Eng. 52 (2001), pp. 273–286.

[36] LOULA, A.F.D., FRANCA, L.P., HUGHES, T.J.R. AND MIRANDA, I *Stability, convergence and accuracy of a new finite element method for the circular arch problem*, Comput. Methods Appl. Mech. Engrg. 63 (1987), 281-303.

[37] LITEWKA, P. , RAKOSWKY, J. *Free vibration of shear- flexible and compresible arches by FEM.* Int. J. Numer. Methods. Appl. Mech. Eng. 52 (2001), pp. 273-286.

[38] MUKHERJEE A. AND MUKHOPADHYAY M., *Finite element free vibration of eccentrically stiffened plates*, Computers and Structures 30 (1988), pp. 1303–1317.

[39] OCHOA O. O. AND REDDY J.N., *Finite element analysis of composite laminates*, Kluwer Academic Publishers, Dordrecht, The Netherlands (1992).

[40] O'LEARY J. AND HARARI I., *Finite Element Analysis of Stiffened Plates*, Computers and Structures 21 (1985), pp. 973–985.

[41] RAVIART P.A. AND THOMAS J. M., *A mixed finite element method for second order elliptic problems*, mathematical aspects of the finite element method, Lecture Notes in Math., Springer, 1977, pp 292–315.

[42] REDDY, B.D. AND VOLPI, M.B. *Mixed finite element methods for the circular arch problem*, Comput. Methods Appl. Mech. Engrg. 97 (1992), pp. 125–145.

[43] REDDY J.N, *Energy and Variational Methods in Applied Mechanics*, Wiley, New York, (1984).

[44] REDDY J.N., *Mechanics of Laminated Composite Plates – Theory and Analysis*, CRC Press, Boca Raton (1997).

[45] ROSS C. T. F.*Advanced applied stress analysis*, Ellis Horwood Limited, England (1987).

[46] SCOTT L. AND ZHANG S., *Finite element interpolation of nonsmooth functions satisfying boundary conditions*, Math. Comp. 54 (1990), pp. 483–493.

[47] TIMOSHENKO S. P. AND WOINOWSKY- KREIGER S.*Theory of Plates and Shells* McGraw-Hill, 1959.